Kinematic Solutions for the Effective Implementation of Parallel Manipulators

by

Leila Notash
B.Sc., Middle East Technical University, Turkey, 1988
M.A.Sc., University of Toronto, 1991

A Dissertation Submitted in Partial Fulfillment of the
Requirements for the Degree of
DOCTOR OF PHILOSOPHY
in the
Department of Mechanical Engineering.

We accept this dissertation as conforming
to the required standard

Dr. R. P. Podhorodeski, Supervisor (Dept. of Mechanical Engineering)

Dr. B. Tabarrok, Departmental Member (Dept. of Mechanical Engineering)

Dr. J. Haddow, Departmental Member (Dept. of Mechanical Engineering)

Dr. M. Nahon, Departmental Member (Dept. of Mechanical Engineering)

Dr. W. S. Lu, Outside Member (Dept. of Electrical and Computer Engineering)

Dr. J. M. McCarthy, External Examiner (Dept. of Mechanical and Aerospace Engineering, University of California at Irvine)

University of Victoria

Supervisor: Dr. Ron P. Podhorodeski

Abstract

Solutions are developed for the effective implementation of parallel manipulators. A class of three-branch parallel manipulators, with three main-arm joints on a branch and a passive spherical branch end joint, is considered. All feasible combinations of revolute and prismatic joints and all feasible combinations of sensing/actuating of the main-arm joints are investigated.

Solutions for the forward displacement problem of the class of three-branch parallel manipulators are introduced. The effect of including redundancy in the main-arm joint displacement sensing on providing closed-form forward displacement solutions and on the reduction of the number of potential assembly modes for the manipulators is investigated. Intersection of loci defining the feasible locations of the branch ends considering individual branches and branch combinations is utilized for the solutions. It is found that closed-form solutions exist for all cases of redundant sensing and for asymmetric non-redundant sensing.

The special configurations of parallel manipulators are considered. The investigation is based on examining potential degeneracies of the screw systems formed by actuated-joint associated wrenches, identifying all potential uncertainties for the considered class of manipulators. The characteristics of the unconstrained instantaneous degrees of freedom corresponding to each uncertainty configuration are discussed. Joint actuation layouts that eliminate the uncertainty configurations are determined through the consideration of all feasible cases of main-arm joint actuation.

The effect of adding a redundant branch in terms of reduction of the number of assembly modes and elimination of potential uncertainty configurations is also investigated. The addition of a redundant branch to the three-branch parallel manipulators

effectively yields a four-branch manipulator class. Considered in particular is a 3-4 form of the manipulator where two branch ends meet at one point on the mobile platform and symmetric main-arm joint sensing and actuation (two sensed/actuated main-arm joints per branch) is utilized. The addition of such a branch is found to be not as effective for assembly mode and uncertainty elimination as redundant sensing/actuation of main-arm joints.

A calibration method for parallel manipulators is introduced which is based on the redundant joint displacement sensing and does not require a calibration fixture when all of the main-arm joints of the considered manipulators are sensed. The procedure is applied and shown to be effective for the calibration of a redesigned parallel hand controller.

A sensor fault detection scheme for fault tolerant operation of parallel manipulators is introduced. The presented forward displacement solutions are used to develop sensor failure safe solutions. The fault detection analysis of the calibrated hand controller is investigated. Data analysis is performed to examine the sources of algorithmic failure. It is concluded that high accuracy in the passive spherical branch end joints is required to facilitate fault detection.

The solutions are implemented in computer simulation and also in real-time operation of a six degree of freedom parallel hand controller.

Examiners:

Dr. R. P. Podhorodeski, Supervisor (Dept. of Mechanical Engineering)

Dr. B. Tabarrok, Departmental Member (Dept. of Mechanical Engineering)

Dr. J. Haddow, Departmental Member (Dept. of Mechanical Engineering)

Dr. M. Nahon, Departmental Member (Dept. of Mechanical Engineering)

Dr. W. S. Lu, Outside Member (Dept. of Electrical and Computer Engineering)

Dr. J. M. McCarthy, External Examiner (Dept. of Mechanical and Aerospace Engineering, University of California at Irvine)

Table of Contents

List of Figures

List of Tables

Acknowledgements

I would like to acknowledge comments of my supervisor, Professor Ron P. Podhorodeski, on the work. I appriciate his willingness in editing any pieces of my work.

Chapter 1

Introduction

1.1 Parallel Manipulators

Manipulators can be thought to range from serial manipulators to fully parallel configurations. Serial manipulators have one branch and all of the joints of the branch are actuated and sensed. Fully parallel manipulators have one actuated and sensed joint in each branch (depending on the context), e.g., a fully parallel spatial manipulator would have six branches with one sensed and actuated joint in each branch. Between the extremes of serial and fully parallel devices are n-branch parallel manipulators (n = 2, 3, 4, or 5 for spatial devices) where one or more joints are active in each branch. For a parallel manipulator to be capable of spatial motion each branch must be able to accommodate six degrees of freedom (dof) of task space motion. Parallel manipulators, in comparison to serial manipulators, have the advantages of not requiring actuation of base distal joints and of having their active joints acting in parallel on a common payload. These advantages lead to manipulators having desirable stiffness, accuracy and dynamic characteristics, Hunt (1978) (1983), and Fichter (1986).

Fully parallel manipulators have been proposed as flight simulators and also utilized in tire test applications for several decades. Recently, parallel manipulators have been employed as master arms in telerobotics applications. Furthermore, combination of parallel manipulators with serial arms have been employed to obtain desirable fine and gross motion characteristics (Sklar and Tesar (1988) and Waldron et al. (1989)).

Implementation of parallel manipulators requires the solution of fundamental kinematic problems including (depending on application): forward and inverse displacement and higher order kinematics solutions; and knowledge of special configurations leading to motion or force degeneracies. Furthermore, for effective real-time implementation of a parallel manipulator the existence of closed-form (analytical) and unique solutions, elimination of special configurations through design, the ability to perform calibrations to enhance accuracy, and operational/failure safe capabilities can be necessary. The next section defines these problems for the parallel manipulators. Subsequent sections of this chapter outline previous work of other researchers and set the objective of this research.

1.2 Kinematic Problems of Parallel Manipulators

Calculation of the end effector pose, velocity, and acceleration for a given joint displacement, velocity, and acceleration of a manipulator, is referred to as the forward kinematic analysis in the literature. For a non-redundant 6 dof serial manipulator forward displacement analysis results in a unique solution whereas the inverse displacement solution (evaluating joint displacements for a given end effector pose) can have up to 16 solutions for a general manipulator layout (Raghavan and Roth (1990)). In contrast to serial manipulators, parallel manipulators can have multiple forward displacement solutions for a known set of actuated joint displacements, each solution

corresponding to a different assembly configuration of the parallel manipulator. The existence of multiple solutions for the forward/inverse displacement problems is an important issue for on-line computations required for manipulator control. Parallel manipulators can possess problems both due to multiple inverse displacement solutions of serial arms and multiple forward displacement solutions of parallel devices.

Degeneracies of parallel manipulators can be classified as branch singularities and uncertainty configurations of the parallel manipulator. At a special configuration a parallel manipulator may not be capable of providing a required end effector motion due to a branch singularity or may not be able to resist/apply an end effector force/moment (wrench) due to a manipulator uncertainty configuration.

Branch singularities correspond to configurations where the joints of the branch are instantaneously aligned such that the branch is incapable of six dof task motion. A branch degeneracy corresponds to the set of joint displacements where the different solutions of the inverse kinematic problem of a branch meet. The encounter (or close encounter) of a branch degeneracy can cause several problems including: required high joint acceleration if the branch leaves the singularity on a different branch configuration (branch switching); and required high joint rates during motions near degenerate configurations. Branch singularities can also be considered potentially attractive since they represent configurations in which certain externally applied loads are not reacted by the actuators, i.e., they are sustained by the structure of the arm. As outlined in the next section, singularities of serial manipulators have been addressed by several researchers. Similar problems exist for parallel manipulators. Most of the work on singularities of serial manipulators should be easy to adapt for parallel manipulators. Therefore, branch degeneracies will not be addressed in this thesis.

In uncertainty configurations the end effector is instantaneously movable even

when all of the actuated joints are locked. Uncertainties correspond to configurations where different solutions of the forward displacement problem (assembly modes) of a parallel manipulator meet. In this case, the common payload (end effector) gains one or more unconstrained task space degrees of freedom and one or more wrenches (generalized forces) cannot be resisted. The loss of the ability to sustain wrenches is critical in manipulator applications. Furthermore, since uncertainties correspond to the configurations where the forward displacement solutions coalesce, false assembly mode switching at uncertainties can occur. That is, the device can leave the uncertainty in an assembly mode that does not correspond to the assembly mode assumed by the model utilized for device control. The false assembly mode switching will lead to unsuccessful task completion and can be extremely dangerous. Knowledge of uncertainty configurations, and potential for their elimination, is critical for effective implementation of parallel manipulators.

Kinematic calibration of a manipulator attempts to accurately identify values for the set of kinematic parameters involved in the relationship of the joint displacements to the end effector pose. The ability to calibrate a manipulator is critical for applications requiring high accuracy. Kinematic calibration of a manipulator typically requires precise measurement of the end effector position and orientation at a number of different manipulator poses, i.e., a calibration fixture is required. For manipulators operating in remote or hazardous environments use of a calibration fixture is not always possible. Research into fixture free calibration of parallel manipulators is required.

Reliable and safe manipulators are required in remote applications and hazardous environments. Kinematically redundant serial manipulators have been proposed for these applications. Appropriate redundancy should be investigated to see if on-line fault detection and fault tolerant operation of parallel manipulators is possible.

1.3 Previous Work

1.3.1 Forward Displacement Analysis

A number of forward displacement solutions have been presented for fully parallel manipulators based on a special class of the so-called Stewart platform (Stewart (1965)). The special class considered consists of parallel manipulators formed by six branches, each branch consisting of an active prismatic joint and passive universal and spherical end joint groups for connection to a common base and mobile platform, respectively. Forward displacement solutions of 3-3[1] and 3-6 platform configurations were formulated in terms of an even powered 16-th order polynomial of a single variable by Griffis and Duffy (1989), and by Nanua et al. (1990). Innocenti and Parenti-Castelli (1990) and Parenti-Castelli and Innocenti (1990) (1992) utilized a model suitable for any spatial parallel mechanism where the branches support the mobile platform at three points via (coincident) spherical joint groups, and the resulting trace paths of the spherical joints would be circles/lines if they were disconnected from the mobile platform. Included in this class are the three branch platforms proposed by Stewart (1965), all 3-3 and 3-6 layouts, and indeed the non-redundant symmetric sensing case of the parallel manipulators considered in this work (Section 1.5). Applying loop-closure Innocenti and Parenti-Castelli, depending on the resulting trace paths, found 8-th, 12-th or 16-th order polynomials of a single variable, the real roots of which corresponded to solutions of the forward displacement problem (FDP). Hunt and Primrose (1993) applied synthetic geometry to deduce the potential number of assembly solutions for fully parallel manipulators based on six actuated prismatic joints. Husain and Waldron (1992) considered the forward displacement solution of

[1] An $m-n$ layout refers to one where the branches in total are connected to the mobile platform and the base at m and n unique locations.

a specific three-branch parallel spatial manipulator having passive spherical joints at the mobile platform and two actuated (and sensed) joints in each branch. Husain and Waldron's formulation led to the generation of a 16-th order polynomial of a single variable.

Commonly applied for resolving FDP solutions are Newton-Raphson based methods intended to resolve a single FDP solution. For example, the early and commonly applied work of Dieudonne et al. (1972) presented a Newton-Raphson iteration solution for fully parallel flight simulators. Cleary and Brooks (1993) solved the FDP of a three-branch parallel manipulator (SMARTee) utilizing a Newton-Raphson iteration method. Podhorodeski (1991) introduced an iterative method based on reciprocal screw quantities for the iterative solution of the FDP and applied the solution to a three-branch parallel hand controller. While fast enough even with fairly modest computational power, single-solution-iteration techniques are handicapped since with multiple potential solutions a danger of unplanned switching between assembly modes becomes a concern, particularly for devices capable of operating near end effector poses where assembly modes coexist (i.e., near uncertainty configurations).

Hunt and Primrose (1993) suggested that for practical considerations, parallel manipulator designs lending themselves to having fewer assembly modes should be of interest. Concurrently, Zhang and Song (1992) considered a class of Stewart platforms where five platform connections are on a line, finding in general up to 16 assemblies could be resolved with a solution involving at highest a 4-th order polynomial. Zlatanov et al. (1992) considered the FDP of a three-branch manipulator comprised of three identical branches, each consisting of three revolute main-arm joints and a passive spherical end joint for support of the common payload, and utilized an asymmetric 3-2-1 distribution of actuators (and also joint sensing) amongst the three branches. The FDP for the particular fully parallel manipulators identified by Zhang

and Song (1992) and the three-branch joint layout and sensing combination proposed by Zlatanov et al. (1992) were demonstrated to be solvable in closed-form.

The inclusion of redundant branches and/or redundant sensing of joints has also been considered for specific parallel manipulators. Cleary and Arai (1991) attached a nonactuated-follow-along branch to the payload platform to allow a unique solution to the forward displacement problem for a parallel manipulator. This, however, introduces potential problems due to serial manipulator degeneracies, branch interference and additional cost. Inoue et al. (1986) employed three extra shaft encoders for a pantograph-linkage based parallel manipulator to measure the rotation of each pantograph link about the edges of the base platform. The forward displacement problem of this parallel manipulator with redundant encoders had a unique solution. Waldron et al. (1989) proposed utilizing redundant shaft encoders to yield a unique solution for the forward displacement problem of a three degree of freedom parallel micromanipulator. Cheok et al. (1993) employed three extra translational displacement sensors (measuring the length of three additional non-actuated branches with variable length) to obtain a unique solution for the end effector pose of a 6-6 Stewart platform. Merlet (1993) investigated the minimum number of extra branches of 3-6 linear-actuated fully parallel manipulators required to obtain a unique solution for the platform pose. Three extra passive branches were found to be required.

1.3.2 Special Configurations

The special configurations of parallel manipulators can be classified as degeneracies related to the branches and uncertainty configurations of the parallel architecture. In a branch degeneracy a serial branch, and hence the entire parallel manipulator, is not capable of providing a required end effector motion. In an uncertainty configuration a parallel manipulator is not able to resist (or apply) a required end effector

force/torque. Near uncertainty configurations the required actuator torque/force corresponding to an end effector loading can be very large. Furthermore, in uncertainty configurations the end effector is instantaneously unconstrained even when all of the actuated joints are locked.

Branch Degeneracies

Raghavan and Roth (1990) determined that there can be up to 16 solutions for the inverse displacement problem of a general non-redundant 6 dof serial manipulator. Litvin et al. (1986) pointed out that special link positions (degeneracies) of serial manipulators (branches) occur when two potential configurations coincide with each other.

Degeneracies of serial manipulators have been investigated in detail and different approaches to compensate for the ill-conditioned motion problem near degeneracies have been proposed. These methods can be classified as: utilization of kinematically redundant arms (Hollerbach (1984), Stanisic and Pennock (1985), Shamir (1990), and Kircanski and Petrovic (1991)); degeneracy avoidance through design (Hollerbach (1984), Trevelyan et al. (1986), and Stanisic and Duta (1990)); and numerical and analytical techniques. Various numerical techniques to overcome the difficulties encountered near kinematic singularities have been investigated. These techniques include pseudo-inverse solution (Klein and Huang (1983)), damped least-square solution with/without numerical filtering (Wampler (1986), Nakamura and Hanafusa (1986), and Maciejewski and Klein (1988)), excessive joint rate truncation (Aboaf and Paul (1987), Lai and Yang (1989), and Podhorodeski (1991)), slowing down the movement and optimal control strategies (Mayorga and Wong (1987), Sampei and Furuta (1987), and Novakovic and Nemec (1990)), branch switching avoidance (Angeles et al. (1988)), and motion planning (Kieffer (1991)).

Hunt (1986), Wang and Waldron (1987), and Kieffer and Lenarcic (1992) proposed taking advantages of degenerate configurations in serial manipulators to improve the mechanical advantages of the arms and to increase the payload capacity of the manipulators.

Parallel manipulators will share the problems of serial manipulators in terms of branch degeneracies. Several of the approaches mentioned above should be adaptable for the parallel manipulators. This adaptation will not be a focus of the research of this thesis.

Uncertainty Configurations

Gosselin and Angeles (1990) classified singularities of closed-chain (parallel) manipulators based on the singularities of Jacobian matrices obtained by differentiating the input/output relationship. Later, Ma and Angeles (1991) examined architecture singularities of linear-actuated fully parallel manipulators. They found that when the mobile and the base platforms are similar and regular polygons, the Jacobian matrix is singular throughout the workspace. In addition, the Jacobian matrix is singular in most subregions of the workspace when the centers of both platforms are coincident, when both platforms have the same orientation, or when the moving and the base platforms are parallel. The last case of architecture singularity, i.e., parallel base and mobile platforms, has also been identified by Merlet (1987) and (1988) for symmetric manipulators. Fichter (1986) has also pointed out the existence of restrictions on the manipulator geometry in order to control the platform.

The uncertainty configurations of parallel manipulators can be investigated by examining potential actuated-joint associated wrench system degeneracies using screw theory. For particular device classes, line geometry considerations can be utilized. The linear dependencies of lines has been studied in detail, e.g., Veblen and Young

(1910), Cheung and Crapo (1976), Hunt (1978), and Dandurand (1984). Hunt (1978) utilized principles of reciprocity and linear dependence of screws to classify screw systems and studied special configurations of a variety of mechanisms. Hunt et al. (1991) also investigated special configurations of multi-finger grippers, which use a mixture of in-parallel and serial actuation. Merlet (1989) utilized line geometry to identify the uncertainty configurations of a special linear-actuated fully parallel manipulator (3-3 Stewart platform), including configurations described earlier by Hunt (1983) and Fichter (1986). The instantaneous screw axes of motion at degenerate configurations of this fully parallel manipulator and their corresponding pitches were also determined by Merlet (1992).

Enhancement of the mechanical performance of parallel manipulators requires a detailed insight of their special configurations. Knowledge of the characteristics of special configurations can be utilized to eliminate the potential uncertainties of parallel manipulators at the design stage by employing appropriate actuation redundancy. Hayward and Kurtz (1992) used actuator redundancy, by employing a redundant branch with a linear actuator which connected the mobile and base platforms with two universal joints, to increase the workspace of a parallel wrist mechanism and to overcome its singularity.

1.3.3 Kinematic Calibration

Roth et al. (1987) classified approaches to manipulator calibration and defined three levels of manipulator calibration. Two are kinematic calibrations and can be classified as joint level calibration to relate the signal from the joint displacement transducer to the actual joint displacement, and calibration of the entire set of kinematic parameters involved in the relationship of the joint displacements to the end effector pose. The third, nonkinematic (nongeometric) calibration of the manipulator corresponds to

nonkinematic error sources in positioning the end effector, e.g., errors due to the joint compliance, friction, clearance, link compliance, and also corrections for changes in dynamic model.

The kinematic parameter identification problem of a serial manipulator can be stated as follows. Given the joint displacements and the measured end effector poses, estimate kinematic parameters which define the transformation between the two. The minimum number of measured poses depends on the number of the parameters to be identified. Because of the measurement noise, the number of measured configurations should be larger than the minimum value. Zhuang and Roth (1993) suggested that twice as many as the necessary number of configurations should be used for robust parameter estimation.

Closed-loop kinematic chain manipulators (mechanisms) have several characteristics that complicate their modeling as compared to the open kinematic chain devices. In the modeling of closed-loop manipulators, there exists a number of dependent parameters (e.g., passive joint displacements) where the relationship between these parameters must be determined from the loop constraint equation.

There have been a number of publications on the calibration of serial manipulators considering geometric or nongeometric parameters, e.g., Hayati (1983), Hayati and Mirmirani (1985), Hayati et. al (1988), Meng et. al (1989), and Borm and Meng (1991).

Previous works on the calibration of parallel manipulators have concentrated on the calibration of 6-6 linear-actuated fully parallel manipulators (Stewart platforms). Non-redundant sensing of the manipulator is considered and the forward displacement solution is calculated utilizing iterative nonlinear optimization algorithms.

Zhuang and Roth (1993) simplified the kinematic identification of a 6-6 Stewart platform by calculating the kinematic parameters of each branch separately, and

hence, not considering the coupling effect among the branches. In their kinematic model the prismatic joints were assumed to be an ideal single degree of freedom pair and the ball joints connecting the branches to the base and mobile platforms were assumed to be perfect.

Wang and Masory (1993) noted that the joint manufacturing tolerances have a minor effect on the end effector pose error of a 6-6 linear-actuated fully parallel manipulator. Based on the simulation results, Wang and Masory (1993) concluded that the end effector pose error is in the same order of magnitude as its manufacturing tolerances. Masory et al. (1993) simulated the identification of the kinematic parameters of a Stewart platform. The full kinematic model (considering manufacturing and installation errors) and also the reduced kinematic model (errors only in joint locations and link offsets) were considered. It was recommended to use the reduced model for the compensation procedure which has to be executed in real time.

Hollerbach and Lokhorst (1993) presented an optimization method for joint level calibration of a three-branch parallel hand controller. The Levenberg-Marquardt algorithm was employed to solve the associated nonlinear least square problem to minimize the error of the distances between branch ends. The optimization was found to converge only if the potentiometers' nominal parameters were within 10% of the corresponding actual values, i.e., it was applicable only when a fairly good nominal parameter set is available. Otherwise, the optimization was found to converge to trivial null solutions. The convergence region is highly dependent on the chosen pose sets and the algorithm has high sensitivity to sensor noise. It is not applicable for larger drift or for complete failure of sensors. The approach considered only sensor parameters (potentiometer gains and offsets) in the calibration.

1.3.4 Fault Detection and Fault Tolerant Operation

Redundant serial manipulators have been proposed for cases where high reliability and safety are demanded, e.g., for hazardous-waste-handling applications (Colbaugh and Jamshidi (1992)), or for space based manipulators (Chladek (1990)). Effective utilization of redundancy was shown to increase the robustness to joint actuator failure and to improve the reliability of the manipulator. In addition, appropriate redundancy will improve the manipulator performance by improving its fault tolerance (while operating with a payload, in close proximity to an obstacle, or in contact with the environment in a constrained motion). There are different levels of fault tolerance in which a manipulator remains in a safely controlled state. These levels are as follows. The manipulator is fully operational after a failure without any degradation in performance (operational safe), or the manipulator can be operated with limited performance or it can terminate the task safely (fail safe).

Redundancy in joint sensing/actuation of a serial manipulator can be achieved employing two functionally equivalent sensors/actuators in a single joint (primary and backup systems). When the primary system fails a fault tolerance program enables the backup system to finish the task. A kinematically redundant serial manipulator may also be used for fault tolerant operation. The additional dof of kinematically redundant serial manipulators may permit the required end effector motion even after a failed actuator is immobilized.

Wu et al. (1991) proposed a fault tolerant joint drive with dual input actuators driving a single load output which can sustain a single actuator failure. The two input actuators run at different speeds and when one of the actuators fails the other actuator can pick up the whole load and continue the task in a single input mode.

Maciejewski (1991) quantified a measure of fault tolerance for an arbitrary pose

of a redundant manipulator and determined the optimal fault tolerant configuration based on the singular value decomposition of the Jacobian matrix. Lewis and Maciejewski (1994) analyzed the workspace of a kinematically redundant serial manipulator to find regions to ensure failure tolerance. The manipulator was defined to be fault tolerant with respect to a given task if it is capable of performing the task after any one of its joints has failed and is locked in place. To insure that the task is completable regardless of which joint fails, constraints on the range of motion of the manipulator were imposed.

1.4 Objective of the Research

As noted above polynomial formulations of the forward displacement problem for specific parallel manipulators have been performed. However, there is no closed-form expression for the solution of the FDP. Polynomial formulations must be solved numerically and they might not be applicable for on-line control of the manipulators. Iterative methods have also been used. Iterative solutions identify only one assembly mode of the device. This solution may not correspond to the required solution, e.g., switching from one assembly mode to another may occur near uncertainty poses. Thus, the problem of including adequate redundancy and determining closed-form solutions still exists and should be addressed for classes of parallel manipulators. In addition, considerations related to reducing the number of forward displacement solutions, and consequently the number of assembly modes of parallel manipulators, should be studied. Special configurations of fully parallel manipulators have been identified for some forms of the Stewart platform (linear-actuated fully parallel manipulators). The degeneracies of classes of parallel manipulators should be identified and methods for their elimination should be investigated.

Presently, continuous operation of parallel manipulators cannot be achieved if any of the sensors/actuators fail. Replacement of the failed parts requires presence of a trained person. In addition, downtime problems could be crucial, especially if the manipulator is operated in remote areas or is used for hazardous applications. Thus, the problem of sensor/actuator failure should be considered and designs and methods allowing failure resolution and robustness to partial failure should be determined.

The objective of this research is to investigate and develop parallel manipulator designs and kinematic solutions allowing the effective implementation of the devices. Specific objectives include: determining classes of structural and sensing designs allowing the potential of closed-form forward displacement solutions and the reduction of potential assembly modes; developing and applying methods to yield such closed-form solutions; and determining designs and techniques allowing recalibration and failure safe implementation. Furthermore, this thesis has the objective of considering and developing designs and/or solution methods allowing the identification and the elimination of the uncertainty configurations of parallel manipulators.

1.5 Considered Class of Parallel Manipulators

Manipulators consisting of three branch main arms supporting a mobile platform (end effector) through passive spherical end-joints are concentrated on in this thesis.[2] The choice of three branches stems largely from two considerations: (1) three or more branches are required to have passive spherical branch-end joints; and (2) a manipulator with three branches can be designed to have a larger relative dextrous work volume than a manipulator with more than three branches. Consideration (1)

[2]An example of a three-branch all-revolute-jointed parallel manipulator is illustrated in Figure 2.4.

is important because it allows base distal joints to be nonactuated and therefore light and, furthermore, it renders the individual branches kinematically simple. The larger relative work volume mentioned in (2) results because the potential of branch interference is reduced. No assumptions about the joint layout or similarity of the branches will be made other than that the main arms will be assumed to consist of three joints and that each main arm in combination with its spherical end joint allows three dimensional translation and rotation (spatial motion) at its end point.

1.6 Summary of Contents

In Chapter 2 forward displacement solutions[3] are developed for the considered class of parallel manipulators for all possible combinations of non-redundant and redundant main-arm joint displacement sensing. In addition, the effect of redundant main-arm joint sensing on the reduction of number of assembly modes is investigated. The forward displacement solutions of an example all-revolute-jointed parallel manipulator is presented.

In Chapter 3 the special configurations of the considered class of parallel manipulators are examined.[4] The uncertainty configurations are discussed utilizing concepts of screw theory. Joint actuation layouts that eliminate the uncertainty configurations are introduced. Furthermore, example configurations which result in the corresponding dependency case of the example manipulator are identified.

Chapter 4 includes an analysis of the FDP and uncertainty configurations of three-branch parallel manipulators with an additional branch, i.e., four-branch manipulators. Symmetric main-arm joint sensing and actuation (two sensed/actuated main-

[3]Notash and Podhorodeski (1994a) and (1995a).
[4]Notash and Podhorodeski (1994b).

arm joints per branch) of the considered class of manipulators are investigated.[5]

A calibration procedure for closed-loop (parallel) manipulation devices is given in Chapter 5.[6] In addition, specific models and calibration results for a redesigned hand controller are presented.

A sensor fault detection scheme for fault tolerant operation of the considered class of parallel manipulators is introduced in Chapter 6.[7] This scheme is based on the forward displacement solutions discussed in Chapter 2.

Chapter 7 includes a discussion and further considerations on topics including: redundant main-arm joint sensing and actuation; inclusion of a redundant branch; calibration; and failure safe operation.

Conclusions and recommendations for future work are given in Chapter 8.

Cayley's and Bezout's Theorems and a discussion of the circularity of the curves and the surfaces are included in Appendix A. Appendix B includes a discussion of the curves and surfaces which define the revolute joint associated branch end loci and the intersections of these curves and surfaces in further detail. Appendix C contains the analytical form of the joint screws of the example parallel manipulator, their associated reciprocal screws, and the structural screws corresponding to branch degeneracies. In addition, a velocity and force analysis of the example manipulator is included. The redesign of a parallel manipulator based hand controller to provide a closed-form forward displacement solution is included in Appendix D. Appendix E considers calibration models for joint sensors.

[5]Notash and Podhorodeski (1994c).
[6]Notash and Podhorodeski (1995b).
[7]Notash and Podhorodeski (1995c).

Chapter 2

Forward Displacement Analysis

Solution of the forward displacement problem (FDP) requires resolving the location and orientation of the payload of a manipulator given displacements at sensed joints. With serial manipulators every joint is sensed and actuated. Therefore, the solution of the FDP is unique and straight-forward, e.g., utilizing homogeneous transforms describing the relative locations of link attached frames (Paul 1981). Parallel manipulators consist of multiple branches acting on a common payload with some joints unsensed. Solution of the FDP can be more involved with parallel manipulators and may not be unique with the feasible number of assembly modes (forward displacement solutions) for the parallel device being dependent on the device layout and the joint sensing utilized.

Redundant joint displacement sensing can be employed to reduce the number of potential assembly modes of a parallel manipulator and to obtain analytical solutions for the FDP. Solutions for the FDP of the considered class of parallel manipulators will be presented in this chapter. Forward displacement solutions will be investigated for all possible combinations of non-redundant and redundant main-arm joint displacement sensing.

2.1 Considered Parallel Manipulators

The forward displacement analysis of the class of parallel manipulators presented in Section 1.5 will be investigated throughout this chapter.

2.1.1 Joint Displacement Sensing

Forward displacement solutions will be discussed for all feasible cases of main-arm joint sensing of the considered class of parallel manipulators. The nomenclature n_1-n_2-n_3 will be used to describe the sensing where n_i corresponds to the number of joints sensed in branch i. For spatial manipulation a minimum of six joints must be sensed. Furthermore, since the main-arm attachments to the platform are passive spherical joints, each branch main-arm must have at least one sensed joint, i.e., with 3-3-0 sensing the rotation of the platform about a line through the passive spherical end joints of branches one and two would not be resolvable. Therefore, all possible combinations of joint sensing are: i) 3-3-3 (nine joints sensed); ii) 3-3-2 (eight joints sensed); iii) 3-3-1 and 3-2-2 (seven joints sensed); and iv) 3-2-1 and 2-2-2 (six joints sensed). Permutations branch/joints sensed of these cases can be achieved by switching the chosen branch indices.

2.2 Forward Displacement Solutions

2.2.1 Nine Joint Displacements Sensed (3-3-3 Sensing)

Sensing all three main-arm joints of a branch i allows the location of the center p_i of its passive spherical branch end to be determined as a function of the sensed joint displacements. With 3-3-3 sensing the locations p_i, $i = 1, 2, 3$, are known. Since

the passive spherical joints are attached to the platform, p_i, $i = 1, 2, 3$, can also be considered to be three points on the mobile platform. With known p_i, $i = 1, 2, 3$, the platform's location and orientation can be uniquely and easily determined.[1]

Let ${}^0\mathbf{p}_i$ be the $\{x, y, z\}^T$ coordinates of p_i with respect to a base mounted frame of reference F_0. The location of the centroid of the branch ends p_c is described by

$$ {}^0\mathbf{p}_c = ({}^0\mathbf{p}_1 + {}^0\mathbf{p}_2 + {}^0\mathbf{p}_3)/3 \tag{2.1} $$

Three orthogonal unit vectors describing the orientation of the mobile platform can be found as:

$$ {}^0\mathbf{u}_{23} = ({}^0\mathbf{p}_3 - {}^0\mathbf{p}_2)/\|\mathbf{p}_3 - \mathbf{p}_2\| \tag{2.2} $$

$$ {}^0\mathbf{u}_n = {}^0\mathbf{u}_{23} \times ({}^0\mathbf{p}_1 - {}^0\mathbf{p}_2)/\|\mathbf{u}_{23} \times (\mathbf{p}_1 - \mathbf{p}_2)\| \tag{2.3} $$

$$ {}^0\mathbf{u}_\perp = {}^0\mathbf{u}_n \times {}^0\mathbf{u}_{23} \tag{2.4} $$

with $\mathbf{u}_n$ being normal to the plane of the mobile platform, $\mathbf{u}_{23}$ being parallel to the p_2p_3 directed towards p_3, $\mathbf{u}_\perp$ being a unit vector perpendicular to $\mathbf{u}_n$ and $\mathbf{u}_{23}$ and directed towards p_1 (refer to Figure 2.1) and with $\|\cdot\|$ denoting the Euclidean norm. Assembly of the unit vectors into a matrix $\mathbf{R}_{0P} = [{}^0\mathbf{u}_{23}\ {}^0\mathbf{u}_\perp\ {}^0\mathbf{u}_n]$ provides a rotation matrix describing the orientation of the platform with respect to F_0.

${}^0\mathbf{p}_c$ and $\mathbf{R}_{0P}$ describe the location and orientation of a platform frame F_P. The location and orientation of the end effector with respect to F_P are known values that

[1]Implicit in the discussion is that the manipulator has been designed such that the three spherical joints attached to the platform are not collinear.

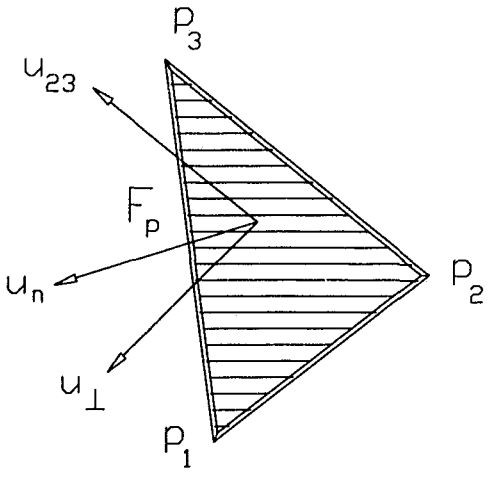

Figure 2.1: Mobile platform and mobile platform frame F_p.

are dependent on the end effector, its mounting to the platform and the application. Therefore, the location and orientation of the end effector with respect to F_0 can be easily calculated.

The above expressions are the forward displacement solution knowing the locations of p_i, $i = 1, 2, 3$. The remainder of the forward displacement solutions, for different combinations of main-arm joint sensing, shall be presented in terms of resolving the locations of p_i, $i = 1, 2, 3$. By determining the number of feasible locations for the p_i the maximum number of potential assembly modes for the parallel manipulator is determined. The further combinations of joint sensing could result from sensor failures from an initial 3-3-3 sensing configuration or may be due to initial design of the device.

The forward displacement solutions discussed in subsequent sections will involve the intersections of potential p_i loci. Appendix B discusses the curves and surfaces, which are the characteristics of revolute joints, and the intersections of these curves and surfaces, in further detail.

Table 2.1: Solutions and maximum assembly modes for 3-3-2 sensing.

Unsensed Joint Type			
R-Joint		P-Joint	
Solution	# of Solutions	Solution	# of Solutions
$C_{1,2} \cap C_3$	2*	$C_{1,2} \cap L_3$	2†

2.2.2 Eight Joint Displacements Sensed (3-3-2 Sensing)

The location of p_1 and p_2 (the branches with 3 sensors) can be expressed in terms of the sensed main-arm joint displacements. Feasible locations of p_3 must be determined.

Let m be the projection of p_3 on edge p_1p_2. The projection point m and the length mp_3 are constant and known from the geometry of the platform. Considering the constraint of branches one and two the loci of possible p_3 locations is a circle $C_{1,2}$ about the line p_1p_2 (i.e., the centerline $S_{C_{1,2}}$ of $C_{1,2}$ is parallel to $\mathbf{u}_{12} = (\mathbf{p}_1 - \mathbf{p}_2)/\|(\mathbf{p}_1 - \mathbf{p}_2)\|$). The circle $C_{1,2}$ has a radius mp_3 and its center point is m. The loci of possible p_3 locations considering the constraints imposed by branch three depends on whether branch three has an unsensed revolute or prismatic joint. The intersections of $C_{1,2}$ and the loci of possible p_3 locations due to the constraints provided by branch three correspond to potential p_3 locations for the assembled manipulator. Table 2.1 summarizes the solutions and the maximum number of assembly modes for cases of 3-3-2 joint displacement sensing. The subsections below detail these FDP solutions.

Unsensed Revolute Main-Arm Joint (3-3-2 Sensing)

The loci of possible p_3 locations considering the constraint provided by branch three is a circle C_3 about the unsensed joint axis S_R (normal direction $\mathbf{u}_{S_R}$) of radius q_3p_3

*If axes of $C_{1,2}$ and C_3 are intersecting, otherwise up to one solution.
†If L_3 is in the plane of $C_{1,2}$, otherwise up to one solution.

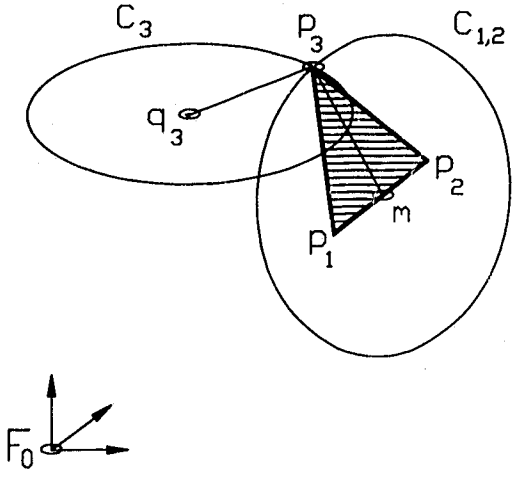

Figure 2.2: Intersection of two circles (3-3-2 case).

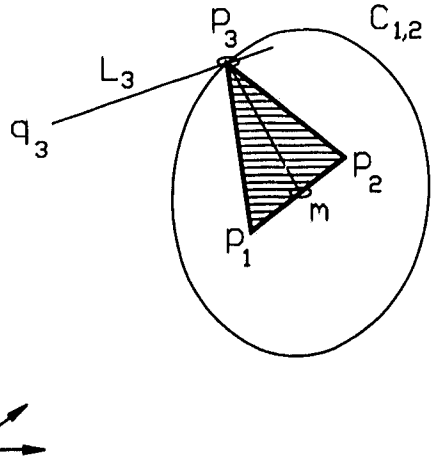

Figure 2.3: Intersection of circle and line (3-3-2 case).

and center point q_3, as illustrated in Figure 2.2. The point q_3 corresponds to the known point on branch three that is closest to p_3. Note that q_3 will lie on S_R and its location will be known as a function of branch geometric parameters and of the sensed joint displacements of branch three. Also note that the length q_3p_3 will be a function of branch geometric parameters and of sensed joint displacements (if S_R is not the base distal joint of the main-arm).

The two spatial circles $\mathsf{C}_{1,2}$ and C_3 can have up to two real intersection points. It is important to note that two intersections is a special case. A necessary condition for two intersections is that the centerlines of the circles, $\mathsf{S}_{\mathsf{C}_{1,2}}$ and S_R, intersect. While this can be possible, for $\mathsf{C}_{1,2}$ and C_3 it generally is not the case. For non-intersecting $\mathsf{S}_{\mathsf{C}_{1,2}}$ and S_R there will be only one intersection and hence only one feasible location for p_3. It is also important to note that although generally two spatial circles do not intersect at even one point, the circles $\mathsf{C}_{1,2}$ and C_3 are generated by an assembled device. That is, $\mathsf{C}_{1,2}$ and C_3 must intersect (within a tolerance due to sensing accuracy) in at least one location.

The intersections of $\mathsf{C}_{1,2}$ and C_3 must occur on the common line (intersection) of the planes in which $\mathsf{C}_{1,2}$ and C_3 lie. These two planes are easily found from the respective normals and center points of $\mathsf{C}_{1,2}$ and C_3, i.e., $\mathbf{u}_{12}$ & m and $\mathbf{u}_{\mathsf{S}_R}$ & q_3. Having found the common line of the planes, intersections of the common line with $\mathsf{C}_{1,2}$ and C_3 yields up to two potential points for each circle. Comparison of the potential points for commonality between the circles yields the feasible p_3 location(s).

If $\mathbf{u}_{12}$ and $\mathbf{u}_{\mathsf{S}_R}$ are parallel ($\mathsf{C}_{1,2}$ and C_3 centerlines intersect at infinity) the planes of $\mathsf{C}_{1,2}$ and C_3 are parallel. Since the directions of $\mathbf{u}_{12}$ and $\mathbf{u}_{\mathsf{S}_R}$ result from an assembled physical device, $\mathsf{C}_{1,2}$ and C_3 in this case must also be coplanar. In Section 2.2.3 (intersecting unsensed joint axes) finding intersections for coplanar circles is discussed.

Unsensed Prismatic Main-Arm Joint (3-3-2 Sensing)

The loci of possible p_3 locations considering the constraint provided by branch three is a line L_3 parallel to the direction $\mathbf{u}_{S_P}$ of the unsensed joint axis S_P. L_3 has a length equal to the total possible displacement of the prismatic joint and a starting point q_3 corresponding to the branch end position at zero displacement of the unsensed prismatic joint, as shown in Figure 2.3.

The circle $C_{1,2}$ and line L_3 can have a maximum of two intersection points. A necessary condition for two intersections is that the line be coplanar with the circle $C_{1,2}$, i.e., $\mathbf{u}_{S_P} \cdot \mathbf{u}_{12} = 0$.[2] In addition, the shortest distance from the center of circle $C_{1,2}$ to L_3 must be smaller than the circle's radius and the available unsensed prismatic joint displacement must be large enough to allow two intersections. Note that $C_{1,2}$ and L_3 being coplanar is generally not the case. For non-coplanar cases of $C_{1,2}$ and L_3 there will be only one intersection.

2.2.3 Seven Joint Displacements Sensed (3-3-1 Sensing)

The locations of p_1 and p_2 can be expressed in terms of the known joint displacements. The potential locations of p_3 must be resolved. As in the case of 3-3-2 sensing the loci of possible p_3 locations considering the constraints of branches one and two is the circle $C_{1,2}$. The potential p_3 locations considering branch three depends on the types of the unsensed joints and their relative positions and directions. Table 2.2 summarizes the solutions and the maximum number of assembly modes for cases of 3-3-1 joint displacement sensing. The following subsections detail these FDP solutions.

[2] $\mathbf{u}_{S_P} \cdot \mathbf{u}_{12} = 0$ is the condition for a plane being parallel to a line, but since $C_{1,2}$ and L_3 are generated by an assembled device they must also be coplanar.

Table 2.2: Solutions and maximum assembly modes for 3-3-1 sensing.

Unsensed Joint Type				
Unsensed Joint Axes	R-pairs		P-pairs	
	Solution	#	Solution	#
Parallel	$C_{1,2} \cap RG_3$	2	-	-
Non-Parallel	$C_{1,2} \cap (SP_3^*, TR_3^\dagger)$	$2^*/4^\dagger$	$C_{1,2} \cap PG_3$	2
Unsensed Joint Axes	R&P-pairs			
	Solution		#	
Parallel	$C_{1,2} \cap RC_3$		4	
Non-Parallel	$C_{1,2} \cap (PC_3^\ddagger, OC_3^\S, RG_3^\P \text{or } FC_3^\|)$		$2^{**}/4^{\dagger\dagger}$	

Unsensed Revolute Main-Arm Joints (3-3-1 Sensing)

The loci of possible p_3 locations due to the constraint of the (third) branch with two unsensed revolute joints will be a sphere, a torus, or a ring depending on the relative positions and directions of the unsensed joint axes.

(i) Intersecting unsensed joint axes

Let q_3 be the intersection point of the two unsensed joint axes. The location of q_3 will be a function of known geometric parameters and of the one sensed joint displacement

*Intersecting unsensed revolute joint axes.

†Non-intersecting (skew) unsensed revolute joint axes.

‡Unsensed revolute joint follows unsensed prismatic joint and the unsensed joint axes are perpendicular.

§Unsensed revolute joint follows unsensed prismatic joint and the unsensed joint axes are not perpendicular.

¶Unsensed prismatic joint follows unsensed revolute joint and the unsensed joint axes are perpendicular.

‖Unsensed prismatic joint follows unsensed revolute joint and the unsensed joint axes are not perpendicular.

**Unsensed joint axes are at right angles, or unsensed joint axes make either acute or obtuse angles and $C_{1,2}$ is parallel to the base plane of spatial surface.

††Unsensed joint axes make either acute or obtuse angles and $C_{1,2}$ is not parallel to the base plane of spatial surface and center of $C_{1,2}$ is located inside the surface.

of branch three (if the unsensed joints are the second and the third joints). The loci of possible p_3 locations considering the unsensed joints of branch three is a sphere SP_3 with center at q_3 and radius q_3p_3. Potential p_3 locations for the assembled three-branch manipulator correspond to $\mathsf{C}_{1,2} \cap \mathsf{SP}_3$. Hence, there will be up to two p_3 locations, i.e., up to two forward displacement solutions.

The intersection point(s) of circle $\mathsf{C}_{1,2}$ and sphere SP_3 will be on the plane of circle $\mathsf{C}_{1,2}$ (the plane passing though m having a normal parallel to $\mathbf{u}_{12}$). The intersection of SP_3 with the plane of $\mathsf{C}_{1,2}$ will be a circle $\mathsf{C}_{\mathsf{SP}_3}$ on this plane, i.e., there are two coplanar circles. The point equation of $\mathsf{C}_{\mathsf{SP}_3}$ and the point equation of $\mathsf{C}_{1,2}$ can both be expressed as quadratic equations in two unknowns. Bezout's theorem can be used to eliminate one of the unknowns of these equations and to reduce the two equations to a single polynomial expression. Since the circularity of both $\mathsf{C}_{\mathsf{SP}_3}$ and $\mathsf{C}_{1,2}$ is one (full circularity) the polynomial of a single variable is quadratic.[3] The solution of this quadratic expression yields values for one of the coordinates of p_3. Substituting these coordinate values back to the expression of $\mathsf{C}_{1,2}$ and the equation for the plane of $\mathsf{C}_{1,2}$ gives the remaining position coordinates of p_3. Since there exists up to two solutions for the quadratic equation, there will be up to two potential points for p_3. Thus, there will be up to two feasible assemblies for the manipulator.

(ii) Non-intersecting (skew) unsensed joint axes

Let q_3' and q_3 be the points on the unsensed joint axes that are closest to p_3. Specifically, let q_3' be on the unsensed joint axis closer to the branch base and q_3 be located on the unsensed joint axis closer to p_3.

The loci of possible p_3 locations considering the unsensed joints of branch three

[3] A discussion of the circularity is presented in Appendix A.

becomes a torus TR_3 with center at q_3', and primary and secondary radii of $q_3'q_3$ and q_3p_3, respectively. Note that both $q_3'q_3$ and q_3p_3 can only be a function of fixed geometric parameters and the sensed joint displacement. The primary radius of the torus corresponds to a circle with a normal vector in the direction of the first unsensed joint axis, i.e., the axis of torus. A general torus is obtained for different combinations of the angle between the skew joint axes, the angles between joint axes and the link connecting them, the link lengths and the joint offsets. If the skew joint axes are perpendicular to each other and to the connecting link and there is no joint offset between the skew joint axes TR_3 will be the special case of a right circular torus.

The potential solutions for the location of p_3 for the assembled three-branch manipulator correspond to $\mathsf{C}_{1,2} \cap \mathsf{TR}_3$. A circle and a torus, noting that the circularity of a circle is one and all circular tori have full circularity, i.e., circularity of two, will intersect at a maximum of four points. Hence, there will be up to four forward displacement solutions.

The intersection of torus TR_3 with circle $\mathsf{C}_{1,2}$ will occur on the plane of $\mathsf{C}_{1,2}$. The curve of intersection of this plane with TR_3 will be of order four (a quartic) in terms of two unknown position coordinates of p_3. $\mathsf{C}_{1,2}$ can be expressed as a quadratic in terms of these two unknowns as well. Eliminating one of the unknowns between the quartic equation and the quadratic equation of $\mathsf{C}_{1,2}$, utilizing Bezout's theorem, yields a polynomial expression in terms of one of the position coordinates. Because $\mathsf{C}_{1,2}$ and TR_3 both have full circularity the resulting polynomial is quartic. Solution of the roots of this quartic yields up to four possible values (corresponding to potential assembly configurations) for the position coordinate. The other two coordinates of p_3 can be obtained by substituting the values found from the solution of the quartic into the expressions for $\mathsf{C}_{1,2}$ and plane of $\mathsf{C}_{1,2}$. To simplify the expression of the quartic curve of intersection, the location of p_3 can be evaluated with respect to a reference

frame having one axis directed parallel to the torus axis and its origin located at the center of the torus. The coordinates of the center of TR_3 will be zero in this frame. This simplifies the single variable quartic equation as well. The transformation of the coordinates of p_3 from this frame to the reference frame F_0 allows calculation of the position and orientation of the end effector.

(iii) Parallel unsensed joint axes

Again, let q_3' and q_3 be points (on the unsensed joint axes) that are closest to p_3, with q_3' being on the unsensed joint axis closer to the branch base and q_3 being on the unsensed joint axis closer to p_3. For parallel unsensed joint axes in branch three, the loci of possible p_3 locations due to the unsensed joints of branch three corresponds to a ring RG_3 with a normal direction parallel to the unsensed joint axes' direction, a center q_3', an inner radius $q_3'q_3 - q_3p_3$, and an outer radius $q_3'q_3 + q_3p_3$. Potential locations for p_3 correspond to the $\mathsf{C}_{1,2} \cap \mathsf{RG}_3$.

In general, there are up to two intersections of $\mathsf{C}_{1,2}$ and RG_3. A degenerate (unconstrained) exception occurs if $\mathbf{u}_{12}$ is parallel to the unsensed axes' direction and there is more than one intersection point, i.e., $\mathsf{C}_{1,2}$ is not tangent to RG_3. Assuming that $\mathbf{u}_{12}$ is not parallel to the unsensed axes' direction the intersections can be resolved by intersecting $\mathsf{C}_{1,2}$ with the plane of the ring (the plane perpendicular to the unsensed axes' direction), and testing the found intersections to see if they correspond to points on the ring.

Unsensed Prismatic Main-Arm Joints (3-3-1 Sensing)

(i) Non-parallel unsensed joint axes

Two unsensed prismatic joints in the third branch generally constrain the loci of possible p_3 locations to a planar surface PG_3 defined by a parallelogram. This parallelogram has one vertex q_3 at the p_3 location corresponding to zero displacements at both unsensed prismatic joints. One side of the parallelogram at q_3 is parallel to the first unsensed prismatic joint axis S_{P_1} and is of length equal to the total allowable displacement of this joint. Similarly, the other side of the parallelogram at q_3 is parallel to the second prismatic joint axis S_{P_2} with a length equal to the total allowable displacement of that joint.

The intersection of $\mathsf{C}_{1,2}$ and PG_3 will occur at a maximum of two points if $\mathsf{C}_{1,2}$ and PG_3 are not coplanar. A degenerate (unconstrained) case occurs if $\mathsf{C}_{1,2}$ lies in the plane of PG_3, i.e., $\mathbf{u}_{12} \cdot \mathbf{u}_{\mathsf{S}_{P_1}} = 0$ and $\mathbf{u}_{12} \cdot \mathbf{u}_{\mathsf{S}_{P_2}} = 0$.

(ii) Parallel unsensed joint axes

A branch with a spherical end joint and three joints in its main-arm will be capable of only five task space degrees of freedom (dof) if it has two parallel prismatic joints in its main-arm assembly. Furthermore a main-arm, having two prismatic joints separated by a revolute joint, that is capable of achieving a configuration with the two parallel prismatic joints aligned will be degenerate in all configurations. This is easily seen by noting that to be capable of aligning the two prismatic joints the intermediate revolute joint must be perpendicular to both. Hence, all three main-arm joints are capable of translational motion of the branch end only in the plane normal to the revolute joint (the plane containing S_{P_1} and S_{P_2}). Such a main-arm layout is unacceptable for the class of considered manipulators.

Unsensed Revolute and Prismatic Main-Arm Joints (3-3-1 Sensing)

The loci of possible p_3 locations due to the constraints of the third branch will be a line segment, a portion of a plane, a ring, part of a right circular or an oblique circular cylinder or a frustum of a right circular cone depending on the relative position and directions of the unsensed revolute and prismatic joint axes.

(i) Non-parallel unsensed joint axes

Revolute joint S_{R_2} *follows prismatic joint* S_{P_1}: Due to the unsensed revolute joint S_{R_2} the branch end p_3 is constrained to lie on a circle C_3 in a plane normal to S_{R_2} with its center q_3 on this axis. The circle radius is equal to the normal from S_{R_2} to p_3 and can be calculated from the branch geometry and the sensed joint displacement. The loci of possible p_3 locations due to the constraints of branch three is the surface that would be generated by sweeping C_3 in the direction of S_{P_1} from zero to maximum displacement of this unsensed prismatic joint. Potential p_3 locations for the assembled device correspond to the intersection of this surface and $C_{1,2}$.

For the case of perpendicular S_{P_1} and S_{R_2} directions ($\mathbf{u}_{S_{R_2}} \cdot \mathbf{u}_{S_{P_1}} = 0$) the loci of potential p_3 locations considering branch three is a planar surface PC_3. The surface PC_3 and $C_{1,2}$ can intersect at up to two locations.

For general cases of non-parallel S_{P_1} and S_{R_2} the surface describing potential p_3 locations considering branch three is a portion of the surface of an oblique circular cylinder OC_3. The intersection of OC_3 and the plane of $C_{1,2}$ is a quadratic curve. Therefore, intersection of OC_3 and $C_{1,2}$ (a second order curve of full circularity) can occur at up to four points. Up to four intersection points can only occur if m (the center of $C_{1,2}$) is located inside OC_3 and the plane of $C_{1,2}$ is not perpendicular to the axis of the unsensed revolute joint, i.e., $\mathbf{u}_{S_{R_2}} \cdot \mathbf{u}_{12} \neq 1$. Otherwise, there will be up to

two intersection points.

Prismatic joint S_{P_2} *follows revolute joint* S_{R_1}: For the case of perpendicular S_{R_1} and S_{P_2} directions ($\mathbf{u}_{S_{P_2}} \cdot \mathbf{u}_{S_{R_1}} = 0$) the loci of potential p_3 locations due to the constraint of branch three is a ring RG_3. This ring lies on a plane normal to, and has a center q_3 on, S_{R_1}. The width of RG_3 is equal to the difference of the distances between q_3 and p_3 positions corresponding to maximum and minimum displacement of the unsensed prismatic joint. In general, there are up to two intersections of $C_{1,2}$ and RG_3 as discussed in Section 2.2.3(*iii*).

For general cases of non-parallel S_{R_1} and S_{P_2} the surface describing potential p_3 locations considering branch three is a frustum of right circular cone FC_3 whose axis corresponds to S_{R_1}. The smaller and larger base radii of FC_3 are respectively equal to the shortest distances from S_{R_1} to p_3 locations corresponding to zero and maximum displacements of the prismatic joint. The circle $C_{1,2}$ can intersect FC_3 at a maximum of four points if m is located inside FC_3 and the plane of $C_{1,2}$ is not perpendicular to S_{R_1} i.e., $\mathbf{u}_{S_{R_1}} \cdot \mathbf{u}_{12} \neq 1$. Otherwise there will be up to two intersection points.

(ii) Parallel unsensed joint axes

Regardless of their order in the branch, if the unsensed revolute (S_R) and the unsensed prismatic (S_P) joints are parallel the loci of possible p_3 locations considering the constraint of branch three is a right circular cylinder RC_3. The radius of RC_3 is equal to the normal (shortest) distance between S_R and p_3. The height of RC_3 is equal to the total possible displacement of S_P. The intersections of $C_{1,2}$ and RC_3 can occur at up to four points if m is located inside RC_3 and $\mathbf{u}_{S_R} \cdot \mathbf{u}_{12} \neq 1$. Otherwise there will be up to two intersection points.

If S_R and S_P are parallel and the line collinear with the revolute joint axis passes

through p_3, the main-arm is degenerate. While degenerate this configuration can possibly be encountered by a nominally nondegenerate main-arm if there is a revolute joint between the unsensed revolute and prismatic joints and no link offsets. In this case, the loci of possible p_3 locations due to branch three is a line L_3 collinear with S_R. The line L_3 has a starting point corresponding to p_3 for zero displacement of the unsensed prismatic joint and a length equal to the total allowable displacement of the joint. The intersections of $\mathsf{C}_{1,2}$ and L_3 can be found similar to 3-3-2 (unsensed prismatic main-arm joint) case considered in Section 2.2.2. Note that this degenerate case can be avoided by design, i.e., by offsetting the unsensed prismatic and revolute joints.

2.2.4 Seven Joint Displacements Sensed (3-2-2 Sensing)

With 3-2-2 sensing, the location of p_1 can be expressed as a function of sensed joint displacements. The feasible locations of p_2 and p_3 must be determined. Due to the constraint of branch one p_2 and p_3 must lie on respective spheres SP_2 and SP_3, both of which are centered at p_1 and have radii of p_1p_2 and p_1p_3, respectively. Table 2.3 summarizes the solutions and the maximum number of assembly modes for cases of 3-2-2 joint displacement sensing. The subsections below detail these FDP solutions.

Unsensed Revolute Main-Arm Joints (3-2-2 Sensing)

The branch ends p_i, $i = 2, 3$, are also constrained by their branches to lie on circles C_i of radius q_ip_i, having centers q_i and normal directions $\mathbf{u}_{\mathsf{S}_{R_i}}$, where q_i is the closest point on the unsensed axis S_{R_i} to the branch end p_i. Note that all q_i, q_ip_i, and $\mathbf{u}_{\mathsf{S}_{R_i}}$ can be found from known geometric parameters and sensed joint displacements.

Table 2.3: Solutions and maximum assembly modes for 3-2-2 sensing.

Unsensed Joint Type					
R-pairs		P-pairs		R&P-pairs	
Solution	#	Solution	#	Solution	#
$\mathsf{SP}_2 \cap \mathsf{C}_2$ & $\mathsf{C}_{1,2_j} \cap \mathsf{C}_3$	4*	$\mathsf{SP}_2 \cap \mathsf{L}_2$ & $\mathsf{C}_{1,2_j} \cap \mathsf{L}_3$	4†	$\mathsf{SP}_2 \cap \mathsf{C}_2$ & $\mathsf{C}_{1,2_j} \cap \mathsf{L}_3$	4†

The intersections $\mathsf{SP}_2 \cap \mathsf{C}_2$ locates the potential p_2 locations. This is similar to the intersecting unsensed joints (3-3-1 sensing) case considered in Section 2.2.3(i). Up to two potential locations p_{2_1} and p_{2_2} will exist. Similarly, intersections of C_3 and SP_3 could be used to resolve up to two potential locations for p_3 leading to the conclusion that up to four assembly modes can exist. However, it is more illustrative to consider resolution of p_3 using intersections of $\mathsf{C}_{1,2_j}$ and C_3. Since this corresponds to the intersection of two spatial circles, in the special case of intersecting $\mathsf{C}_{1,2_j}$ and C_3 centerlines, up to two feasible locations for p_3 will exist for a p_{2_j}. This again leads to the conclusion that up to a maximum of four solutions can exist. Note, however, that a necessary condition of the center lines $p_1p_{2_1}$, $p_1p_{2_2}$ and S_{R_3} be coplanar or that S_{R_3} intersect p_1 would have to be satisfied to be capable of four solutions. For nonintersecting centerlines only up to one p_3 will be found for each p_{2_j}. It is important to also note that in many cases a p_3 location may not exist for one of the p_{2_j} due to C_3 being further from p_{2_j} than p_2p_3.

*If centerlines of C_3 and $\mathsf{C}_{1,2_j}$, $j = 1, 2$, intersect, or up to three solutions if centerline of C_3 intersects centerline of one of $\mathsf{C}_{1,2_j}$, $j = 1, 2$, otherwise up to two solutions.

†If direction of L_3 is collinear with the intersection line of planes of $\mathsf{C}_{1,2_j}$, $j = 1, 2$, or up to three solutions if L_3 is coplanar with one of $\mathsf{C}_{1,2_j}$, otherwise up to two solutions.

Unsensed Prismatic Main-Arm Joints (3-2-2 Sensing)

The branch ends, p_i, $i = 2, 3$, are constrained by their branches to lie on lines L_i in the direction of the corresponding prismatic joint axes S_{P_i}. The lengths of the L_i will be equal to the total displacement possible for the related unsensed joints and the L_i will have starting points q_i corresponding to the p_i locations for related zero unsensed joint displacements.

$\mathsf{SP}_2 \cap \mathsf{L}_2$ locates potential p_2 locations. There will be up to two intersections between SP_2 and L_2, i.e., two solutions if L_2 passes through SP_2 and is long enough to cut it twice. For each potential p_2, feasible p_3 locations can be found from $\mathsf{C}_{1,2_j} \cap \mathsf{L}_3$ (see Section 2.2.2). Up to two p_3 locations can exist for a p_{2_j} location if L_3 is coplanar with the respective $\mathsf{C}_{1,2_j}$, i.e., $\mathbf{u}_{\mathsf{S}_{P_3}} \cdot \mathbf{u}_{12_j} = 0$. This leads to the conclusion that up to four solutions for p_3 and hence for the end effector location and orientation can exist. However, note that again four solutions is a very special case requiring L_3 to be coplanar with both $\mathsf{C}_{1,2_1}$ and $\mathsf{C}_{1,2_2}$, i.e., L_3 would have to be collinear with the common line of planes of $\mathsf{C}_{1,2_1}$ and $\mathsf{C}_{1,2_2}$. In general (noncoplanar $\mathsf{C}_{1,2_j}$ and L_3), only up to one p_3 will be found for each p_{2_j}. It is important to also note that in many cases a p_3 location may not exist for one of the p_{2_j} due to L_3 being further from p_{2_j} than p_2p_3.

Unsensed Revolute and Prismatic Main-Arm Joints (3-2-2 Sensing)

If the second branch has an unsensed revolute main-arm joint, the loci of possible p_2 locations due to branch two is a circle C_2 as defined earlier in this section. If the unsensed joint of the third branch is prismatic, p_3 will be constrained by the third branch to lie on a line L_3 as defined earlier in this section.

Intersections of SP_2 and C_2 will yield up to two potential locations for p_2. For

each potential p_2 location $\mathsf{C}_{1,2_j} \cap \mathsf{L}_3$ will yield up to two feasible locations for p_3 if $\mathbf{u}_{\mathsf{S}_{P_3}} \cdot \mathbf{u}_{12_j} = 0$. Again this leads to the conclusion that up to four assembly modes could exist. However, as previously noted, four solutions is a very special case requiring as a necessary condition that L_3 be collinear with the line of intersection of the planes $\mathsf{C}_{1,2_1}$ and $\mathsf{C}_{1,2_2}$. In general (noncoplanar L_3 and $\mathsf{C}_{1,2_j}$), only up to one p_3 will be found for each of p_{2_j}. Similar to the previous cases, a p_3 location may not exist for one of the p_{2_j} due to L_3 being further from p_{2_j} than p_2p_3.

2.2.5 Six Joint Displacements Sensed (3-2-1 Sensing)

In this case, the location of p_1 is known in terms of sensed joint displacements and geometric parameters of branch one. Feasible locations of p_2 and p_3 must be determined. Due to branch one both p_2 and p_3 are also constrained to lie on spheres SP_2 and SP_3 centered at p_1 as described in Section 2.2.4.

Unsensed Revolute Main-Arm Joints (3-2-1 Sensing)

The loci of potential p_2 locations due to the constraint of branch two is a circle C_2 as defined in Section 2.2.4. Feasible locations of p_2 correspond to $\mathsf{SP}_2 \cap \mathsf{C}_2$. Thus, there will be up to two locations for p_2.

For each location of p_2 resolving potential p_3 locations reduces to a 3-3-1 problem. The methodology described in Section 2.2.3 can be applied to resolve for each feasible p_2 location: up to two p_3 locations if the two unsensed joint axes of the third branch are intersecting (or parallel); or up to four p_3 locations if the axes are skew. Therefore, there will be up to four forward displacement solutions for intersecting (or parallel) unsensed revolute joint axes in the branch with one sensor and up to eight solutions for skew unsensed revolute joint axes.

Unsensed Prismatic Main-Arm Joints (3-2-1 Sensing)

Due to the second branch p_2 is constrained to lie on line L_2 as defined in Section 2.2.4. Feasible locations of p_2 correspond to $\mathsf{SP}_2 \cap \mathsf{L}_2$. Thus, there will be up to two locations for p_2.

For each location of p_2 resolving potential p_3 locations reduces to a 3-3-1 problem. The methodology described in Section 2.2.3 can be applied to resolve for each feasible p_2 location up to two p_3 locations. Therefore, there will be up to four forward displacement solutions for two unsensed prismatic joint axes in the branch with one sensor.

Unsensed Revolute S_R and Prismatic S_P Main-Arm Joints (3-2-1 Sensing)

Up to two potential locations of p_2 can be found as outlined in Section 2.2.4 based on $\mathsf{SP}_2 \cap \mathsf{C}_2$ or $\mathsf{SP}_2 \cap \mathsf{L}_2$ (depending on the type of the unsensed joint of branch two).

For each location of p_2 resolving potential p_3 locations reduces to a 3-3-1 problem. For one unsensed revolute and one unsensed prismatic joint in branch three the methodology described in Section 2.2.3 can be applied to resolve for each feasible p_2 location: up to two p_3 locations for perpendicular S_R and S_P; or up to four p_3 locations if S_R and S_P are not perpendicular. Therefore, there will be up to four forward displacement solutions for perpendicular S_R and S_P and up to eight solutions for non-perpendicular S_R and S_P.

2.2.6 Six Joint Displacements Sensed (2-2-2 Sensing)

Unsensed Revolute Main-Arm Joints (2-2-2 Sensing)

In this case, six sensors are used but none of the branch end locations are known. The loci of potential p_i, $i = 1, 2, 3$, locations will be circles C_i with centers q_i, normals in the direction of the respective unsensed joints, and radii $q_i p_i$. Feasible assembly modes correspond to the intersection of these circles with the platform geometry. The 2-2-2 sensing case is kinematically identical to the model proposed by Innocenti and Parenti-Castelli (1990) for a particular class of Stewart platforms. In their work loop closure was utilized in the derivation of a 16-th order polynomial of a single variable indicating that up to sixteen assemblies (forward solutions) can exist. This solution is directly applicable to 2-2-2 sensing for the class of manipulators considered in this thesis.

This maximum number of assembly modes can be verified utilizing Bezout's theorem and Cayley's theorem (refer to Appendix A) as follows. Since C_1 and C_2 both have orders of two and circularity of one (full circularity), the ruled surface generated by line (platform edge) p_1p_2 is of eighth order provided that the circles C_1 and C_2 are not in parallel planes.[4] For a fixed position of p_1 and p_2, branch end p_3 will trace a circle $C_{1,2}$ (order two), with center m, about line p_1p_2 where m is the projection of p_3 on p_1p_2. The order of the surface traced by p_3 while p_1 and p_2 are free to move on their respective circles, constrained by the constant length p_1p_2, is the product of the orders (degrees) of the two connections and is fully circular, i.e., the surface is of order sixteen and its circularity is eight. This surface can have up to sixteen real points in common with the circle C_3. Thus, confirming that there can be up to

[4] If two circles C_1 and C_2 lie in parallel planes then the order of the line series traced by p_1p_2 will be 6 and there will be up to 12 assembly configurations.

sixteen forward displacement solutions for a 2-2-2 sensing for the considered class of three-branch parallel manipulators if all unsensed main-arm joints are revolute.

Unsensed Prismatic Main-Arm Joints (2-2-2 Sensing)

The loci of potential p_i, $i = 1, 2, 3$, locations will be a line L_i in the direction of unsensed prismatic joint axis and with starting point q_i on this line corresponding to the location of branch end for zero displacement of the unsensed prismatic joint. Feasible assembly modes correspond to the intersection of these lines with the platform geometry.

Cayley's theorem (Appendix A) can be employed to show that the order of the line series traced by the line p_1p_2, while p_1 and p_2 trace their loci L_1 and L_2, is four. Since p_3 traces a circle $\mathsf{C}_{1,2}$ about line p_1p_2, the order of the surface traced by p_3 while p_1 and p_2 trace their loci is eight. The number of intersection points of this surface and the line L_3 on which p_3 lies cannot exceed eight. Hence, there will be up to eight forward displacement solution sets for the considered class of three-branch parallel manipulators if all unsensed main-arm joints are prismatic. Parenti-Castelli and Innocenti (1990) derived polynomial solutions (8-th order polynomials of a single variable) of the forward displacement problem for this case.

Unsensed Revolute and Prismatic Main-Arm Joints (2-2-2 Sensing)

The loci of potential branch end locations for each branch end will be either a circle C_i with center q_i, a normal in the direction of the unsensed revolute joint axis and a radius q_ip_i, or a line L_i in the direction of unsensed prismatic joint axis and with starting point q_i on this line corresponding to the location of branch end for zero displacement of the unsensed prismatic joint. Feasible assembly modes correspond to

the intersection of these circle(s) and line(s) with the platform geometry.

One prismatic and two revolute unsensed joints

If p_1 and p_2 are the branch end points corresponding to the branches with unsensed revolute joints the loci of p_1 and p_2 will be respectively on circles C_1 and C_2. If C_1 and C_2 are not in parallel planes the line p_1p_2 generates a ruled surface of degree eight as p_1 and p_2 trace their respective loci. For a fixed position of p_1 and p_2, p_3 traces a circle $C_{1,2}$ (order two) about line p_1p_2 with center m, where m is the projection of p_3 on p_1p_2. Since p_1 and p_2 are free to move on their circles the overall effect is equivalent to a two in-series algebraic connection with an order of sixteen. Thus, p_3 traces a surface of order sixteen and it can have up to sixteen real points in common with the line L_3 in the direction of unsensed prismatic joint of the third branch on which p_3 also lies. Therefore, if the unsensed joints of the main arms of two branches are revolute and the third branch's unsensed main-arm joint is prismatic there will exist up to sixteen forward displacement solutions. Husain and Waldron (1992) and Parenti-Castelli and Innocenti (1992) derived polynomial solutions (16-th order polynomials of a single variable) of the forward displacement problem for this case.

One revolute and two prismatic unsensed joints

When the unsensed joint of one branch is revolute and the unsensed joint of other two branches are prismatic the degree of the ruled surface obtained by line p_1p_2, when p_1 traces the circle C_1 with center on the unsensed revolute joint and p_2 traces the line L_2 in the direction of the unsensed prismatic joint of the second branch, is six. Branch end p_3 would trace a circle $C_{1,2}$ about the line p_1p_2 with center at m for a given position of p_1 and p_2. Therefore, the overall surface traced by p_3 while p_1 and p_2 trace their loci is of order twelve. There will be up to twelve intersection points between this

Table 2.4: Maximum assembly modes for non-redundant sensing.

# of Sensors of Branches	Unsensed Joint Type				
	R-pairs		P-pairs	R&P-pairs	
3-2-1	Parallel Axes	4	4	Parallel Axes	8
	Non-Parallel Axes	4*/8†	-	Non-Parallel Axes	4‡/8§
2-2-2	16		8	2R&1P-pairs	16
				1R&2P-pairs	12

surface and line L_3 on which p_3 lies. Thus, there will be up to twelve assembly modes for a three branch parallel manipulator with symmetric and non-redundant sensing which has one revolute and two prismatic unsensed main-arm joints. The polynomial solution (a 12-th degree polynomial expression) of the forward displacement problem of this case has also been derived by Parenti-Castelli and Innocenti (1992).

The number of solutions for the forward displacement problem of non-redundant (symmetric and asymmetric) sensed main-arm joints of three-branch parallel manipulators are summarized in Table 2.4. The analysis has considered branches with unsensed revolute, unsensed prismatic and combinations of unsensed revolute and prismatic main-arm joints.

2.3 Closed-Form Forward Displacement Solutions

Direct analytical solutions for the locations of p_i, $i = 1, 2, 3$, and hence direct analytical forward displacement solutions can be obtained for all cases of redundant

*Unsensed revolute joint axes are intersectiong.
†Unsensed revolute joint axes are skew.
‡Unsensed joint axes are at right angles.
§Unsensed joint axes make either acute or obtuse angles.

main-arm joint displacement sensing and for asymmetric non-redundant sensing as described below.

As discussed in Section 2.2 when the location of two branch ends p_1 and p_2 are known, the loci of possible p_3 locations due to branches one and two will be a circle $C_{1,2}$. The branch end p_3 is also constrained due to branch three to lie on a circle, a line, a sphere, a ring, a torus, a plane, an oblique circular cylinder, a frustum of circular cone, or a right circular cylinder depending on the layout, type and number of unsensed joint(s) of branch three as discussed in Sections 2.2.2 and 2.2.3.

For the planar curves or surfaces the intersection points can be found by first intersecting the plane of $C_{1,2}$ and the plane of the curve/surface (circle C_3, ring RG_3, or planar surfaces PG_3 or PC_3). Intersection of $C_{1,2}$ with the common line of the planes then provides potential p_3 locations. For planar surfaces feasible p_3 locations are those located within the boundaries of the surface. For C_3 the feasible p_3 locations can be found by also intersecting C_3 with the common line of the planes and comparing these intersections with the potential p_3 locations found from the $C_{1,2}$ intersection with the line. If the planes of $C_{1,2}$ and C_3 are coplanar their corresponding 2nd order expressions of two unknowns (and of full circularity) can be combined and reduced into a 2nd order polynomial of a single variable.

Direct solutions for the intersection points of $C_{1,2}$ and a line L_3 or of $C_{1,2}$ and spatial surfaces (sphere SP_3, torus TR_3, oblique circular cylinder OC_3, frustum of circular cone FC_3 or right circular cylinder RC_3) can be found by noting the intersections must be on the plane of $C_{1,2}$. The intersection of the plane of $C_{1,2}$ and these spatial surfaces will be either a circle (for SP_3; or for OC_3, FC_3 or RC_3 if the plane of $C_{1,2}$ is parallel to the base of the surface), an ellipse (for OC_3, or RC_3 if the plane of $C_{1,2}$ is not parallel to the base of the cylinder), an oval (for FC_3 if the plane of $C_{1,2}$ is not normal to the axis of FC_3), or a quartic curve (for TR_3). Intersection of the corresponding curve for

the case and $\mathsf{C}_{1,2}$ yields the potential p_3 locations.

For 3-2-2 and 3-2-1 sensing the location of one branch end is known. As discussed in Section 2.2.4 and 2.2.5, the loci of p_2 considering the constraint provided by the first branch will be a sphere SP_2. Also as previously discussed, p_2 is further constrained due to the second branch to lie either on a line L_2 or a circle C_2. Furthermore, p_3 is constrained to various curves or surfaces (see previous paragraphs) depending on the type, number and relative position of the unsensed joint(s) in the third branch. Intersection of a sphere and a circle/line can be calculated as discussed above to find potential p_2 locations. Similarly, the intersections required to find the corresponding p_3 locations for each potential p_2 can be found as detailed above.

All of the above (redundant or asymmetric non-redundant sensing) solutions can be expressed in terms of single variable polynomials having factors of order four or less. Therefore, they can be resolved in terms of analytical expressions. The highest order (4-th order) factors occur in the solutions involving any of $\mathsf{C}_{1,2} \cap \mathsf{TR}_3$, $\mathsf{C}_{1,2} \cap \mathsf{OC}_3$, $\mathsf{C}_{1,2} \cap \mathsf{FC}_3$, or $\mathsf{C}_{1,2} \cap \mathsf{RC}_3$ (see Tables 2.2 and 2.3).

2.4 Example

To illustrate the forward displacement solutions of Section 2.2, the three-branch parallel manipulator illustrated in Figure 2.4 is considered. The three branches of the example manipulator have identical layouts. The axes of the first and the second joints are parallel and the third joint axis intersects and is perpendicular to the second joint axis for each branch. The branch main-arm joints are separated by a length g between the first and the second joints and an offset h between the intersection of the second and the third joint and the spherical branch end as illustrated in Figures 2.5 and 2.6. The first joints of each branch are tangent to and equally spaced ($\frac{2\pi}{3}$

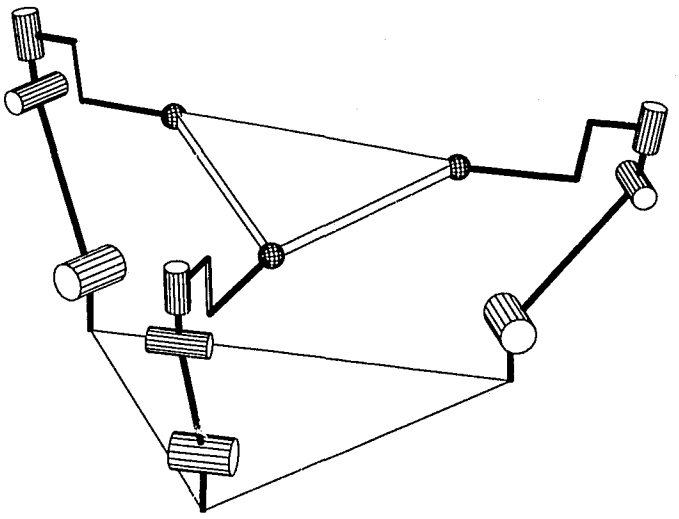

Figure 2.4: Example three-branch parallel manipulator.

radians apart) about a base circle of radius r_b. The placement of the first joints can be seen in Figure 2.4. Similarly, the branch ends p_i are attached to the common mobile platform such that p_i, $i = 1, 2$, and 3, define an equilateral triangle contained in a circle of radius r_p.

A reference frame F_0 is located at the center of the base platform (base center) with Z_0 normal to the platform plane and Y_0 in the direction of a line from the center of the base to the first joint of branch one. The branch i reference frame F_{B_i} has been established at the branch base point b_i with the z-axis being tangent to the base circle and collinear with the first joint axis of branch i. The positive z-axes of the branch reference frames are in the CCW direction about the Z_0-axis of the base reference frame. The x-axis of branch i is in the direction of a line from b_i to the origin of the base reference frame (base platform center), and the y-axis is in the direction of the base reference frame's Z_0-axis.

The loci of branch end p_i corresponding to an unsensed revolute main-arm joint

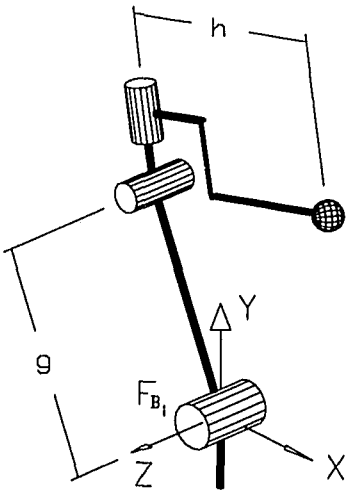

Figure 2.5: Branch layout of the example parallel manipulator.

is a circle C_{j_i} about the axis of unsensed joint j, $j = 1, 2$, or 3 of branch i, as depicted in Figure 2.6. The radius of C_{j_i} will be the shortest distance between the unsensed joint axis and p_i, e.g., C_{3_i} would have a radius of $q_i p_i$, and the radius of C_{1_i} or C_{2_i} would depend on the displacements of the sensed joints.

2.4.1 Forward Displacement

Denavit-Hartenberg parameters for the joints of a branch i are given in Table 2.5. If all main-arm joints of a branch i are sensed, the location of p_i with respect to F_{B_i} is

$$ {}^{B_i}\mathbf{p}_i = \begin{bmatrix} p_x \\ p_y \\ p_z \end{bmatrix}_i = \begin{bmatrix} hC_{12}S_3 + gC_1 \\ hS_{12}S_3 + gS_1 \\ hC_3 \end{bmatrix}_i \tag{2.5} $$

where $C_j = \cos\theta_j$, $S_j = \sin\theta_j$, $C_{jk} = \cos(\theta_j + \theta_k)$ and so on, with θ_j being the

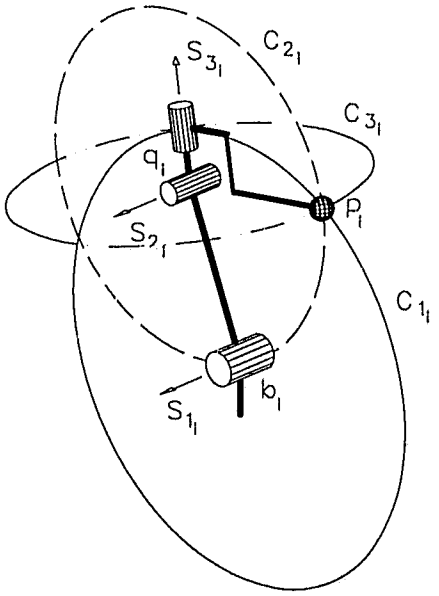

Figure 2.6: Loci of branch end p_i corresponding to each main-arm joint of example manipulator branch.

displacement at joint j. The homogeneous transform describing F_{Bi} with respect to F_0 is

$$T_{0,B_i} = \begin{bmatrix} C_\phi & 0 & S_\phi & -r_b C_\phi \\ S_\phi & 0 & -C_\phi & -r_b S_\phi \\ 0 & 1 & 0 & 0 \\ 0 & 0 & 0 & 1 \end{bmatrix}_i \tag{2.6}$$

where ϕ is the angle from the X_0 axis to the x-axis of the branch reference frame. Hence, with respect to F_0 the position coordinates of p_i are

Table 2.5: DH parameters of the example manipulator branch.

Denavit-Hartenberg Parameters				
Joint #	θ_i	a_i	α_i	d_i
1	θ_1	g	0	0
2	θ_2	0	-90	0
3	θ_3	0	90	0
4	θ_4	0	-90	h
5	θ_5	0	90	0
6	θ_6	0	0	0

$$\begin{bmatrix} {}^0\mathbf{p}_i \\ 1 \end{bmatrix} = \begin{bmatrix} {}^0p_x \\ {}^0p_y \\ {}^0p_z \\ 1 \end{bmatrix}_i = T_{0,B_i} \begin{bmatrix} {}^{B_i}\mathbf{p}_i \\ 1 \end{bmatrix} = \begin{bmatrix} (p_x - r_b)C_\phi + p_z S_\phi \\ (p_x - r_b)S_\phi - p_z C_\phi \\ p_y \\ 1 \end{bmatrix}_i \tag{2.7}$$

For branches $i = 1, 2$, and 3 the angle $\phi = \frac{-\pi}{2}$ $(-90°)$, $\frac{\pi}{6}$ $(30°)$, and $\frac{5\pi}{6}$ $(150°)$, respectively.

In the following discussion, the point coordinates and the directions will be defined with respect to the branch reference frame unless otherwise specified.

3-3-3 Sensing

If all main-arm joints are sensed for branches $i = 1, 2$, and 3 the forward displacement solution presented in Section 2.2.1 (3-3-3 sensing) can be directly applied.

3-3-2 Sensing

If all main-arm joints of branches i and j, $i, j = 1, 2$ or 3, $j \neq i$ are sensed the locations ${}^0\mathbf{p}_i$ and ${}^0\mathbf{p}_j$ can be evaluated. The location of the k-th branch end, ${}^0\mathbf{p}_k$,

$k \neq i, j$, will be located on a circle, $C_{i,j}$, with center at ${}^0\mathbf{m} = \frac{1}{2}({}^0\mathbf{p}_i + {}^0\mathbf{p}_j)$ and radius $mp_k = 1.5r_p$. The plane of circle $C_{i,j}$ is normal to the platform edge p_ip_j, i.e., $C_{i,j}$ has a unit normal vector parallel to $\mathbf{u}_{ij} = ({}^0\mathbf{p}_j - {}^0\mathbf{p}_i)/\|\mathbf{p}_j - \mathbf{p}_i\|$. The location of p_k will be at the intersection(s) of $C_{i,j}$ and a circle C_k. The forward displacement solution presented in Section 2.2.2 (3-3-2 sensing) can be applied.

- If the first joint of branch k is unsensed, C_k has a center q_k having coordinates of $\{0, 0, hC_3\}_k^T$ and a radius $q_kp_k = (|g^2 + h^2{S_3}^2 + 2ghC_2S_3|_k)^{\frac{1}{2}}$. The normal to the plane of C_k is $\{0, 0, 1\}_k^T$, i.e., the direction of the first joint.

- If the second joint of branch k is unsensed, C_k has a center q_k having coordinates of $\{gC_1, gS_1, hC_3\}_k^T$ and a radius $q_kp_k = |hS_3|_k$. The normal to the plane of C_k is $\{0, 0, 1\}_k^T$, i.e., the direction of the second joint.

- If the third joint of branch k is unsensed, C_k has a center q_k having coordinates of $\{gC_1, gS_1, 0\}_k^T$ and a radius $q_kp_k = h$. The normal to the plane of C_k is $\{-S_{12}, C_{12}, 0\}_k^T$, i.e., the direction of the third joint.

3-3-1 Sensing

If two joints of branch k are unsensed, the location of p_k will be at the intersection(s) of $C_{i,j}$ and a sphere, a torus, or a ring depending on the unsensed joints. The solutions outlined in Section 2.2.3 (3-3-1 sensing) can be applied.

- If the second and third joints of branch k are unsensed, intersection of $C_{i,j}$ and a sphere SP_k having a center at $\{gC_1, gS_1, 0\}_k^T$ and a radius equal to h, defines the potential p_k locations.

- If the first and third joints of branch k are unsensed, intersection of $\mathsf{C}_{i,j}$ and the torus TR_k having a center at $\{0,0,0\}_k^T$ with an offset of $|gS_2|_k$ and primary and secondary radii of $|gC_2|_k$ and h respectively - yields the potential p_k locations.

- If the first and second joints of branch k are unsensed, intersection of $\mathsf{C}_{i,j}$ and the ring RG_k having a center at $\{0,0,hC_3\}_k^T$, an axis direction $\{0,0,1\}_k^T$, and smaller and larger radii of $|g - hS_3|_k$ and $|g + hS_3|_k$, defines the potential p_k locations.

3-2-2 and 3-2-1 Sensing

If all main-arm joints of branch i are sensed the location of p_i can be evaluated. The potential locations of the end of branch j (the branch with two sensors) can be evaluated by considering the intersection of a sphere SP_j and the circle C_j. The sphere SP_j will be centered at p_i and will have a radius equal to $p_ip_j = 2r_p\cos(\frac{\pi}{3})$. The potential circles for C_j were described above in the discussion on 3-3-2 sensing.

- If two joints are sensed for branch k (3-2-2 sensing, Section 2.2.2) the potential p_k can be found for each p_j as described in the above discussion on 3-3-2 sensing.

- If one joint is sensed for branch k (3-2-1 sensing, Section 2.2.3) the potential p_k can be found for each p_j as described in the above discussion on 3-3-1 sensing.

2-2-2 Sensing

Branch end circles C_i, C_j, and C_k, dependent on the passive joints of each branch, will be as described in the discussion on 3-3-2 sensing. The 16-th order polynomial formulation of Innocenti and Parenti-Castelli (1990) can be applied in the resolution of potential assembly modes.

2.4.2 Inverse Displacement

A solution for the main-arm joint displacements knowing the location of i-th branch end can be found by considering the expressions in equation (2.5) to be

$$\theta_3 = \pm\cos^{-1}\left(\frac{p_z}{h}\right) \tag{2.8}$$

$$\theta_2 = -\sigma\cos^{-1}\left(\frac{{p_x}^2 + {p_y}^2 - h^2{S_3}^2 - g^2}{2ghS_3}\right) \tag{2.9}$$

$$\theta_1 = \tan^{-1}\left(\frac{p_y}{p_x}\right) + \sigma\cos^{-1}\left(\frac{{p_x}^2 + {p_y}^2 - h^2{S_3}^2 + g^2}{2g\sqrt{{p_x}^2 + {p_y}^2}}\right) \tag{2.10}$$

where $\sigma = \pm 1$. Thus, for each branch there could exist four sets of main-arm joint inverse displacement solutions.

2.4.3 Example Displacement Solutions

Forward and inverse displacement solutions of example three-branch parallel manipulator have been implemented in a computer simulation. The computer program is capable of performing forward displacement solutions for any combinations of redundant joint displacement sensing and also for non-redundant asymmetrical sensing. The number of excluded sensor(s) - indicating the corresponding branch number(s) - and the mobile platform pose are the inputs to the program. The inverse displacement solution is utilized to check if the considered mobile platform pose is achievable by the parallel manipulator. The displacements of the selected joints are used to calculate the forward displacement solution of the manipulator as discussed in Section 2.2 utilizing the loci characteristics given in Section 2.4.1

Table 2.6: Joint displacements for the example parallel manipulator.

Main-Arm Joint Displacements (radians)			
	Joint #		
Branch #	1	2	3
1	1.473	-2.203	1.814
2	1.365	-2.159	1.602
3	1.512	-2.431	1.638

An example of main-arm joint displacements in radians and corresponding mobile platform position and orientation are given in Tables 2.6 and 2.7, respectively. In this example, the lengths of the arms of the branches are $g = 3.2$ and $h = 4.0$ inches, and the radii of the base and the mobile platforms, r_b and r_p, are 4.5 and 1.5 inches, respectively. Table 2.7 presents potential mobile platform pose solutions for all 3-3-3, 3-3-2, 3-3-1, 3-2-2, and 3-2-1 sensing combinations of the main-arm joints. The first column of Table 2.7 gives the total number of sensors of each branch. The second column of this table indicates the unsensed joint(s) of each branch. The roll, pitch, and yaw (RPY) angles of the mobile platform frame F_P and the coordinates of the location of F_P with respect to F_0 are given in columns three to eight, respectively.

2.5 Implementation on RSI Hand Controller

The presented forward displacement solutions have been implemented for real-time applications of the six degree of freedom hand controller of RSI Research Ltd. (refer to Appendix D). Figure 2.7 depicts photographs of the hand controller. The hand controller is also used in Chapters 5 and 6 for real-time applications. Note that the basic model of the device is identical to the example of Section 2.4.

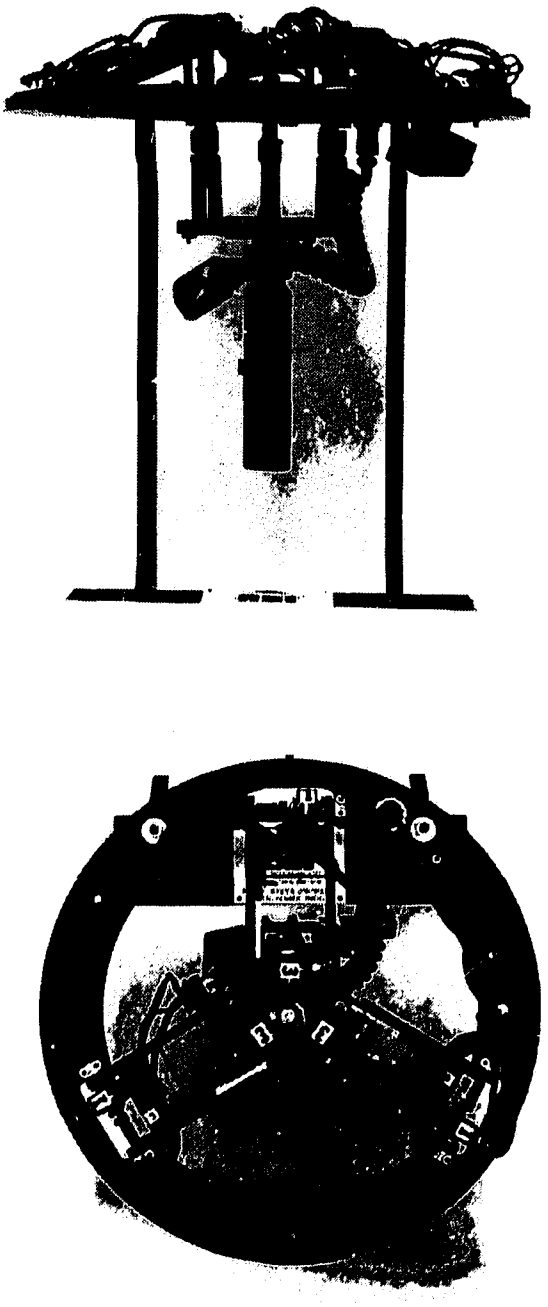

Figure 2.7: RSI hand controller.

2.6 Summary

For the considered class of three-branch parallel manipulators (branches composed of three joints in the main-arm and a passive spherical end attached to the payload platform) closed-form forward displacement solutions can be found for all cases (3-3-3, 3-3-2, 3-2-2, 3-3-1) of redundant sensing of main-arm joint displacements. Furthermore, a closed-form solution can be found for asymmetric (3-2-1) non-redundant main-arm joint displacement sensing.

A unique forward displacement solution exists for 3-3-3 sensing. Furthermore, normally only one forward displacement solution exists for 3-3-2 sensing, the existence of two solutions requiring the satisfaction of special conditions. For an unsensed revolute main-arm joint S_R intersection of a line collinear with S_R and the line passing through the centers of the passive spherical end joints of the two branches with all main-arm joints sensed is necessary to have up to two solutions. For an unsensed prismatic main-arm joint S_P the direction of S_P must lie on a plane normal to the line passing through the centers of the passive spherical end joints of the branches with all main-arm joints sensed.

The presented forward displacement solutions have been implemented in a computer simulation for an example parallel manipulator and also for real-time implementation of a three-branch parallel manipulator based hand controller.

Redundant sensing of main-arm joint displacements provides an ability to have closed-form forward displacement solutions and an inherent reduction in potential assembly modes for known joint displacements. Later, it will be presented that redundant sensing also provides the potential for the consideration of sensor-failure-safe implementations (Chapter 6). Therefore, appropriate redundancy in joint displacement sensing is an important consideration in the design of parallel manipulators.

Table 2.7: Orientation and position of mobile platform.

Main-Arm Joint Sensing Case	Unsensed Joint # for Branches	Platform Pose: RPY-Angles and F_P Location in Frame F_0					
3-3-3	0-0-0	-0.300	0.100	0.200	0.500	-0.100	0.300
3-3-2	All Combinations	-0.300	0.100	0.200	0.500	-0.100	0.300
3-3-1	All Combinations	-0.300	0.100	0.200	0.500	-0.100	0.300
	1&2-0-0	-0.300	0.100	0.424	0.500	-0.154	0.459
	1&3-0-0	-0.300	0.100	1.874	0.271	-1.033	0.864
		-0.300	0.100	-2.008	0.110	-1.081	-0.524
		-0.300	0.100	-0.314	0.457	-0.109	-0.079
	2&3-0-0	-0.300	0.100	0.892	0.463	-0.365	0.732
	0-1&2-0	-0.916	-0.743	1.070	0.935	0.151	-0.372
	0-1&3-0	-1.683	1.251	-1.941	1.354	-0.084	1.036
		-1.551	-0.809	1.791	1.312	0.243	-0.413
		-0.299	0.104	0.198	0.500	-0.101	0.304
	0-2&3-0	-0.468	1.045	-0.508	0.935	-0.159	0.963
	0-0-1&2	-0.197	-0.813	-0.419	0.260	0.038	1.016
	0-0-1&3	1.725	-0.654	-2.873	-0.429	0.834	0.913
		1.680	0.343	2.779	-0.412	0.965	0.095
		-0.320	-0.019	0.129	0.499	-0.118	0.403
	0-0-2&3	0.126	-1.070	-0.868	0.089	0.207	1.146
3-2-2	All Combinations	-0.300	0.100	0.200	0.500	-0.100	0.300
3-2-1	All Combinations	-0.300	0.100	0.200	0.500	-0.100	0.300
	1&2-any-any	-0.300	0.100	0.424	0.500	-0.154	0.459
	1&2-1-0	-0.301	-0.106	-0.155	0.501	-0.093	-0.230
	1&2-2-0	-0.612	0.635	-0.681	0.752	0.059	0.412
		-0.612	0.635	2.085	0.752	-1.104	1.318
	1&2-3-0	0.809	0.339	1.443	0.760	-1.822	1.155
	1&2-0-2	0.000	-1.113	-0.736	0.059	0.140	1.225
		0.000	-1.113	-2.405	0.059	-0.972	1.225
	1&3-any-any	-0.300	0.100	-0.314	0.457	-0.109	-0.079
	1&3-any-any	0.809	0.339	1.419	0.746	-1.810	1.153
	1&3-any-any	0.809	0.339	-1.035	0.233	-1.958	-0.154
	1&3-0-3	-0.576	0.065	-0.717	0.402	-0.630	-0.296
		-0.576	0.065	0.918	0.402	-0.761	0.791
	1&3-1-0	-0.301	-0.106	2.004	0.108	-1.076	0.562
		-0.301	-0.106	-1.880	0.274	-1.037	-0.826
		-0.301	-0.106	-0.206	0.502	-0.101	-0.268
		-0.301	-0.106	0.309	0.458	-0.108	0.112

Table 2.7: Orientation and position of mobile platform (cont'd).

Main-Arm Joint Sensing Case	Unsensed Joint # for Branches	Platform Pose: RPY-Angles and F_P Location in Frame F_0					
3-2-1(cont'd)	1&3-2-0	-0.612	0.635	-2.631	0.093	-0.990	0.498
		-0.612	0.635	1.315	1.109	-0.671	1.377
		-0.612	0.635	-0.249	0.975	0.079	0.644
		-0.612	0.635	-0.801	0.685	0.031	0.359
	1&3-3-0	-0.300	0.100	1.874	0.271	-1.033	0.864
		-0.300	0.100	-2.008	0.110	-1.081	-0.524
	1&3-0-1	-0.301	0.007	1.881	0.211	-1.021	0.987
		-0.301	0.007	-1.995	0.178	-1.095	-0.411
		-0.301	0.007	-0.296	0.486	-0.116	0.053
		-0.301	0.007	0 186	0.494	-0.098	0.411
	1&3-0-2	0.000	-1.113	1.682	-1.061	-0.499	1.776
		0.000	-1.113	-2.186	0.157	-0.849	1.776
		0.000	-1.113	-0.680	0.031	0.167	1.239
		0.000	-1.113	0.291	-0.585	0.303	1.542
	1&3-0-3	-0.576	0.065	1.708	0.106	-1.234	0.937
		-0.576	0.065	-1.878	-0.042	-1.286	-0.517
	2&3-any-any	-0.300	0.100	0.892	0.463	-0.365	0.732
	2&3-1-0	-0.301	-0.106	0.318	0.457	-0.109	0.118
		-0.301	-0.106	0.596	0.336	-0.365	0.494
	2&3-0-1	-0.301	0.007	0.123	0.496	-0.091	0.365
		-0.301	0.007	0.986	0.401	-0.407	0.898
	2&3-0-2	0.000	-1.113	0.778	0.080	0.118	1.215
		0.000	-1.113	0.959	-0.943	0.015	1.718
	any-1&2-any	-0.916	-0.743	1.070	0.935	0.151	-0.372
	1-1&2-0	-0.946	0 747	-1.107	0.952	0.159	0.413
		-0.300	-0.099	-0.209	0.500	-0.102	-0.262
	2-1&2-0	-1.792	-0.123	1.982	1.511	0.226	0.544
		-0.307	0.150	0.865	0.507	-0.354	0.780
	3-1&2-0	-0.903	-0.741	1.062	0.923	0.146	-0.372
		-0.298	0.081	0.210	0.493	-0.102	0.283
	0-1&2-2	-0.035	-1.113	-0.674	0.082	0.154	1.011
	any-1&3-any	-1.683	1.251	-1.941	1.354	-0.084	1.036
	any-1&3-any	-1.551	-0.809	1.791	1.312	0.243	-0.413
	any-1&3-any	-0.299	0.104	0.198	0.500	-0.101	0.304
	1-1&3-0	-1.542	0.803	-1.781	1.306	0.245	0.447
		-1.710	-1.256	1.972	1.360	-0.091	-0.999

Table 2.7: Orientation and position of mobile platform (cont'd).

Main-Arm Joint Sensing Case	Unsensed Joint # for Branches	Platform Pose: RPY-Angles and F_P Location in Frame F_0					
3-2-1(cont'd)	1-1&3-0	-0.289	-0.154	-0.179	0.503	-0.112	-0.308
		-0.306	-0.071	-0.225	0.500	-0.096	-0.237
	2-1&3-0	-1.493	-0.214	1.753	1.258	0.231	0.467
		1.793	1.281	1.503	1.378	-0.854	1.481
		-0.281	0.172	0.849	0.503	-0.376	0.799
		0.054	0.501	0.694	0.565	-0.653	1.067
	3-1&3-0	-1.681	1.250	-1.946	1.349	-0.084	1.035
		-1.551	-0.809	1.798	1.307	0.242	-0.414
		-0.309	0.033	0.237	0.494	-0.092	0.242
		-0.282	0.168	0.161	0.498	-0.118	0.358
	0-1&3-1	-1.725	-1.036	2.032	1.444	0.051	-0.088
		-1.321	1.013	-1.561	1.263	0.059	1.391
	0-1&3-2	-0.347	-0.875	-0.579	-0.057	0.330	1.123
		-0.105	-1.071	-0.643	0.052	0.184	1.028
	0-1&3-3	0.905	0.274	-0.284	2.166	0.496	1.002
		0.955	-0.430	0.140	2.226	0.509	0.406
	any-2&3-any	-0.468	1.045	-0.508	0.935	-0.159	0.963
	1-2&3-0	-0.578	0.498	-0.662	0.686	0.059	0.238
		-0.384	0.177	-0.381	0.533	-0.037	-0.023
	2-2&3-0	-0.333	0.128	0.881	0.511	-0.332	0.761
		0.736	1.070	0.764	1.015	-0.891	1.411
	3-2&3-0	-0.295	0.096	0.201	0.494	-0.105	0.296
		-0.466	1.047	-0.513	0.931	-0.161	0.963
	0-2&3-1	-0.666	0.839	-0.780	0.921	-0.028	1.301
		-0.283	-0.148	0.046	0.554	-0.146	0.529
	0-2&3-2	-0.732	-0.435	-0.653	-0.119	0.666	1.423
		-0.286	-0.932	-0.588	-0.030	0.286	1.092
	any-any-1&2	-0.197	-0.813	-0.419	0.260	0.038	1.016
	1-0-1&2	0.016	1.123	0.758	0.049	0.145	-0.670
		-0.300	-0.091	-0.283	0.501	-0.116	0.190
	2-0-1&2	2.044	-1.152	2.897	-0.484	0.238	1.542
		-0.298	0.160	0.815	0.494	-0.326	0.613
	3-0-1&2	2.309	0.758	1.790	-1.820	0.764	0.080
		1.684	-1.293	-1.091	-1.423	0.535	1.348
	0-1-1&2	-0.240	-0.638	-0.328	0.346	-0.015	0.985

Table 2.7: Orientation and position of mobile platform (cont'd).

Main-Arm Joint Sensing Case	Unsensed Joint # for Branches	Platform Pose: RPY-Angles and F_P Location in Frame F_0					
3-2-1(cont'd)	0-1-1&2	-0.292	0.197	0.203	0.483	-0.094	0.300
	0-2-1&2	2.895	0.892	-2.192	-0.171	0.680	1.362
		-0.748	0.690	-0.875	0.846	0.093	1.485
	0-3-1&2	-0.343	-0.912	-0.591	-0.078	0.344	1.108
		-0.394	0.554	0.516	0.102	0.240	-0.033
	any-any-1&3	1.725	-0.654	-2.873	-0.429	0.834	0.913
	any-any-1&3	1.680	0.343	2.779	-0.412	0.965	0.095
	any-any-1&3	-0.320	-0.019	0.129	0.499	-0.118	0.403
	1-0-1&3	1.630	-0.330	-2.690	-0.372	0.957	0.392
		1.783	0.581	3.033	-0.476	0.847	-0.363
		-0.352	0.153	-0.140	0.480	-0.157	-0.020
		-0.319	-0.019	-0.239	0.499	-0.133	0.128
	2-0-1&3	1.927	-0.929	2.865	-0.504	0.410	1.445
		1.628	-0.312	2.650	-0.370	0.748	1.017
		-0.488	-0.055	0.638	0.440	-0.481	0.798
		-0.326	0.134	0.789	0.490	-0.350	0.635
	3-0-1&3	1.916	0.758	1.352	-1.609	0.890	-0.080
		2.888	-1.201	-2.463	-1.699	0.377	1.323
	0-1-1&3	1.689	-0.639	-2.812	-0.412	0.841	0.986
		1.694	0.370	2.821	-0.429	0.952	0.156
	0-2-1&3	1.221	-0.031	-1.781	0.654	1.360	2.063
		2.436	0.629	-2.268	-0.177	1.001	1.527
	0-3-1&3	1.326	-0.858	-2.628	-0.440	1.072	1.078
		1.335	0.537	2.643	-0.404	1.246	-0.020
	any-any-2&3	0.126	-1.070	-0.868	0.089	0.207	1.146
	1-0-2&3	0.375	-0.806	-1.187	0.235	0.359	0.737
		-0.344	0.102	-0.169	0.488	-0.152	0.024
	2-0-2&3	-0.357	0.102	0.759	0.484	-0.376	0.663
		-0.977	-0.979	0.266	-0.053	-0.475	1.470
	0-1-2&3	0.200	-1.040	-0.956	0.099	0.238	1.217
		-0.303	0.143	0.169	0.488	-0.105	0.347
	0-2-2&3	0.556	-0.030	-1.359	1.092	1.004	2.062
		-1.143	0.904	-0.959	0.579	0.060	1.355
	0-3-2&3	-0.384	-0.871	-0.530	-0.060	0.314	1.085
		-0.588	-0.108	0.054	0.139	0.045	0.516

Chapter 3

Uncertainty Configurations

In uncertainty configurations the end effector of a parallel manipulator is instantaneously movable even when all of the actuated joints are locked. Near uncertainty configurations the required actuator torque/force corresponding to an end effector loading may be very large. Identification and elimination of uncertainties is critical in the design of effective parallel manipulators.

At uncertainty configurations a parallel manipulator gains at least one unconstrained instantaneous degree of freedom (dof). Associated with each actuated joint in a branch is a reciprocal screw (wrench) that does not perform work for tip motions due to instantaneous motion at any other joint of the branch, i.e., it is reciprocal to all of the other joints of the branch. The wrenches that can be applied and resisted by the end effector of a parallel manipulator can be expressed as the sum of wrench intensities acting on the reciprocal screws associated with the actuated joints. A parallel manipulator is in an uncertainty configuration if the set of reciprocal screws associated with the actuated joints are linearly dependent such that the associated reciprocal screws do not span the six-system of all generalized forces. In an uncertainty, the end effector can instantaneously twist about a screw reciprocal to the

screw system spanned by the reciprocal screws associated with the actuated joints. This twist is uncontrollable (unconstrained) and is undesirable.

Potential uncertainty configurations of the considered class of three-branch parallel manipulators are discussed in this chapter utilizing concepts of screw theory. All feasible cases of main-arm joint actuation are considered. The characteristics of the unconstrained instantaneous dofs corresponding to each uncertainty configuration are discussed. In addition, joint actuation layouts that eliminate the uncertainty configurations are recommended. Furthermore, example configurations which result in the corresponding dependency case for the parallel manipulator of Figure 2.4 are identified.

3.1 Considered Parallel Manipulators

3.1.1 Associated Reciprocal Screws

For the considered parallel manipulators the reciprocal screw associated with an actuated main-arm joint of a branch must be reciprocal to the passive spherical branch-end joint. The wrench system which is reciprocal to a spherical joint, i.e., has zero contribution to the rate of working of motions allowed by the spherical joint, is the three-system of all zero-pitch wrenches (pure forces) passing through the spherical joint center. In addition, the reciprocal screw associated with an actuated joint will be reciprocal to the other main-arm joints of the branch, i.e., it will intersect the other revolute joint axes and it will be perpendicular to the prismatic joint axes. For the mobile platform to be constrained for all generalized forces the order of the system defined by all of the associated reciprocal screws must be six.

3.1.2 Joint Actuation

Uncertainty configurations will be identified for all possible combinations of non-redundant and redundant main-arm joint actuations. The nomenclature n_1-n_2-n_3 will be used to describe the actuation, where n_i corresponds to the number of joints actuated in branch i. For spatial manipulation a minimum of six joints must be actuated. Furthermore, because the main-arm attachments to the platform are passive spherical joints, each branch must have at least one actuated joint, i.e., with 3-3-0 actuation the platform cannot apply/resist any torque about the line connecting the passive spherical end-joints of branches with three actuated joints. Therefore, all possible combinations of joint actuation are (1) 3-3-3 (nine joints actuated); (2) 3-3-2 (eight joints actuated); (3) 3-3-1 and 3-2-2 (seven joints actuated); and (4) 3-2-1 and 2-2-2 (six joints actuated). Permutations of branch/joints actuated of these cases can be achieved by switching the chosen branch indices.

3.2 Identification and Elimination of Uncertainties

As noted above the reciprocal screws associated with the actuated joints of the branches for the considered manipulator class, are zero-pitch screws passing through their corresponding branch-end passive spherical joint. Since the associated reciprocal screws are of zero-pitch, the conditions required for dependency of the system of associated reciprocal screws are identical to the linear dependency cases of lines.

A set of lines is a variety if no line outside the set is dependent on the lines in the set, e.g., see Dandurand (1984). The line varieties of rank $2, \ldots, 5$ are summarized in Figure 3.1 and are discussed further in the next section. The rank of any line

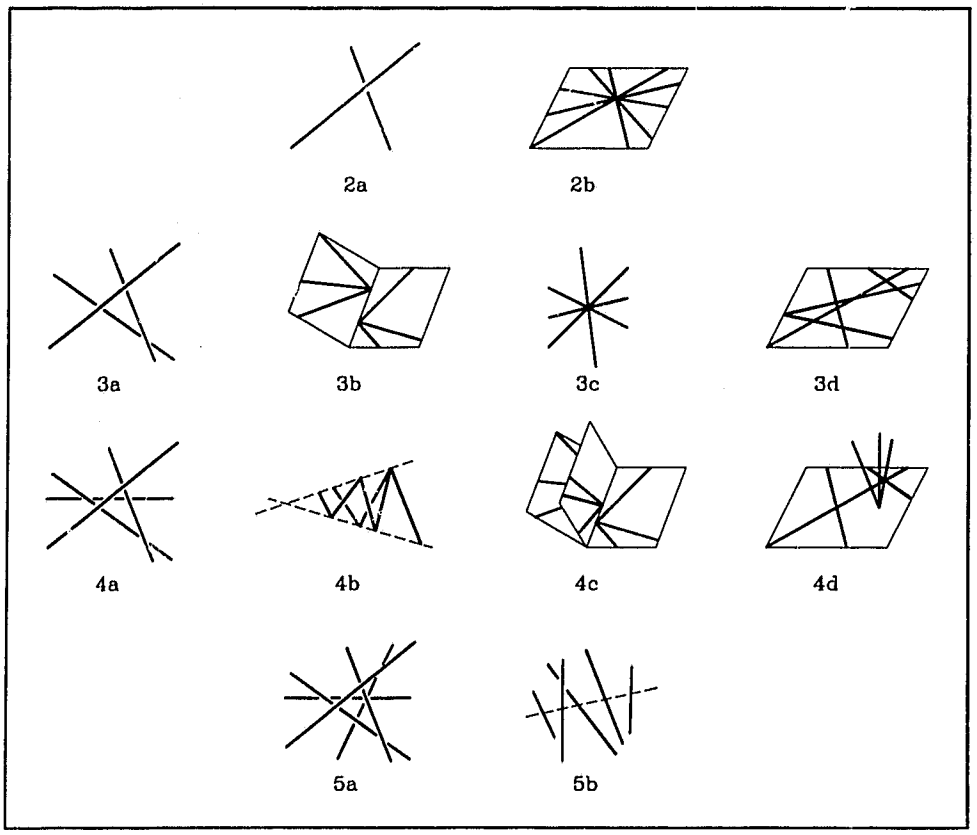

Figure 3.1: Line varieties of rank two, three, four, and five.

variety also represents the order of the corresponding zero-pitch screw system. If n lines (zero-pitch screws) belong to a variety (system) of rank (order) less than n, the lines (zero-pitch screws) are linearly dependent.

3.2.1 Possible Uncertainties and their Elimination

A six-system defines all the screws in space, i.e., there will be no screws reciprocal to six linearly independent wrenches. Reciprocal to an m-system of screws, $m \leq 6$, is a $(6-m)$-system.

The condition(s) required for n associated reciprocal screws of the considered three-branch parallel manipulators to define a screw system with an order m, where $m \leq 6 \leq n$ with n being the total number of actuated joints, is determined in this section considering the potential line dependencies. The possibility of occurrence of each dependency case is examined. For each existing dependency case the characteristics of the screw reciprocal to the dependent wrenches (the screw of the unconstrained instantaneous twist) of the mobile platform is discussed. The minimum number of actuated joints required to eliminate the uncertainty of each case is also presented.

In the presentation it will be assumed that the parallel manipulator will be non-redundantly actuated and that each branch has two actuated main-arm joints (2-2-2 actuation), unless otherwise stated.

Case 1 - Collinear lines: Two zero (finite) pitch wrenches are dependent if they lie on the same axis and have the same pitch. Therefore, Case 1 arises whenever one associated reciprocal screw (wrench) of branch i is collinear with one of branch j. For the considered class this is possible only if the wrenches are collinear with p_ip_j. The constrained dof will be translation along the axis of the wrenches. The remaining four wrenches of the branches will constrain motion (rotation/translation) in only four (of the five remaining) directions.

With redundant actuation of one joint of any branch the instantaneous (generally non-zero pitch) unconstrained twist of the mobile platform resulting from Case 1 will be constrained completely and the uncertainty configuration arising from this case will be eliminated. Case 1 will exist doubly when one wrench of both branches i and j are collinear with p_ip_j and another wrench of branch i is collinear with a wrench of branch k. When Case 1 exists doubly (triply) the four (six) wrenches will be coplanar and they will belong to Case 3d. Case 1 will exist triply if the two wrenches of branch

i, $i = 1, 2, 3$, are collinear with $p_i p_j$ and $p_i p_k$ $(j, k \neq i)$. It should be noted that Case 1 cannot exist triply for 3-2-1 and 3-3-1 actuation layouts.

Case 2a - Two skew lines: Because two skew zero-pitch screws are only dependent on themselves this case is not a potential case of an uncertainty.

Case 2b - Coplanar concurrent lines: Three wrenches will belong to a flat pencil if: (1) one wrench of branch j passes through p_i and lies on the plane of the wrenches of branch i, or (2) one wrench of each of the branches intersects at a common point lying on the plane of $p_i p_j p_k$. In these configurations the three coplanar intersecting wrenches belong to the same flat pencil with rank two and they will constrain the motion of platform point concurrent with the pencil center in the two translational dof on the plane of wrenches. The remaining three wrenches (e.g., for sub-case (1) the other wrench of branch j and the two wrenches of branch k) will constrain three of the remaining four dof.

Redundant joint actuation of any branch, i.e., 3-2-2 and 3-3-1 actuations, will eliminate the uncertainty configuration resulting from cases (1) and (2). If sub-case (1) occurs doubly, e.g., one wrench of branch j passes through p_i lying on the plane of the wrenches of branch i and the other wrench of branch j passes through p_k lying on the plane of the wrenches of branch k, the uncertainty configuration will be eliminated with two redundant actuated joints, i.e., 3-3-2 actuation. Note that for the 3-2-1 and 3-3-1 actuations sub-case (2) will reduce to Case 5b.

Case 3a - Regulus: A family of skew lines that generate a regulus intersects with every line of the complementary regulus. The wrenches of branch i, $\mathbf{W}_{l_i}$ & $\mathbf{W}_{m_i}$, $l, m = 1, 2,$ or 3 and $l \neq m$, intersect at the spherical joint center p_i. If $\mathbf{W}_{l_i}$ belongs to the regulus, $\mathbf{W}_{m_i}$ belongs to the complementary regulus. Thus, four of the lines (zero-pitch wrenches) cannot belong to the same regulus and this case does not exist

for the considered class of three-branch parallel manipulators.

Case 3b - Union of two flat pencils: This case will exist when the only common line of the planes defined by the wrenches of branches i and j is p_ip_j, i.e., the plane of $\mathbf{W}_{l_i}$ & $\mathbf{W}_{m_i}$ contains p_j and the plane of $\mathbf{W}_{l_j}$ & $\mathbf{W}_{m_j}$ contains p_i and the two planes are not coplanar. These wrenches will constrain translation of the line on the mobile platform coincident with p_ip_j in three directions. The three-system of unconstrained instantaneous dof can be represented by linear combinations of twists about p_ip_j and about lines having directions normal to p_ip_j lying on the planes of $\mathbf{W}_{l_i}$ & $\mathbf{W}_{m_i}$ ($\mathbf{W}_{l_j}$ & $\mathbf{W}_{m_j}$) and passing through p_j (p_i). These three twists define an unconstrained three-system of twists. The two-system of remaining constraint wrenches provided by branch k will reduce the unconstrained twists to a one-system. Generally, the screw characterizing the unconstrained one-system will be a non-zero pitch screw. Redundant joint actuation of one branch will resist the unconstrained twist.

Case 3c - A bundle of lines: Regardless of the number of actuated joints on a branch, for this class of parallel manipulators, the bundle center of four concurrent wrenches can only be p_i, p_j, or p_k. If branch k has two actuated joints and one wrench of each of branches i and j pass through branch end p_k, four non-coplanar wrenches will intersect at bundle center p_k and will be linearly dependent. The end effector point coincident with p_k would be constrained in three translational dof by the four concurrent wrenches, i.e., the bundle of zero-pitch wrenches defines the freedoms in spherical motion. Two of the rotational dof of the end effector about the bundle center p_k would be resisted with the remaining two wrenches of branches $i\&j$. The third unconstrained instantaneous motion would be a rotational dof defined by the zero-pitch screw passing through the bundle center and intersecting the wrenches of branches $i\&j$. This unconstrained dof can be eliminated if at least one of branches i or j have three actuated joints.

This uncertainty would also occur for 3-2-1 actuation if one wrench of the branch with two actuators passes through the branch end of the branch with three actuators. The unconstrained twist dof would be identical to that described for 2-2-2 actuation. One case of a special complex (case 5b) would result if the one wrench of the branch with one actuator passes through the branch end point of the branch with three actuators.

There can be up to five concurrent wrenches if branch k has three actuated joints (3-2-1 actuation, or 3-2-2 and 3-3-1 redundant actuations) and one wrench of branches $i\&j$ pass through the branch end p_k. Redundant actuation of two joints, i.e., 3-3-2 actuation, will be necessary to completely eliminate the possibility of uncertainty configurations due to this case.

Case 3d - Coplanar non-concurrent lines: If four wrenches $\mathbf{W}_{l_i}$, $\mathbf{W}_{m_i}$, $\mathbf{W}_{l_j}$, and $\mathbf{W}_{m_j}$, $l, m = 1, 2$, or 3 and $l \neq m$, are coplanar the mobile platform will have three unconstrained dof. This unconstrained three-system consists of all linear combinations of the translational dof in the direction normal to the plane of coplanar wrenches and the two rotational dof about lines lying on this plane. Due to the two wrenches associated with branch k, the unconstrained twisting of the end effector will be reduced to a one-system. The two wrenches of branch k will intersect the plane of coplanar wrenches at two points (or one wrench of branch k will intersect this plane and the other one will be parallel to the plane). The unconstrained instantaneous twist of the mobile platform for this uncertainty will correspond to a twist about the zero-pitch screw passing through the two intersection points (or the line passing through the intersection point and in the direction of the wrench which is parallel to the plane of coplanar wrenches). Redundant actuation can be utilized to resist this rotational dof.

If branch i has three actuated joints and two of their wrenches are coplanar with

the two wrenches of branch j, as long as p_i does not lie on the line connecting the intersection points of the wrenches of branch k with the plane, the wrench associated with the redundant actuator will eliminate the uncertainty. If both branches $i\&j$ have three actuated joints and if p_i lies on the line connecting the intersection points, p_j generally will not be on this line and it will resist rotation about this line. If the line of intersection points is collinear with p_ip_j, i.e., the wrenches of branch k lie on the mobile platform, Case 5b will arise.

Case 4a - Four independent skew lines: Similar to Case 3a since three wrenches of the considered three-branch parallel manipulators intersect the other three wrenches, it is not possible to have five skew lines (or four independent skew wrenches). Thus, Case 4a is not a concern.

Case 4b - Lines concurrent with two skew lines: Degenerate cases of Case 4b can be investigated by finding potential line(s) that can intersect five wrenches, seeing if two such lines can be intersected at the same time, and checking if these lines are skew. For the considered class of manipulators there are several potential lines which might intersect five wrenches. (1) Any edge p_ip_j of the mobile platform can be one of the skew lines if one wrench of branch k lies on the mobile platform plane. (2) The common line of the planes of $\mathbf{W}_{l_i}$ & $\mathbf{W}_{m_i}$ and $\mathbf{W}_{l_j}$ & $\mathbf{W}_{m_j}$ is a potential line if it intersects one wrench of branch k. (3) When p_j lies on the plane of $\mathbf{W}_{l_i}$ & $\mathbf{W}_{m_i}$, a line on this plane passing through p_j and the intersection point of the wrench of branch k with the plane could be one of the skew lines. (4) Line p_ip_j will intersect five wrenches if one of the branches i or j has three actuated joints. If any two of these lines intersect the same five wrenches and are skew, Case 4b will exist and the manipulator will be in an uncertainty configuration when only six joints are actuated.

The unconstrained dof of the mobile platform when five wrenches are linearly

dependent, due to being concurrent with two skew lines, is a two-system of twists. This two-system is comprised of all linear combinations of twists about the zero-pitch screws along the two skew lines. The sixth wrench will reduce the unconstrained twist system to a system of order one (assuming that the sixth wrench does not also intersect both of the skew lines). The one-system of unconstrained twists will be characterized by a non-zero pitch screw, except for the special case when the sixth wrench intersects one of the skew lines and the unconstrained twist will be characterized by the zero-pitch screw collinear with the line intersecting the six wrenches. The unconstrained one-system can be constrained by redundant actuation of at least one branch.

Case 4c - One-parameter family of flat pencils: The wrenches of branch i, $\mathbf{W}_{l_i}$ & $\mathbf{W}_{m_i}$, intersect at the spherical joint center p_i. The three branch end points p_1, p_2, and p_3 must not be collinear, otherwise the design would be fundamentally degenerate (unconstrained rotation about the line $p_1p_2p_3$). Therefore, uncertainties due to three collinear spherical joint centers cannot exist.

Case 4d - Lines on a plane or passing through one point on the plane: For degeneracies of this case to exist there will be at least five wrenches where a minimum of two wrenches are coplanar and the remaining wrenches, which must number larger than or equal to one, intersect the plane of the coplanar wrenches at a common point. Potential sub-cases include: (1) Three wrenches are coplanar and the intersection point of the other two wrenches lies on this plane, e.g., one of the wrenches of branch i lies on the plane of wrenches of branch j and one wrench of branch k passes through p_i. (2) The plane of two wrenches passes through the common point of the other three wrenches, e.g., one wrench of branch j as well as the plane of two wrenches of branch k pass through p_i with branch i having two actuated joints, or the plane of two wrenches of branch j or k passes through the branch end point p_i of the branch with three actuators (3-2-1 actuation). The two-system unconstrained by the five

linearly dependent wrenches can be described as combinations of twists about two non-collinear zero-pitch screws lying on the plane of wrenches and passing through p_i. Redundant actuation of branch j or k leading to an additional associated wrench that neither lies on the plane of coplanar wrenches nor passes through the common point will eliminate the uncertainty.

As mentioned above, this dependency case can occur for five or six wrenches. That is, a maximum of three wrenches can be concurrent without being dependent because of Case 3c, and a maximum of three wrenches can be coplanar (non-concurrent) without being dependent because of Case 3d. Therefore, redundant actuation of at least two branches will eliminate this uncertainty configuration. It should be noted that a maximum of five wrenches can be concurrent, and a maximum of six coplanar wrenches (coplanar with the mobile platform) can exist and the seventh and eighth wrenches cannot pass through a common point on this plane.

Case 5a - General complex: The coplanar lines of a complex meet at a common point. This property can be utilized to identify the condition that six wrenches belong to a complex. This can occur if the three flat pencils defined by wrenches $\mathbf{W}_{l_i}$ & $\mathbf{W}_{m_i}$, $i = 1, 2$, and 3, each has a line on the plane of $p_1p_2p_3$ with a common point on this mobile platform plane. In this configuration, the components of the zero-pitch wrenches on the plane of $p_1p_2p_3$ pass through one point. Thus, the six wrenches cannot resist any twist amplitude acting on a non-zero pitch screw along the normal to the plane $p_1p_2p_3$ which passes through the common point. Redundant actuation of at least one branch will provide a wrench to resist this unconstrained motion.

Case 5b - Special complex: When all six wrenches intersect one line they will be linearly dependent. Reciprocal to the six wrenches is any twist amplitude acting on

the zero-pitch screw along the common line. The wrench system of two branch ends p_i and p_j generally has order four (five if branch i and/or j has three actuated joints). The wrenches of branch k must resist any force/torque which results in the rotation of the mobile platform about p_ip_j and must also resist rotation about the common line of the planes defined by the wrenches of branches i and j.

Several potential sub-cases on this uncertainty can occur for the considered class of manipulators. (1) If the two wrenches of branch k lie on the plane of the mobile platform, line p_ip_j will intersect six wrenches and instantaneous rotation about p_ip_j cannot be resisted. (2) If the common line of the planes of $\mathbf{W}_{l_i}$ & $\mathbf{W}_{m_i}$ and $\mathbf{W}_{l_j}$ & $\mathbf{W}_{m_j}$ passes through p_k, i.e., intersects the two wrenches of branch k, it will intersect six wrenches. Note that p_k will lie on the plane of $\mathbf{W}_{l_i}$ & $\mathbf{W}_{m_i}$ ($\mathbf{W}_{l_j}$ & $\mathbf{W}_{m_j}$) if line p_ip_k (p_jp_k) lies on this plane. (3) If a common line of the planes of $\mathbf{W}_{l_{i,j,k}}$ & $\mathbf{W}_{m_{i,j,k}}$ exists, it will intersect six wrenches, e.g., when $\mathbf{W}_{l_{i,j,k}}$ & $\mathbf{W}_{m_{i,j,k}}$ lie on the vertical planes passing through the mobile platform center. (4) If the plane of $\mathbf{W}_{l_i}$ & $\mathbf{W}_{m_i}$ passes through p_j, and the intersection points of the wrenches of branch k with the plane of $\mathbf{W}_{l_i}$ & $\mathbf{W}_{m_i}$ are collinear with p_j, the line passing through these three collinear points will intersect all six wrenches.

Redundant actuation of branch k will prevent the unconstrained instantaneous rotation for sub-case (1). Hence, to eliminate this configuration for all of the branches, 3-3-3 actuation is required. Redundant actuation of branch i or j will constrain the instantaneous motion of sub-case (2), however, 3-2-2 actuation will not eliminate the uncertainty configuration of this case if branch k corresponds to the branch with three actuated joints. The twist about the common line of sub-case (3) will be resisted by redundant actuation of one branch, i.e., 3-2-2 actuation. Redundant actuation of either branch i or k (two branches) will completely eliminate the possibility of the motion of sub-case (4), i.e., 3-3-2 actuation. Therefore, Case 5b will not cause an

uncertainty configuration if all main-arm joints are redundantly actuated, i.e., 3-3-3 actuation.

3.3 Example

Consider the example all-revolute-jointed parallel manipulator of Figure 2.4. The three branches are identical, a branch i being illustrated in Figure 3.2. The axes of the first and the second joints are parallel and the third joint axis intersects and is perpendicular to the second joint for each branch. The first joints of each branch are tangent to and equally spaced ($\frac{2\pi}{3}$ radians apart) about a base circle (branch base points b_i). Similarly, the branch ends p_i are attached to the common mobile platform such that p_i, $i = 1, 2$, and 3, define an equilateral triangle.

3.3.1 Associated Reciprocal Screws

The reciprocal screws associated with the main-arm joints of a branch i can be obtained as follows. The reciprocal screw associated with the first joint, $\mathbf{W}_{1i}$, is a zero-pitch screw passing through spherical joint center p_i and the intersection q_i of the second and the third joints, i.e., $\mathbf{W}_{1i}$ will be in the direction of the upper-arm q_ip_i. $\mathbf{W}_{2i}$ is a zero-pitch screw passing through spherical joint center p_i and intersecting the first and the third joint axes, $\mathbf{S}_{1i}$ and $\mathbf{S}_{3i}$. Reciprocal screw $\mathbf{W}_{3i}$, which is also a zero-pitch screw, passes through p_i and intersects $\mathbf{S}_{1i}$ and $\mathbf{S}_{2i}$ at infinity, i.e., it is parallel to $\mathbf{S}_{1i}$ and $\mathbf{S}_{2i}$. Figure 3.2 depicts these associated reciprocal wrenches. It is important to note that $\mathbf{W}_{1i}$, $\mathbf{W}_{2i}$, and $\mathbf{W}_{3i}$ only contribute a constraint of the platform if joints one, two, and three are respectively actuated. The analytical form (screw coordinates) of the joint screws of the example parallel manipulator and their associated reciprocal screws are given in Appendix C.

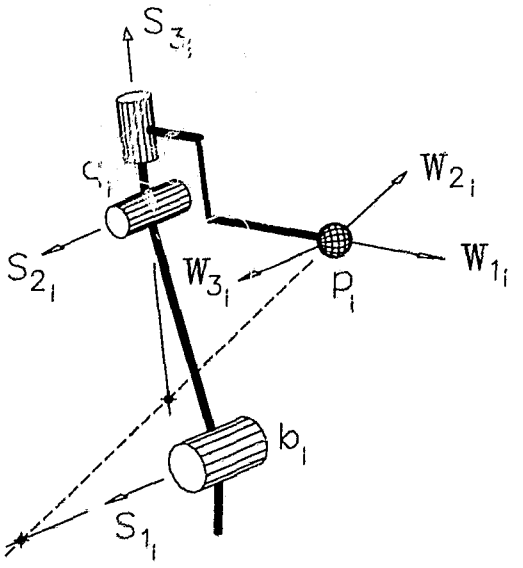

Figure 3.2: Reciprocal screws associated with the main-arm joints of example manipulator branch

3.3.2 Example Uncertainty Configurations

Case 1 - Collinear lines: For the example parallel manipulator the reciprocal screws associated with the actuated first joints of branches i and j, $\mathbf{W}_{1i}$ and $\mathbf{W}_{1j}$, are coaxial if they are collinear with the line p_ip_j, i.e., the four points q_i, p_i, p_j, and q_j are collinear.

Case 2b - Coplanar concurrent lines: The reciprocal screws associated with the actuated third joints of branches of the example manipulator will belong to Case 2b when the mobile platform is horizontal (parallel to the base platform) and is rotated about its normal by $\frac{\pi}{2}$ radians. In this configuration $\mathbf{W}_{3i}$, $i = 1, 2, 3$, will intersect at the mobile platform center and their order will be two.

Case 3b - Union of two flat pencils: For any joint actuation layout of the example

parallel manipulator the only configuration for which p_ip_j lies on the planes of the corresponding wrenches is when four wrenches are coplanar (Case 3d). Therefore, Case 3b does not exist for the example manipulator.

Case 3c - A bundle of lines: The wrenches associated with the actuated first joints of branches i and j will pass through p_k, where the wrenches of branch k pass as well, when $\mathbf{W}_{1_i}\&\mathbf{W}_{1_j}$ lie on the mobile platform plane and pass through p_k, i.e., q_i, p_i, and p_k are collinear, and also q_j, p_j, and p_k are collinear.

Case 3d - Coplanar non-concurrent lines: When the first and the third joints of branches i and j of the example manipulator are actuated the wrenches associated with the third joints ($\mathbf{W}_{3_i}\&\mathbf{W}_{3_j}$) can be coplanar if they lie on a plane parallel to the base platform plane, i.e., p_ip_j is parallel to the base platform. As well, $\mathbf{W}_{1_i}$ and $\mathbf{W}_{1_j}$ will lie on this plane if the upper-arms are parallel to the base platform, i.e., $q_ip_i\&q_jp_j$ lie on a plane parallel to the base platform resulting in four coplanar zero-pitch wrenches.

Case 4b - Lines concurrent with two skew lines: When the first and the third joints of the branches of the example manipulator are actuated and $\mathbf{W}_{1_k}$ (q_kp_k) lies on the mobile platform plane, p_ip_j will intersect at least five wrenches. When p_ip_j is a horizontal line and the plane of branch k, i.e., the plane defined by b_k, q_k, and p_k, is a vertical plane, the common line of the planes of $\mathbf{W}_{1_i}$ & $\mathbf{W}_{3_i}$ and $\mathbf{W}_{1_j}$ & $\mathbf{W}_{3_j}$ will intersect $\mathbf{W}_{1_k}$. Hence, this common line is a skew line with respect to p_ip_j and the skew lines intersect five wrenches, $\mathbf{W}_{1_i}$, $\mathbf{W}_{3_i}$, $\mathbf{W}_{1_j}$, $\mathbf{W}_{3_j}$, and $\mathbf{W}_{1_k}$, if p_ip_j is a horizontal line, the plane of branch k is a vertical plane and q_kp_k lies on the mobile platform plane.

Case 4d - Lines on a plane or passing through one point on the plane: This case can occur with 3-2-1 actuation of the example manipulator as follows. Let

branches i, j, and k have, respectively, three, two, and one actuated joints with the first joint of branch j and the second joint of branch k actuated (the other actuated joint of branch j can be either joint two or three). When p_ip_k is a horizontal line on the base platform plane $\mathbf{W}_{2_i}$, $\mathbf{W}_{3_i}$, and $\mathbf{W}_{2_k}$ are coplanar and if q_jp_j passes through p_i the four wrenches $\mathbf{W}_{1_i}$, $\mathbf{W}_{2_i}$, $\mathbf{W}_{3_i}$, and $\mathbf{W}_{1_j}$ will be concurrent at p_i. In this configuration the five wrenches $\mathbf{W}_{1_i}$, $\mathbf{W}_{2_i}$, $\mathbf{W}_{3_i}$, $\mathbf{W}_{1_j}$, and $\mathbf{W}_{2_k}$ will belong to Case 4d.

Case 5a - General complex: When the planes of wrenches associated with any joint actuation layout pass through the mobile platform center either the planes have a common line, Case 5b (e.g., when the first and second joints are actuated), or one of the wrenches of each branch pass through the mobile platform center, Case 2b (e.g., when the third joints are one of the actuated joints). Thus, Case 5a does not exist for the example parallel manipulator.

Case 5b - Special complex: When the first and the third joints of branch k are actuated, line p_ip_j will intersect wrenches $\mathbf{W}_{1_k}$ and $\mathbf{W}_{3_k}$ (in addition to the wrenches of branches i and j) if q_kp_k lies on the mobile platform plane while the mobile platform is parallel to the first joint axis S_{1k}.

3.4 Effect of Branch Degeneracies on Uncertainties

When n_i main-arm joints of a branch i are actuated, the reciprocal screws associated with the actuated joints of the branch will span a system of order m_i where $m_i \leq n_i$, with $m_i = n_i$ if the reciprocal screws are independent. In a main-arm branch degeneracy the rank will be $m_i - 1$ (at double degeneracy the rank will be $m_i - 2$ if

$2 \leq m_i$) indicating that an $(m_i - 1)$-system ($(m_i - 2)$-system) of wrenches can be applied by the branch. However, at a branch degeneracy there will be one (two) wrench(es) reciprocal to all of the joints of the branch. This wrench(es) corresponds to a generalized force(s) that can be resisted structurally without any input from the actuators, but cannot be applied by the branch. These branch degeneracy "structural wrenches" combined with the degenerate system spanned by the actuated-joint associated wrenches will span a system of screws of order larger than or equal to m_i. It can be concluded that a branch degeneracy will not result in an uncertainty configuration of a spatial parallel manipulator, unless the reciprocal screws associated with the actuated joints of all of branches and the structural wrenches of degenerate branches are linearly dependent and the screw system spanned by them has an order less than six.

3.5 Summary

Uncertainty configurations of three-branch parallel manipulators with spherical branch-end joints can be eliminated by actuation of all main-arm joints. With 3-3-3 actuation the screw system spanned by the reciprocal screws associated with the actuated joints of the branches and also by the structural wrenches corresponding to degenerate branch configurations, will always have an order of six.

Uncertainty configurations can exist for all other combinations of redundant joint actuation. Table 3.1 summarizes potential uncertainties for the different actuation cases, where the symbol $(\times)$ denotes a potential for the case to exist and the symbol $(-)$ indicates that the case cannot exist.

Uncertainties are largely eliminated by 3-3-2 actuation, an actuation for which there can exist only one form of uncertainty configuration. Considering combinations

Table 3.1: Potential uncertainties for three-branch parallel manipulators

Dependency Case	Three-Branch Manipulators Non-Redundant/Redundant Actuations					
	2-2-2	3-2-1	3-2-2	3-3-1	3-3-2	3-3-3
Case 1	×	×	–	–	–	–
Case 2b	×	×	×	×	–	–
Case 3a	–	–	–	–	–	–
Case 3b	×	×	–	–	–	–
Case 3c	×	×	×	×	–	–
Case 3d	×	×	×	×	–	–
Case 4a	–	–	–	–	–	–
Case 4b	×	×	–	–	–	–
Case 4c	–	–	–	–	–	–
Case 4d	×	×	×	×	–	–
Case 5a	×	–	–	–	–	–
Case 5b	×	×	×	×	×	–

of seven and six actuators, uncertainties can potentially occur more frequently and in a more significant part of the task space for 3-3-1 and 3-2-1 actuations in comparison to 3-2-2 and 2-2-2 actuations, respectively. Hence, 3-2-2 actuation can be concluded to be the preferred actuation layout for a single redundant actuator.

Chapter 4

Redundant Branch Number

The effect of adding a redundant branch in terms of reduction of the number of assembly modes and elimination of potential uncertainty configurations is investigated for the considered class of three-branch parallel manipulators in this chapter. The addition of a redundant branch effectively yields a four-branch manipulator class. The 3-4 form of the resulting manipulator class is considered. This form is obtained when two branch ends meet at one point (have coincident passive spherical joint) on the mobile platform. The goal of this investigation is to determine the effectiveness of the addition of parallel redundant sensing/actuation (the addition of a redundant branch) in comparison to serial redundant sensing/actuation.

4.1 Considered Parallel Manipulators

Symmetric main-arm joint sensing and actuation (two sensed/actuated main-arm joints per branch) of the class of manipulators of Section 1.5 with an additional branch will be investigated.

4.1.1 Joint Sensing and Actuation

The 2-2-2-2 symmetric main-arm joint sensing and actuation is considered. The passive (unactuated) main-arm joint of each branch can be either a revolute or a prismatic joint.

4.1.2 Loci of Branch-End Locations

For the considered class of parallel manipulators the loci of possible locations for a branch end (if disconnected from the mobile platform) would be either a circle about the joint axis for an unsensed revolute joint, or a line in the direction of the joint axis for an unsensed prismatic joint.

4.2 Assembly Configurations

Let p_i represent the spherical end-joint center of branch i where $i = 1, \ldots, 4$, and let the location of p_1 and p_2 be identical, i.e., branches one and two meet at one point on the mobile platform. The number of assembly configurations of this four-branch parallel manipulator can be evaluated utilizing synthetic geometry as follows.

4.2.1 Unsensed Revolute Main-Arm Joints

The loci of possible p_1 and p_2 locations considering the constraint provided by branches one and two are respectively circles C_1 and C_2 with centers on the corresponding unsensed main-arm joint axes of branches one and two. The branch ends p_1 and p_2 meet at one point on the mobile platform. Therefore, the location of $p_{1,2}$ must correspond

to common point(s) of C_1 and C_2. Two spatial circles can have up to two real intersection points. Therefore, there will be up to two locations for point $p_{1,2}$. A necessary condition for two intersections is that the centerlines of the circles intersect. For non-intersecting centerlines of the circles there will be only one intersection of the circles. It is important to note that although generally two spatial circles do not intersect at even one point, the circles C_1 and C_2 are generated by an assembled device. That is, C_1 and C_2 must intersect (within a tolerance due to sensing accuracy) in at least one location.

For each location of $p_{1,2}$, spherical joint center p_3 must be at the intersection of a sphere with center at $p_{1,2}$ and a radius $p_{1,2}p_3$ (known from the mobile platform geometry), and the constraint circle C_3 provided by branch three. Hence, there will be a maximum of four locations for p_3, i.e., two locations for each potential location of $p_{1,2}$. Knowing $p_{1,2}$ and p_3 locations, p_4 will be at the intersection of a circle with center, m, at the projection of p_4 on $p_{1,2}p_3$, and a radius p_4m (known from the mobile platform geometry), and the constraint circle C_4 provided by branch four. For each location of $p_{1,2}$ and p_3 there could be up to two locations for p_4, i.e., totally there could be up to eight locations for p_4. Thus, there will be a maximum of eight assembly configurations for a 3-4 parallel actuated manipulator with unsensed revolute joints.

The intersection points of two circles can be found by first intersecting the planes of the circles. The feasible branch-end locations will be the common solution(s) of the intersection of each circle with the common line of the planes. The problem of intersecting two spatial circles can be formulated as finding the roots of two second-order polynomials in terms of one unknown. Hence, the forward displacement problem can be reduced to finding the roots of five second-order polynomials (corresponding to the intersection of two circle and line for each intersection of two circles, and one for the intersection of the sphere and the circle), each polynomial in terms of one

unknown. That is, a closed-form solution exists for the forward displacement problem (FDP).

With appropriate design it is possible to ensure that only one intersection point will exist for C_1 and C_2. Explicitly, there will exist one location for $p_{1,2}$ if the manipulator is designed such that the unsensed joint axes of branches one and two always remain skew with respect to each other within the workspace of the parallel manipulator. Furthermore, at the design stage it can potentially be ensured that the unsensed joint axis of branch four is never coplanar with the branch ends $p_{1,2}$ and p_3. Therefore, with an appropriate design it is possible to obtain one location for $p_{1,2}$, and for the found location of $p_{1,2}$ up to two locations for p_3, and finally one solution for p_4 for each p_3 location. Hence, the maximum number of assembly solutions can potentially be reduced to two through appropriate design.

4.2.2 Unsensed Prismatic Main-Arm Joints

The loci of possible p_1 (and p_2) locations due to the constraint provided by branch one (two) is a line L_1 (L_2) in the direction of the corresponding unsensed prismatic joint axis. L_1 (L_2) has a length equal to the total possible displacement of the prismatic joint and a starting point corresponding to the branch-end location at zero displacement of the unsensed prismatic joint. Because p_1 and p_2 meet at $p_{1,2}$ on the mobile platform, the intersection of L_1 and L_2 will correspond to the location of $p_{1,2}$. Thus, there will be a unique location for $p_{1,2}$. p_3 will be at the intersection of a sphere with center at $p_{1,2}$ and a radius $p_{1,2}p_3$, and the constraint line L_3 provided by branch three. There will be up to two locations for p_3. Considering each p_3 and the location of $p_{1,2}$, p_4 will be at the intersection of a circle $C_{1,2\&3}$ with center at the projection of p_4 on $p_{1,2}p_3$ and the constraint line L_4 provided by branch four. Therefore, there will be a maximum of four assembly configurations if the unsensed main-arm joints of branches are all

prismatic.

The forward displacement problem can be formulated as finding the root(s) of one first-order polynomial (corresponding to two intersecting lines) and two second-order polynomials (corresponding to the intersection of a line and a sphere and also a line and a circle), each polynomial in terms of one unknown. Therefore, there will be a closed-form solution for the FDP. There exist a maximum of two intersection points between a sphere and a line, and also between a circle and a line. A necessary condition for two intersections of circle $C_{1,2\&3}$ and line L_4 is that the line be coplanar with the circle. In addition, the shortest distance from the center of circle $C_{1,2\&3}$ to L_4 must be smaller than the circle's radius and the available unsensed prismatic joint displacement must be large enough to allow two intersections. For non-coplanar cases of $C_{1,2\&3}$ and L_4 there will be only one intersection. By proper design it can potentially be ensured that $C_{1,2\&3}$ and L_4 do not lie on the same plane, and hence, the maximum number of assembly modes can be reduced to two.

4.2.3 Unsensed Revolute and Prismatic Main-Arm Joints

If the unsensed main-arm joint of branch one is revolute and the unsensed main-arm joint of branch two is prismatic, $p_{1,2}$ will be at the intersection point(s) of a circle C_1 with a center on the unsensed revolute joint axis and a line L_2 in the direction of the unsensed prismatic joint axis. L_2 will have a length equal to the total displacement and a starting point corresponding to the zero displacement of the unsensed prismatic joint of the second branch. There will be up to two intersections of C_1 and L_2. Hence, there will be up to two locations for $p_{1,2}$. A necessary condition for two intersection points to exist is that C_1 and L_2 lie on the same plane. With proper design it can be ensured that the unsensed revolute and prismatic joint axes of the first and the second branches cannot be perpendicular, resulting in non-coplanar C_1 and L_2, hence

allowing only one location for $p_{1,2}$. As discussed in Section 4.2.1, up to two solutions for the location of $p_{1,2}$ can exist if the unsensed joints of both branches are revolute, with design considerations allowing this to be reduced to one location. Furthermore, as discussed in Section 4.2.2, if the unsensed joints of both branches are prismatic there will be a unique location for $p_{1,2}$.

The number of potential p_3 and p_4 locations for each possible location of $p_{1,2}$ is invariant of the type of unsensed main-arm joints of branches three and four. There will be up to two p_3 locations, that can be resolved by intersection of a sphere with center at $p_{1,2}$ and radius $p_{1,2}p_3$ and the circle C_3 (if the unsensed joint of branch three is revolute) or the line L_3 (if the unsensed joint of branch three is prismatic). For each potential pair of $p_{1,2}$ and p_3 up to two locations can exist for p_4. These p_4 locations correspond to the intersections of two circles (if the unsensed joint of branch four is revolute) or the intersection of a circle and a line (if the unsensed joint of branch four is prismatic). As discussed in the previous subsections, there is the potential of ensuring that one p_4 location will exist for each $p_{1,2}p_3$ pair through proper design.

Summarizing, up to eight forward displacement solutions can exist for the 3-4 (2-2-2-2 sensed) layouts with unsensed revolute and prismatic joints, if the branches with the concurrent spherical end joints have unsensed revolute joints in both branches or an unsensed revolute in one branch and an unsensed prismatic in the other. Also, up to four forward displacement solutions can exist if the branches with the concurrent spherical end joints have unsensed prismatic joints in both branches. Furthermore, elimination of the potential existence of necessary conditions through design, could be used to reduce the potential solutions to two solutions.

4.3 Identification of Uncertainty Configurations

Each branch of the considered class of four-branch parallel manipulators has two actuated main-arm joints. Therefore, each branch end p_i, $i = 1, \ldots, 4$, will apply two wrenches on the mobile platform, each wrench associated with one of the actuated joints of the branch and expressible as an intensity acting on the associated reciprocal screw. The condition(s) required for the eight associated reciprocal screws of the considered four-branch parallel manipulators to define a screw system with an order m, where $m \leq 6$, is determined in this section utilizing the discussion of line dependencies of Chapter 3. The possibility of occurrence of each dependency case summarized in Figure 3.1 is examined. For each existing dependency case which can potentially result in an uncertainty configuration, the characteristics of the screw(s) (unconstrained instantaneous twist(s)) which represents the gained instantaneous degree of freedom (dof) of the mobile platform is discussed.

Case 1 - Collinear lines: Two zero-pitch wrenches are dependent if they lie on the same line. This case arises whenever one wrench of branch k is collinear with a wrench of branch h. For the considered class this is possible only if the wrenches of two non-concurrent branches k and h are collinear with $p_k p_h$. When the collinear wrenches of concurrent branches i and j lie on the same axis, the coaxial wrenches and one of the remaining wrenches of branches i or j will belong to Case 2b. The two collinear wrenches for the two non-concurrent branches will constrain one dof translation along the axis of the wrenches. The remaining six wrenches of the branches will constrain the motion (rotation/translation) in the five remaining directions. Hence, even if Case 1 exists doubly or for the special case of the three coaxial wrenches, the reciprocal screw system will still be of full order and the motion of the mobile platform will be constrained completely. Note that when Case 1 exists doubly (triply) the four (six)

dependent wrenches will belong to Case 2b (Case 3d).

Case 2a - Two skew lines: A zero-pitch screw cannot be a nontrivial linear combination of two skew zero-pitch screws, i.e., two skew zero-pitch screws are only dependent on themselves. Therefore, Case 2a cannot be a case of linear dependency for the considered class of manipulators.

Case 2b - Coplanar concurrent lines: When one wrench of branch j passes through p_i and lies on the plane of the two wrenches of branch i, or if one wrench of each of the three branches meet at a common point on the plane of the mobile platform, the order of the three coplanar wrenches will be two. If there is no other dependency among the eight wrenches the rank of the matrix of reciprocal screws will remain six and Case 2b will not cause an uncertainty configuration. The order of the eight wrenches will remain six even if one wrench of each branch (four branches) meet at a common point on the plane of the mobile platform, if four wrenches of the concurrent branches are coplanar, or even if Case 2b exists doubly.

Case 3a - Regulus: A family of skew lines that generate a regulus intersects with every line of the complementary regulus. When $\mathbf{W}_{l_i}$ belongs to the regulus, $\mathbf{W}_{m_i}$ will belong to the complementary regulus and four of the zero-pitch wrenches cannot belong to the same regulus. Thus, this dependency case does not exist for the 3-4 form of four-branch parallel manipulators.

Case 3b - Union of two flat pencils: This case will exist when the common line of the planes defined by the wrenches of non-concurrent branches k and h is $p_k p_h$, i.e., the plane of $\mathbf{W}_{l_k}$ & $\mathbf{W}_{m_k}$ contains p_h and the plane of $\mathbf{W}_{l_h}$ & $\mathbf{W}_{m_h}$ contains p_k and the two planes are not coplanar. These wrenches will constrain translation of the line on the mobile platform coincident with $p_k p_h$ in three directions. Assuming that the

branch ends p_i and p_j correspond to the same point (concurrent branches), at a special case when the common line of the planes of wrenches of branches i, j and k is $p_{i,j}p_k$ there exist ∞^1 lines passing through $p_{i,j}$ and intersecting wrenches of branch k (lying on the plane of branch k wrenches), i.e., there exist ∞^1 lines intersecting six wrenches, which is Case 4d. These six wrenches allow an unconstrained two-system of twists which will correspond to the unconstrained rotation at the bundle center $p_{i,j}$ about any two perpendicular directions on the plane defined by the wrenches of branch k (e.g., direction of $p_{i,j}p_k$ and a direction normal to $p_{i,j}p_k$ passing through $p_{i,j}$ and lying in the plane of wrenches of branch k). Normally, the two unconstrained dof will be resisted by the wrenches of branch h. However, if the wrenches of branch h intersect any line collinear with these unconstrained directions the mobile platform cannot resist the rotation about that line and the manipulator will gain one instantaneous unconstrained dof, which corresponds to Case 5b. Therefore, Case 3b by itself will not cause rank deficiency of the matrix of reciprocal screws for the 2-2-2-2 actuated four-branch manipulators.

Case 3c - A bundle of lines: If one wrench of each branch (four in total) meet at a common point and are not coplanar, the four wrenches will form a bundle (a three-system of screws). Assuming that the remaining four associated reciprocal wrenches do not form another sub-system of order less than three (multiple dependency) or none of them belong to the bundle of the other four wrenches, the order of wrench system for the manipulator will remain six and Case 3c will not be a problem. However, if the remaining wrenches of branches (four wrenches) meet at another common point (or all of the remaining wrenches intersect a line passing through the common point of the first four wrenches), the order of wrench system will reduce to five and the mobile platform will gain an instantaneous rotational dof about the line connecting the two common points (or about the line which intersects all the wrenches). This

however corresponds to Case 5b.

The four wrenches of two concurrent branches i and j belong to the variety of Case 3c. If one wrench of each of branches k and h passes through the bundle center $p_{i,j}$ the three-system of six concurrent wrenches will define the freedoms in spherical motion. The remaining wrenches of branches k and h will constrain two of the rotational dof of the end effector about the bundle center $p_{i,j}$. The mobile platform will gain an instantaneous unconstrained rotational dof about the line passing through $p_{i,j}$ and intersecting the remaining wrenches of branches k and h. Hence, Case 3c can potentially correspond to an uncertainty configuration for the 3-4 form of four-branch parallel manipulators.

Case 3d - Coplanar non-concurrent lines: The parallel manipulator will be in an uncertainty configuration if at least six wrenches are coplanar. The mobile platform considering the six coplanar wrenches would have three unconstrained dof. The corresponding unconstrained three-system consist of all linear combinations of the translational dof in the direction normal to the plane of the coplanar wrenches and the two rotational dof about the lines lying on this plane. Due to the remaining two wrenches the unconstrained twist of the end effector would be reduced to a one-system. The unconstrained twist of the mobile platform for this potential uncertainty would correspond to a twist about the zero-pitch screw passing through the two intersection points of the remaining two wrenches with the plane of coplanar wrenches. When seven wrenches are coplanar the eighth wrench will intersect the plane of the coplanar wrenches and the dependency case will correspond to Case 4d. If all of the eight wrenches are coplanar, i.e., they all lie on the plane of the mobile platform, the mobile platform will gain three instantaneous dof as described earlier for six coplanar wrenches.

Case 4a - Four independent skew lines: For the 3-4 form of the class of four-branch parallel manipulators there are a maximum of three skew wrenches and it is not possible to have five skew wrenches, dependent or not. Thus, Case 4a is not a concern.

Case 4b - Lines concurrent with two skew lines: This case will result in an uncertainty if at least seven wrenches are concurrent with two skew lines. Degenerate cases can be investigated by finding potential line(s) that can intersect seven wrenches, seeing if two such lines can be intersected at the same time, and checking if these lines are skew. There are several potential lines which might intersect seven wrenches of the 3-4 form. (1) The platform edge $p_{i,j}p_k$ will intersect seven wrenches if one wrench of branch h lies on the mobile platform plane. (2) When the wrenches of the concurrent branches i and j are coplanar, the common line of the plane of coplanar wrenches of branches i and j with the plane of wrenches of branch k is a potential line if it intersects one wrench of branch h. (3) When $p_{i,j}$ lies on the plane of $\mathbf{W}_{l_k}$ & $\mathbf{W}_{m_k}$, a line on this plane passing through $p_{i,j}$ and the intersection point of a wrench of branch h with the plane could be one of the skew lines. If any two of the lines intersect the same seven wrenches and are skew uncertainty due to dependence Case 4b will exist.

Case 4c - One-parameter family of flat pencils: The wrenches of branch i, $\mathbf{W}_{l_i}$ & $\mathbf{W}_{m_i}$, intersect at the spherical joint center p_i. The three branch-end locations $p_{i,j}$, p_k and p_h must not be collinear, otherwise the design would be fundamentally degenerate (unconstrained rotation about the line $p_{i,j}p_kp_h$). For non-collinear $p_{i,j}$, p_k, and p_h dependency Case 4c will not exist for the 3-4 form of four-branch parallel manipulators.

Case 4d - Lines on a plane or passing through one point on the plane: This

case will result in the rank deficiency of the set of eight wrenches if at least seven of the wrenches are coplanar or pass through one point on the plane of the coplanar wrenches. When the plane of the wrenches of branch k passes through $p_{i,j}$ there exist ∞^1 lines passing through $p_{i,j}$ and intersecting the wrenches of branch k (lying on the plane of branch k wrenches), i.e., there exist ∞^1 lines intersecting the six associated wrenches. In this configuration, if one wrench of branch h passes through $p_{i,j}$, Case 4d will result in an uncertainty and the eight wrenches associated with the actuated joints will define a five-system of constraint. The unconstrained one-system of twists would correspond to rotation about the line passing through $p_{i,j}$ and the intersection point of the remaining wrench of branch h with the plane of the wrenches of branch k.

Case 5a - General complex: The coplanar lines of a complex meet at a common point. This property can be utilized to identify the condition that eight wrenches belong to a complex. The flat pencils of wrenches $\mathbf{W}_{l_i}$ & $\mathbf{W}_{m_i}$, $i = 1, \ldots, 4$, each has a line on the plane of $p_{1,2}p_3p_4$. If these lines intersect at one point (on the mobile platform plane) the rank of the set of associated reciprocal screws will be five and the eight wrenches will not resist any non-zero pitch twist about the normal to the plane $p_{1,2}p_3p_4$ which passes through the common point. Therefore, it is possible to have an unconstrained mobile platform for the class of four-branch parallel manipulators as a result of Case 5a dependency.

Case 5b - Special complex: If all eight wrenches meet one line they will form a five-system of constraint wrenches and the mobile platform will gain an instantaneous unconstrained zero-pitch twist about the line concurrent with the wrenches. If both associated wrenches of the non-concurrent branch h lie on the mobile platform, line $p_{i,j}p_k$ will intersect eight wrenches. It should be noted that the eight wrenches might

intersect any line, e.g., when a common line of the planes defined by $\mathbf{W}_{l_i}$ & $\mathbf{W}_{m_i}$, $i = 1, \cdots, 4$, exists, it will intersect eight wrenches.

4.4 Comparison with Redundantly Sensed and Actuated Three-Branch Manipulators

It was presented in Chapter 3 that redundant sensing and actuation of all main-arm joints (nine joints) of the three-branch parallel manipulators provides a unique solution for the FDP and eliminates all uncertainty configurations. It was also presented that sensing and actuation of a total of eight main-arm joints results in a maximum of two solutions for the FDP and eliminates all of the potential uncertainties for the considered class of parallel manipulators except those corresponding to Case 5b.

The symmetric 2-2-2-2 joint sensing of 3-4 form of four-branch parallel manipulators provides a maximum of four or eight solutions for the FDP (depending on the type of unsensed main-arm joints). Symmetrically sensed and actuated four-branch parallel manipulators (2-2-2-2 sensing and actuation) have more potential assembly modes and uncertainty cases compared to the redundant sensing and actuation of eight main-arm joints (3-3-2 actuation) of the class of three-branch manipulators even though both possess eight sensed and actuated joints. A summary of potential uncertainty cases that exist for the symmetric actuations of the 3-4 form and the general form (4-4 form) of the four-branch manipulators, and also for the non-redundant symmetric and asymmetric actuations (2-2-2 and 3-2-1) and redundant actuations (3-2-2, 3-3-1, 3-3-2, 3-3-3) of three-branch parallel manipulators is given in Table 4.1

Having the redundant branch will increase cases of workspace limitations due to the interference between the branches. In addition, an extra branch increases the

Table 4.1: Potential uncertainties for four- and three-branch parallel manipulators.

Dependency Case	Four-Branch 2-2-2-2 Actuation		Three-Branch Non-Redundant/Redundant Actuations					
	3-4 form	4-4 form	2-2-2	3-2-1	3-2-2	3-3-1	3-3-2	3-3-3
Case 1	–	–	×	×	–	–	–	–
Case 2b	–	–	×	×	×	×	–	–
Case 3a	–	–	–	–	–	–	–	–
Case 3b	–	–	×	×	–	–	–	–
Case 3c	×	–	×	×	×	×	–	–
Case 3d	×	×	×	×	×	×	–	–
Case 4a	–	–	–	–	–	–	–	–
Case 4b	×	–	×	×	–	–	–	–
Case 4c	–	–	–	–	–	–	–	–
Case 4d	×	×	×	×	×	×	–	–
Case 5a	×	×	×	–	–	–	–	–
Case 5b	×	×	×	×	×	×	×	–

cost and the overall weight of the manipulator. Furthermore, although redundancy in individual branches decreases the number of assembly modes and consequently decreases the number of uncertainty configurations, it will increase the number of motion singular points due to branch degeneracies.

Therefore, it can be concluded that adding a redundant branch (in-parallel redundant sensing and actuation) to a three-branch parallel manipulator is not as efficient and practical of a solution as compared to utilization of redundant sensing and actuation (serial redundant sensing and actuation) of main-arm joints. It is recommended that a redundant branch(es) only be employed when redundant serial sensing and/or actuation of the main-arm joints is undesirable.

4.5 Summary

The number of assembly modes of three-branch parallel manipulators are reduced by adding a redundant branch. Up to eight and up to four assembly modes can exist for four-branch symmetrically sensed 3-4 manipulators when all main-arm unsensed joints are revolute and when all unsensed joints are prismatic, respectively. Similarly, up to eight and up to four assembly modes can exist for manipulators with combinations of unsensed revolute and prismatic joints when one of the concurrent branches and both of the concurrent branches has an unsensed prismatic joint, respectively.

Resolving the potential assembly modes require the consideration of at highest second-order single-variable polynomials. Furthermore, it may be possible through appropriate design to limit the feasible assembly modes to two for all cases. However, with one redundant branch and symmetric 2-2-2-2 sensing it is not possible to get a unique solution for the forward displacement problem (a unique assembly mode).

Not all of the potential wrench dependencies leading to the uncertainty configurations of three-branch parallel manipulators with spherical branch-end joints can be eliminated utilizing a redundant branch.

Considering potential assembly modes and uncertainty configurations redundant sensing and actuation (3-3-2) of three-branch manipulators is more effective than adding a fourth branch (2-2-2-2 sensing and actuation). In addition, a redundant branch will limit the workspace due to branch interference, will increase overall weight and cost of the device, and will increase motion singularities due to branch degeneracies. Redundant branch(es) should only be employed when redundant serial sensing and/or actuation of the main-arm joints is undesirable.

Chapter 5

Kinematic Calibration

Kinematic calibration can be employed to enhance a manipulator's accuracy allowing compensation for manufacturing tolerances and assembly inaccuracies. The manipulator accuracy can be improved by modifying the manipulator software model rather than physically altering the manipulator.

Kinematic calibration of a manipulator identifies the set of kinematic parameters involved in the relationship of the joint displacements to the end effector pose. Kinematic calibration of a manipulator will typically consist of the following steps. Identification of potential error sources and construction of a kinematic model; precise measurement of the end effector position and orientation at a number of different manipulator configurations; identification of the kinematic parameters; and finally compensation for the inaccuracies using the identified values of the parameters.

Some of the factors that affect the manipulator parameter identification are as follows. Type of measurement method, e.g., position and/or orientation of the end effector; number of measurements; accuracy of measurements (accuracy of identification will approach the accuracy of measurement after a large number of measure-

ments and it will never be more accurate than the accuracy of measurement); noise in measurements; initial estimate of parameters; observation strategy, i.e., selection of manipulator configurations during measurements; range of joints' motion; and type of identification parameters (geometric, nongeometric). The set of manipulator configurations should be chosen such that it results in a relatively large position error so that the effects of measurement and unmodeled errors can be minimized. In addition, the measurement data at each configuration should provide the best observability of the calibration parameters. Optimal measurement configurations should be well spaced in the joint space as well as in the Cartesian space.

This chapter studies the kinematic calibration of closed-loop (parallel) manipulation devices. Section 5.1 introduces an identification procedure suited to parallel manipulators and devices. Specific models for a redesigned hand controller are presented in Section 5.2.[1] The identification procedure and models are applied in the calibration of the hand controller and calibration results are given in Section 5.3.

5.1 Identification Objective Functions

Kinematic calibration identifies more accurate values for kinematic parameters involved in the relationship of the joint displacements to the end effector pose. The identification problem can be formulated as a nonlinear optimization problem. For a parallel manipulator the objective function might be the error between the measured end effector pose and the end effector pose calculated based on the sensor readings and the device model, or the error of the distance between the branch end locations calculated based on the model. The error can be expressed as the Euclidean norm

[1]The redesign of a parallel manipulator based hand controller to provide a closed-form forward displacement solution is discussed in Appendix D.

of individual errors over several poses in the workspace. The minimum number of manipulator configurations for the estimation of the parameters will be equal to the number of independent parameters. To reduce the effect of measurement noise, a large number of measurements are required.

For a closed-loop manipulator, because not all of the joints are actuated/sensed, the end effector pose might be expressed in terms of the unsensed joints (dependent variables). This increases the complexity of the forward displacement problem (FDP). For the class of three-branch parallel manipulators with passive spherical branch-end joints, when all of the main-arm joints are sensed (three sensed joints per branch), there is a unique solution for the end effector pose.

5.1.1 End Effector Pose Error

The location of the centroid of the branch ends p_c for a three-branch parallel manipulator is described by

$$\mathbf{p}_c = \frac{1}{3}(\mathbf{p}_1 + \mathbf{p}_2 + \mathbf{p}_3) \tag{5.1}$$

If the end effector reference point is located at the centroid of the three branch ends, then $\mathbf{p}_c$ also corresponds to the position of the end effector reference point, $\mathbf{p}$. Otherwise, an offset must be included yielding

$$\mathbf{p} = \mathbf{p}_c + \mathbf{p}_{offset} \tag{5.2}$$

where $\mathbf{p}_{offset}$ would be a constant with respect to a mobile platform frame.

The orientation of the mobile platform frame with respect to the base frame can be expressed either in the form of a rotation matrix as

$$\mathbf{R}_{0P} = \left[{}^0\mathbf{u}_{23}\ {}^0\mathbf{u}_{\perp}\ {}^0\mathbf{u}_n\right] \tag{5.3}$$

where

$$\begin{cases} {}^0\mathbf{u}_{23} = ({}^0\mathbf{p}_3 - {}^0\mathbf{p}_2)/\|(\mathbf{p}_3 - \mathbf{p}_2)\| \\ {}^0\mathbf{u}_n = {}^0\mathbf{u}_{23} \times ({}^0\mathbf{p}_1 - {}^0\mathbf{p}_2)/\|\mathbf{u}_{23} \times (\mathbf{p}_1 - \mathbf{p}_2)\| \\ {}^0\mathbf{u}_{\perp} = {}^0\mathbf{u}_n \times {}^0\mathbf{u}_{23} \end{cases} \tag{5.4}$$

or in terms of roll, pitch, and yaw angles as $\mathrm{RPY}(\phi, \theta, \psi) = \mathrm{Rot}(z, \phi)\ \mathrm{Rot}(y, \theta)\ \mathrm{Rot}(x, \psi)$, where ϕ_z, θ_y, and ψ_x can be determined from $\mathbf{R}_{0P}$.

Defining a vector $\mathbf{\Theta}$ as

$$\mathbf{\Theta} = [\psi_x\ \theta_y\ \phi_z]^T \tag{5.5}$$

an error function related to the error of end effector pose can be defined as

$$f_l = \left[(\mathbf{p}_m - \mathbf{p})^T(\mathbf{p}_m - \mathbf{p}) + w(\mathbf{\Theta}_m - \mathbf{\Theta})^T(\mathbf{\Theta}_m - \mathbf{\Theta})\right]_l \tag{5.6}$$

where $\mathbf{p}_m$, $\mathbf{\Theta}_m$, and w are respectively the measured location and orientation of the end effector[2], and a weighting factor. The error function can also be just the error of end effector location

$$f_l = \left[(\mathbf{p}_m - \mathbf{p})^T(\mathbf{p}_m - \mathbf{p})\right]_l \tag{5.7}$$

---

[2]The error in orientation can be approximated as $\tilde{\Theta}_{error} = \mathbf{R}_{0P}^T\mathbf{R}_{0P_m} - \mathbf{I} \cong \begin{bmatrix} 0 & -\delta_z & \delta_y \\ \delta_z & 0 & -\delta_x \\ -\delta_y & \delta_x & 0 \end{bmatrix}$

The error function of equation (5.7) is much simpler than equation (5.6). Therefore, the gradient vector of equation (5.7) will have simpler expressions. However, this error function does not account for the fact that an end effector location can be achieved with different end effector orientations.

The objective of a nonlinear least-square problem can be expressed as

$$\texttt{Minimize} \quad \sum_l f_l^2 \tag{5.8}$$

The end effector position error as the objective function was found in implementation not to be sensitive enough to variations (errors) of the kinematic parameters. This is because the end effector pose is obtained by taking the average of three branch end positions which has the effect of filtering the inaccuracies. In addition, the end effector poses must be measured using a calibration fixture. These measurements will be uncertain if, as in this case, the fixture has not been calibrated. Hence, there is a need for an objective function sensitive to the variations of kinematic parameters which requires no measurement for different poses except the joint displacements. An objective function can be formed by noting that the manipulator structure is comprised of three closed loops, i.e , the loops formed by branches one and two, two and three, and one and three, and their respective base and mobile platform mounts. Because the distance between the branch end locations on the mobile platform is constant and known, it allows an objective based on branch end distance errors to be formed.

5.1.2 Branch End Distance Errors

The distance between branch end points $\mathbf{p}_i$ and $\mathbf{p}_j$, $i, j = 1, 2, 3$, $i \neq j$, can be obtained using three loop closure equations and can be defined as the Euclidean norm of the

vector $(\mathbf{p}_i - \mathbf{p}_j)$.

Objective functions related to the errors of the distances between the three branch ends over the workspace can be defined. The branch end distance errors for a pose l are

$$\begin{aligned} f_{1l} &= \left[(\mathbf{p}_1 - \mathbf{p}_2)^T(\mathbf{p}_1 - \mathbf{p}_2) - {p_1p_2}^2\right]_l = \left[(\mathbf{p}_1^T\mathbf{p}_1 + \mathbf{p}_2^T\mathbf{p}_2 - 2\mathbf{p}_1^T\mathbf{p}_2) - {p_1p_2}^2\right]_l \\ f_{2l} &= \left[(\mathbf{p}_2 - \mathbf{p}_3)^T(\mathbf{p}_2 - \mathbf{p}_3) - {p_2p_3}^2\right]_l = \left[(\mathbf{p}_2^T\mathbf{p}_2 + \mathbf{p}_3^T\mathbf{p}_3 - 2\mathbf{p}_2^T\mathbf{p}_3) - {p_2p_3}^2\right]_l \\ f_{3l} &= \left[(\mathbf{p}_1 - \mathbf{p}_3)^T(\mathbf{p}_1 - \mathbf{p}_3) - {p_1p_3}^2\right]_l = \left[(\mathbf{p}_1^T\mathbf{p}_1 + \mathbf{p}_3^T\mathbf{p}_3 - 2\mathbf{p}_1^T\mathbf{p}_3) - {p_1p_3}^2\right]_l \end{aligned} \tag{5.9}$$

where p_1p_2, p_2p_3, and p_1p_3 are the known constant branch end distances on the mobile platform.

An appropriate objective function must be related to the errors of all of the distances between the branch ends over the workspace. There will be three error functions corresponding to the three constant lengths p_1p_2, p_2p_3, and p_1p_3. These error functions must be minimized simultaneously. Therefore, an error vector is defined as

$$\mathbf{f}_l = \begin{bmatrix} f_1 \\ f_2 \\ f_3 \end{bmatrix}_l \tag{5.10}$$

to be used in the least-square problem

$$\texttt{Minimize} \quad \sum_l \mathbf{f}_l^T\mathbf{f}_l \tag{5.11}$$

The error function of equation (5.10) is more adequate compared to equation (5.7) which only includes the error of the end effector location. This is due to the fact that the end effector location and orientation can be expressed in terms of branch end positions.

The objective function of equation (5.11) allows the minimization of the summation of the squares of each of the elements of the error vector. Note that each error function will depend on the kinematic parameters of the two corresponding branches and will be independent of the parameters of the third branch.

The identification Jacobian $\mathbf{J}$, i.e., the gradient matrix of equation (5.10), is a $3m \times n_p$ matrix, where m is the number of sampled manipulator configurations, n_p represents the number of kinematic parameters to be identified, and $m \geq n_p$.

5.2 Identification Models

The hand controller considered as an example in the previous chapters will be modeled using three levels of kinematic parameters. These models will be referred to as original, improved, and complete models. All three models will assume that the three branch distal joints form a spherical joint. The original model will only consider the parameters that are specified by the manufacturer (RSI Research Ltd.). The improved model includes the parameters of the original model and assumes that the first and the second main-arm joint axes are parallel and that the second and the third joint axes are intersecting and perpendicular. The remaining positional parameters used in the transformation from the hand controller base frame to the branch base frame are included in the improved model. The complete model includes the remaining geometric parameters between the three branch base proximal joints in addition to the parameters considered for the improved model.

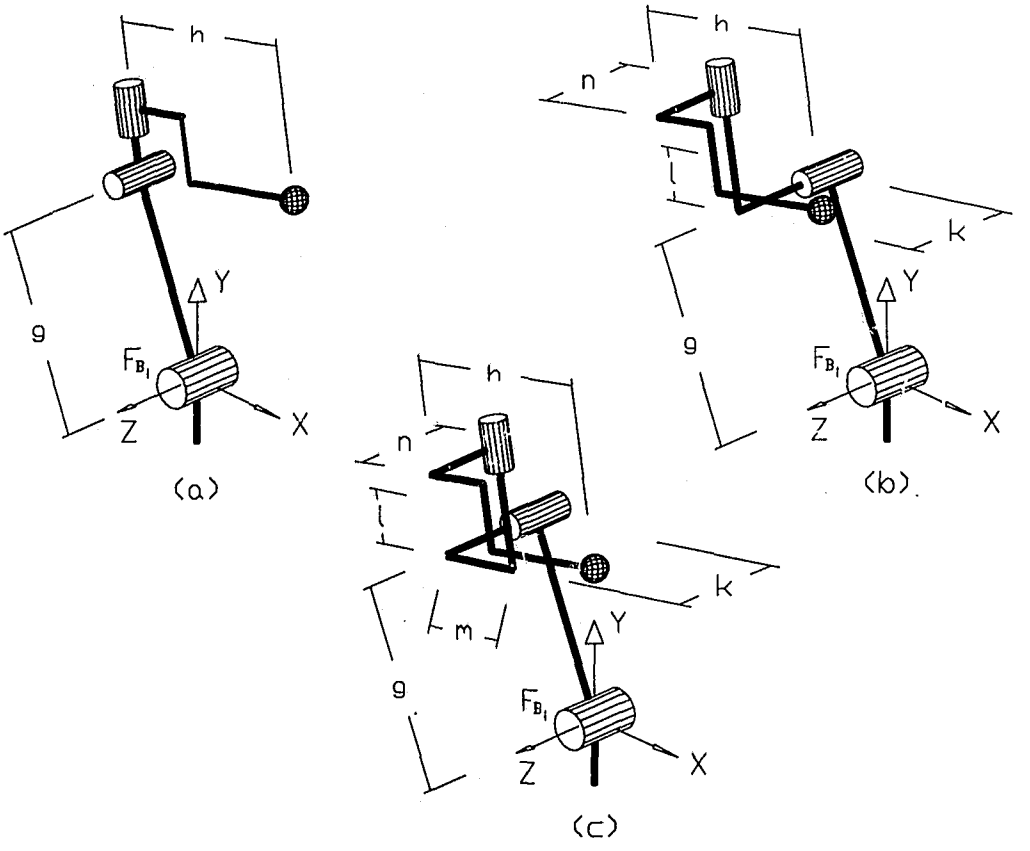

Figure 5.1: Branch layout: (*a*) Original model; (*b*) Improved model; (*c*) Complete model.

5.2.1 Original Model

Kinematic parameters

In the original kinematic modeling of the hand controller it is assumed that the major inaccuracy sources are the two link lengths (g_i, h_i, refer to Figure 5.1*a*) and the branch base positions as described by base platform radii r_{b_i}, and angles ϕ_i. Hence, twelve geometric parameters of the model exist and are

$$\mathbf{a} = \{g_1, h_1, r_{b_1}, \phi_1, g_2, h_2, r_{b_2}, \phi_2, g_3, h_3, r_{b_3}, \phi_3\} \tag{5.12}$$

In addition, the gain and offset of each joint potentiometer can be included in the calibration. This increases the number of kinematic parameters to 30, i.e., 10 parameters for each branch. ϕ_1 can be considered a constant parameter since the sum of ϕ_1, ϕ_2, and ϕ_3 is equal to 2π. This reduces the total number of parameters to 29.

For the original model, identification is performed with $r_p = 1.5$ inches. The nominal hand controller parameters can be used as the initial estimates required for the calibration. These correspond to $\phi = \{\frac{-\pi}{2}, \frac{5\pi}{6}, \frac{\pi}{6}\}$, $r_{b_i} = 4.5$ inches, $h_i = 3.971$ inches, and $g_i = 3.2$ inches. The nominal values of the gain and offset of potentiometers can be obtained from the joint level calibration employing linear regression analysis (Section 5.3.1).

Forward displacement

The location of a branch end $\mathbf{p}_i$ in the branch base frame can be expressed as

$$^{B_i}\mathbf{p}_i = \begin{bmatrix} p_x \\ p_y \\ p_z \end{bmatrix}_i = \begin{bmatrix} hC_{12}S_3 + gC_1 \\ hS_{12}S_3 + gS_1 \\ hC_3 \end{bmatrix}_i \tag{5.13}$$

where $C_j = \cos\theta_j$, $S_j = \sin\theta_j$, $C_{jk} = \cos(\theta_j + \theta_k)$ and so on, with θ_j being the displacement at joint j. The homogeneous transform describing branch base frame with respect to the base platform frame is

$$\mathbf{T}_{0,B_i} = \begin{bmatrix} C_\phi & 0 & S_\phi & -r_b C_\phi \\ S_\phi & 0 & -C_\phi & -r_b S_\phi \\ 0 & 1 & 0 & 0 \\ 0 & 0 & 0 & 1 \end{bmatrix}_i \tag{5.14}$$

Hence, the location of the branch end in the base reference frame will be

$$\begin{bmatrix} {}^0\mathbf{p}_i \\ 1 \end{bmatrix} = \begin{bmatrix} {}^0p_x \\ {}^0p_y \\ {}^0p_z \\ 1 \end{bmatrix}_i = \mathbf{T}_{0,B_i} \begin{bmatrix} {}^{B_i}\mathbf{p}_i \\ 1 \end{bmatrix} = \begin{bmatrix} (p_x - r_b)C_\phi + p_z S_\phi \\ (p_x - r_b)S_\phi - p_z C_\phi \\ p_y \\ 1 \end{bmatrix}_i \tag{5.15}$$

Inverse displacement

A solution for the main-arm joint displacements knowing the position of i-th branch end can be found by considering the expressions in Equation (5.13) to be

$$\theta_3 = \pm\cos^{-1}\left(\frac{p_z}{h}\right) \tag{5.16}$$

$$\theta_2 = -\sigma \cos^{-1}\left(\frac{{p_x}^2 + {p_y}^2 - h^2 {S_3}^2 - g^2}{2ghS_3}\right) \tag{5.17}$$

$$\theta_1 = \tan^{-1}\left(\frac{p_y}{p_x}\right) + \sigma \cos^{-1}\left(\frac{{p_x}^2 + {p_y}^2 - h^2 {S_3}^2 + g^2}{2g\sqrt{{p_x}^2 + {p_y}^2}}\right) \tag{5.18}$$

where $\sigma = \pm 1$. Thus, for each branch there could exist four sets of main-arm joint inverse displacement solutions. The solutions corresponding to $-\cos^{-1}(.)$ are unacceptable considering the joint displacement limitations of the hand controller's branches

and only one solution will exist. This inverse displacement solution will be utilized in the joint level calibration of Section 5.3.1.

5.2.2 Improved Model

In the original model it was assumed that the branch base points were located on a horizontal plane, i.e., $z_{b_i} = 0$, $i = 1, 2, 3$. It was also assumed that the z-axes of the hand controller base frame and of the branch reference frame are perpendicular, i.e., $\alpha_{b_i} = \frac{\pi}{2}$. The fact that the three branch base points might not be coplanar, and that the z-axes of the hand controller base frame and of the branch reference frame might not be perpendicular are included in the improved model. In addition, the joint offset of the parallel first and second joints and also the joint offset and link length between the third and the fourth joints are included (Figure 5.1*b*). The assumptions made for the improved model of a branch are that the first and the second joint axes are parallel, that the second and the third joint axes are intersecting and perpendicular, and that the last three joints of each branch define a spherical joint group with center at the intersection of the fifth joint with the mobile platform.

Kinematic parameters

Introducing five more geometric parameters per branch, i.e., two joint offsets, one link length, the branch base position in Z_0 direction, and the branch base orientation, increases the number of kinematic parameters to a total of 45, i.e., 15 parameters per branch. The geometric parameters of a branch i, $i = 1, 2, 3$ correspond to

$$\mathbf{a}_i = \{g_i, h_i, r_{b_i}, \phi_i, z_{b_i}, \alpha_{b_i}, l_i, k_i, n_i\} \tag{5.19}$$

where k_i represents the joint offset of the second joint, and l_i and n_i correspond to the link offset and link length of the third joint, respectively. Similar to the original model ϕ_1 will be considered as a constant parameter in the calibration. However, the model still is not complete. This is because of the assumptions made for the modeling, i.e., parallelism of the first and the second joint axes, intersection and perpendicularity of the second and the third joint axes, and the spherical branch end joints.

Forward displacement

The location of the end point of branch i in the branch base frame for the improved model is

$$ {}^{B_i}\mathbf{p}_i = \begin{bmatrix} p_x \\ p_y \\ p_z \end{bmatrix}_i = \begin{bmatrix} hC_{12}S_3 + gC_1 - lS_{12} + nC_{12}C_3 \\ hS_{12}S_3 + gS_1 + lC_{12} + nS_{12}C_3 \\ hC_3 + k - nS_3 \end{bmatrix}_i \tag{5.20} $$

For the improved model the homogeneous transform describing branch base frame with respect to the base platform frame becomes

$$ \mathbf{T}_{0,B_i} = \begin{bmatrix} C_\phi & -S_\phi C_{\alpha_b} & S_\phi S_{\alpha_b} & -r_b C_\phi \\ S_\phi & C_\phi C_{\alpha_b} & -C_\phi S_{\alpha_b} & -r_b S_\phi \\ 0 & S_{\alpha_b} & C_{\alpha_b} & z_b \\ 0 & 0 & 0 & 1 \end{bmatrix}_i \tag{5.21} $$

i.e.,

$$ \mathbf{T}_{0,B_i} = \mathbf{Rot}(Z_0, \phi_i)\ \mathbf{Trans}(Z_0, z_{b_i})\ \mathbf{Trans}(x_{b_i}, -r_{b_i})\ \mathbf{Rot}(x_{b_i}, \alpha_{b_i}) \tag{5.22} $$

Inverse displacement

The position of i-th branch end in the branch reference frame given in equation (5.20) can be used to solve for the main-arm joint displacements as follows.

$$\theta_3 = -\tan^{-1}\left(\frac{n}{h}\right) \pm \cos^{-1}\left(\frac{p_z - k}{\sqrt{h^2+n^2}}\right) \tag{5.23}$$

$$\theta_2 = -\tan^{-1}\left(\frac{l}{hS_3+nC_3}\right) - \sigma\cos^{-1}\left(\frac{{p_x}^2+{p_y}^2-[g^2+l^2+(hS_3+nC_3)^2]}{2g\sqrt{(hS_3+nC_3)^2+l^2}}\right) \tag{5.24}$$

$$\theta_1 = \tan^{-1}\left(\frac{p_y}{p_x}\right) + \sigma\cos^{-1}\left(\frac{g+hS_3C_2-lS_2+nC_3C_2}{\sqrt{{p_x}^2+{p_y}^2}}\right) \tag{5.25}$$

where $\sigma = \pm 1$.

5.2.3 Complete Model

The model termed the "complete model" considers all potential uncertainties in the branch link parameters. In addition to the ones which are considered for the improved model, the link twists of the parallel first and second joint axes and also of the perpendicular second and third joint axes are included. The non-parallelism of the two consecutive "parallel" joint axes is included by using the set of link parameters introduced by Hayati (1983). Utilization of the parameters introduced by Hayati (1983) allows small variations in the two consecutive "parallel" joint axes to be modeled by small variations of the link parameters. The last three joints of each branch are still modeled as spherical joints, i.e., the link length, joint offset, and link twist of the branch distal joints are not investigated.

Kinematic parameters

For a branch i the geometric parameters to be identified are

$$\mathbf{a}_i = \{g_i, h_i, r_{b_i}, \phi_i, z_{b_i}, \alpha_{b_i}, l_i, k_i, n_i, m_i, \alpha_{1i}, \beta_{1i}, \alpha_{2i}, \alpha_{3i}\} \tag{5.26}$$

where m_i represents the link length of the second joint (the length parameters are illustrated in Figure 5.1*c*) and α_{1i}, α_{2i}, and α_{3i} model the first, the second, and the third link twists. β_{1i} corresponds to the small misalignment of the parallel joint axes due to the manufacturing tolerances. Similar to the previous models ϕ_1 will be considered as a constant parameter in the calibration. This yields a total of 59 kinematic parameters to be considered.

Forward displacement

The location of the end point of branch i in the branch base frame can be calculated employing homogeneous transformation matrices. The homogeneous transformation for a revolute joint j is

$$\mathbf{T}_{j-1,j} = \begin{bmatrix} C_\theta & -S_\theta C_\alpha & S_\theta S_\alpha & aC_\theta \\ S_\theta & C_\theta C_\alpha & -C_\theta S_\alpha & aS_\theta \\ 0 & S_\alpha & C_\alpha & d \\ 0 & 0 & 0 & 1 \end{bmatrix}_j \tag{5.27}$$

where a, d, and α are Denavit-Hartenberg (DH) link parameters. Table 5.1 represents the DH parameters of the complete model including the modified DH parameters[3] of

[3]The Denavit-Hartenberg method can be employed to represent the relative positional relation between two adjacent links in terms of a homogeneous transformation matrix. However, the DH

Table 5.1: Modified DH parameters for the complete model.

Joint #	θ_j	a_j	α_j	d_j	β_j
1	θ_1	g	α_1	0	β_1
2	θ_2	m	α_2	k	-
3	θ_3	n	α_3	l	-
4	θ_4	0	-90	h	-
5	θ_5	0	90	0	-
6	θ_6	0	0	0	-

the parallel first and second joint axes. The modified DH parameters for two consecutive parallel or near parallel revolute joint axes will result in the transformation matrix

$$\mathbf{T}_{j-1,j} = \begin{bmatrix} C_\theta C_\beta - S_\theta S_\alpha S_\beta & -S_\theta C_\alpha & C_\theta S_\beta + S_\theta S_\alpha C_\beta & aC_\theta \\ S_\theta C_\beta + C_\theta S_\alpha S_\beta & C_\theta C_\alpha & S_\theta S_\beta - C_\theta S_\alpha C_\beta & aS_\theta \\ -C_\alpha S_\beta & S_\alpha & C_\alpha C_\beta & 0 \\ 0 & 0 & 0 & 1 \end{bmatrix}_j \tag{5.28}$$

or

$$\mathbf{T}_{j-1,j} = [\mathtt{Rot}(z,\theta)\ \mathtt{Trans}(x',a)\ \mathtt{Rot}(x'',\alpha)\ \mathtt{Rot}(y''',\beta)]_j \tag{5.29}$$

method results in a problem in the calibration. The limitation of the DH formalism is the treatment of consecutive revolute and prismatic joints with nearly parallel axes. For two parallel revolute joint axes there is no unique common normal. If the two axes are actually not parallel and they are inclined slightly, the common normal becomes unique and the location of the coordinate frame may change significantly. On the other hand, small changes in the position and orientation of two consecutive links cannot necessarily be modeled by small link parameter variations if DH parameters are used. Hayati (1983), and Hayati and Mirmirani (1995) pointed out the proportionality problems inherent in the standard DH approach, and introduced a new set of link parameters which allows first order error modeling of the two consecutive parallel or near parallel revolute and prismatic joint axes.

where x' denotes the x-axis direction after $\texttt{Rot}(z,\theta)$ and y''' denotes the y-axis direction after the $\texttt{Rot}(z,\theta)$ $\texttt{Trans}(x',a)$ $\texttt{Rot}(x'',\alpha)$.

5.3 Calibration Example

The position and orientation of the end effector can be measured using the calibration fixture provided by RSI Research Ltd. (refer to Figure 5.2). The joint displacements can be calculated from the inverse displacement analysis of the original model for each end effector pose. It is initially assumed that there are no inaccuracies in the link lengths and the spacing of branch ends, and that the kinematic model of the hand controller is known precisely (perfect machining, assembly, and joint displacement sensing). In addition, it is initially assumed that the calibration fixture is manufactured precisely so that the exact end effector pose corresponding to a fixture pose is known.

Linear regression analysis (Numerical Recipes in C and MATLAB Package) was employed to calculate the nominal gain k_{j_1} and offset k_{j_2} of potentiometer j from the relationship between the joint displacement θ_j and the potentiometer reading η_j. The relationship between θ_j and η_j can be defined as $\theta_j = k_{j_1}\eta_j + k_{j_2}$. The relationship is assumed to be linear because the potentiometers are mounted on the joint axes directly and the potentiometers are designed to be linear (refer to Appendix E). The plot of joint displacements versus potentiometer readings verified the assumption of a linear relationship (Figures 5.3, 5.4, and 5.5). The readings can be filtered to reduce the noise in the potentiometers, e.g., several samples can be averaged. The values of gains and offsets which are calculated, assuming a precise model, can be used as the nominal values for the kinematic calibration of the hand controller.

The parameter identification study for the three-branch parallel manipulator has

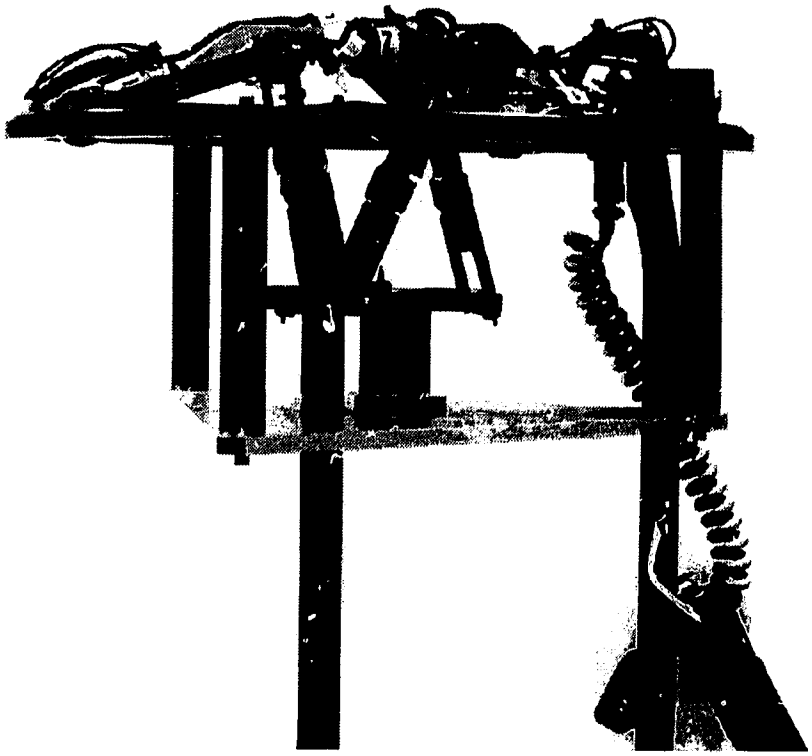

Figure 5.2: RSI hand controller with the calibration fixture.

been performed by implementing the kinematic models of Section 5.2 in a computer program. The developed program can perform the calibration procedure considering any combination of the parameters used in the complete kinematic model of Section 5.2.3. In addition, any combinations of previously collected input data (potentiometer readings) can be used in the investigation.

The Levenberg-Marquardt nonlinear least square algorithm[4] is employed to identify kinematic parameters of the hand controller. The solution is obtained by providing the analytical forms of the cost function(s) and of the gradient matrix of the cost function(s) with respect to the identification parameters. The cost function of the calibration was chosen to be the Euclidean norm of the error of the branch end distances as given by equation (5.11).

The identification procedure can be utilized for the class of three-branch paralliel manipulators where each branch is connected to the mobile platform with a spherical joint and the three branch base proximal joints are all sensed. The calibration program can be used for any manipulator of this class after providing routines that calculate positions of the branch ends expressed in the base reference frame and derivatives of the branch ends' positions with respect to the calibration parameters, and also after providing joint displacement data for a sufficient set of mobile platform poses.

[4]The Levenberg-Marquardt (LM) algorithm has been introduced as an improvement to the familiar iterative linear least-squares algorithm also known as Gauss-Newton method. The technique overcomes problems due to the singularity of the matrix $\mathbf{J}^T\mathbf{J}$ of the problem $\mathbf{J}^T\mathbf{J}\mathbf{x} = \mathbf{J}^T\mathbf{y}$ by adding a varying nonnegative scalar coefficient μ to yield $\mathbf{J}^T\mathbf{J} + \mu\mathbf{I}$ while maintaining the Gauss-Newton convergence properties near the optimal solution, i.e., as the solution approaches the optimum the scalar μ is adjusted to have smaller and smaller values, Mooring et al. (1991).

5.3.1 Joint Level Calibration

The nominal values of gain and offset of the potentiometers were determined employing linear regression analysis and fitting a straight line to a set of potentiometer readings and the corresponding joint displacements. The joint displacements were calculated from the inverse displacement analysis of the original model for each end effector pose neglecting uncertainties of the kinematic model and also uncertainties of the calibration fixture. The calibration fixture can be mounted to the hand controller in three different configurations, where each configuration can be achieved by rotating the fixture by $\frac{2\pi}{3}$ about the Z_0-axis of the hand controller's base reference frame. The calibration fixture, when mounted to the hand controller, is capable of providing 18 poses for the hand controller, i.e., a total of 54 poses. 48 poses (out of 54) are considered in the analysis. Due to the adjustable constraints provided to restrict the first and the third main-arm joints of the branches only 43 of these poses were achievable by the hand controller. The 43 poses of the hand controller are given in Table 5.2.

The potentiometer readings were filtered by averaging twenty samplings for each pose. The standard deviation of each sampling was calculated. The potentiometer readings were captured after the variations in the standard deviation of each potentiometer reading reached a "steady state" value for a configuration. The averaged readings and the corresponding standard deviations were stored in a file to be used in the calibration. Figures 5.3, 5.4, and 5.5 verify the assumption of a linear relationship between the potentiometer readings and the joint displacements. The calculated potentiometer gains and offsets will be used as the nominal values of the potentiometers' parameters in the following calibration procedure. The nominal gains and offsets of joints one, two, and three of each branch are as follows:

for the first branch (branch A) -

$\{-0.002835, 6.107738; -0.002854, 3.941238; 0.002866, -4.312349\}$;

for the second branch (branch B) -

$\{-0.002862, 6.137053; -0.002897, 3.938330; 0.002916, -4.426159\}$;

and for the third branch (branch C) -

$\{-0.002900, 6.264743; -0.002877, 3.899044; 0.002834, -4.257495\}$.

The sensor noise level was investigated by sampling potentiometer readings during 100 milliseconds for a hand controller pose, refer to Figures 5.6, 5.7, and 5.8. This data was taken by averaging 5 readings of the potentiometers for each sample. It can be seen that the noise level is very low with the averaged readings being between less than 1 5 counts (0.0045 radians) of each other, i.e., very close to the resolution of the potentiometers. For the original model of the hand controller the resulting noise of the branch end distances, due to the potentiometers' noise, for the same hand controller pose are given in Figure 5.9. It can be seen that the noise results in variations in the branch end distances of a total of 0.03 inches. The noise level dictates the accuracy level of the calibration that can be achieved provided that the exact kinematic model of the hand controller is available. The noise level should also be taken into consideration in sensor failure detection routines (Chapter 6) in order to define an error band (tolerance) on the branch end distances.

Table 5.2: Hand controller poses on calibration fixture.

Pose #	Reachable	Platform Pose: X	Y	Z	θ_X	θ_Y	θ_Z
1	×	0	0	-3.966	0	0	0
2	×	0	0	-3.966	0	0	-1.5708
3	×	0	0	-2.666	0	0	0
4	×	0	0	-2.666	0	0	-1.5708
5	×	0	-1.5	-3.966	0	0	0
6	×	0	-1.5	-3.966	0	0	0.7859
7	×	0	-1.5	-2.666	0	0	0
8	×	0	-1.5	-2.666	0	0	0.7859
9	×	-1.5	0	-3.966	0	0	0
10	×	-1.5	0	-3.966	0	0	0.7859
11	×	-1.5	0	-2.666	0	0	0
12	×	-1.5	0	-2.666	0	0	0.7859
13	×	0	0	0.033	0	0	0
14	×	0	0	0.033	0	0	-1.5708
15	×	0	-1.5	0.033	0	0	0
16	×	0	-1.5	0.033	0	0	0.7859
17	×	-1.5	0	0.033	0	0	0
18	×	-1.5	0	0.033	0	0	0.7859
19	×	0	0	-3.966	0	0	-1.0472
20	×	0	0	-2.666	0	0	-1.0472
21	×	1.299	0.75	-3.966	0	0	-1.0472
22	×	1.299	0.75	-3.966	0	0	-0.2618
23	×	1.299	0.75	-2.666	0	0	-1.0472
24	×	1.299	0.75	-2.666	0	0	-0.2618

Table 5.2: Hand controller poses on calibration fixture (cont'd).

Pose #	Reachable	Platform Pose: X	Y	Z	θ_X	θ_Y	θ_Z
25	×	0.75	-1.299	-3.966	0	0	-1.0472
26	×	0.75	-1.299	-3.966	0	0	-0.2618
27	×	0.75	-1.299	-2.666	0	0	-1.0472
28	×	0.75	-1.299	-2.666	0	0	-0.2618
29	×	0	0	0.033	0	0	-1.0472
30	×	1.299	0.75	0.033	0	0	-1.0472
31	×	1.299	0.75	0.033	0	0	-0.2618
32	×	0.75	-1.299	0.033	0	0	-1.0472
33	×	0.75	-1.299	0.033	0	0	-0.2618
34	×	0	0	-3.966	0	0	1.0472
35	×	0	0	-2.666	0	0	1.0472
36	×	-1.299	0.75	-3.966	0	0	1.0472
37	–	-1.299	0.75	-3.966	0	0	1.8326
38	×	-1.299	0.75	-2.666	0	0	1.0472
39	–	-1.299	0.75	-2.666	0	0	1.8326
40	×	0.75	1.299	-3.966	0	0	1.0472
41	–	0.75	1.299	-3.966	0	0	1.8326
42	×	0.75	1.299	-2.666	0	0	1.0472
43	×	0.75	1.299	-2.666	0	0	1.8326
44	×	0	0	0.033	0	0	1.0472
45	×	-1.299	0.75	0.033	0	0	1.0472
46	–	-1.299	0.75	0.033	0	0	1.8326
47	×	0.75	1.299	0.033	0	0	1.0472
48	–	0.75	1.299	0.033	0	0	1.8326

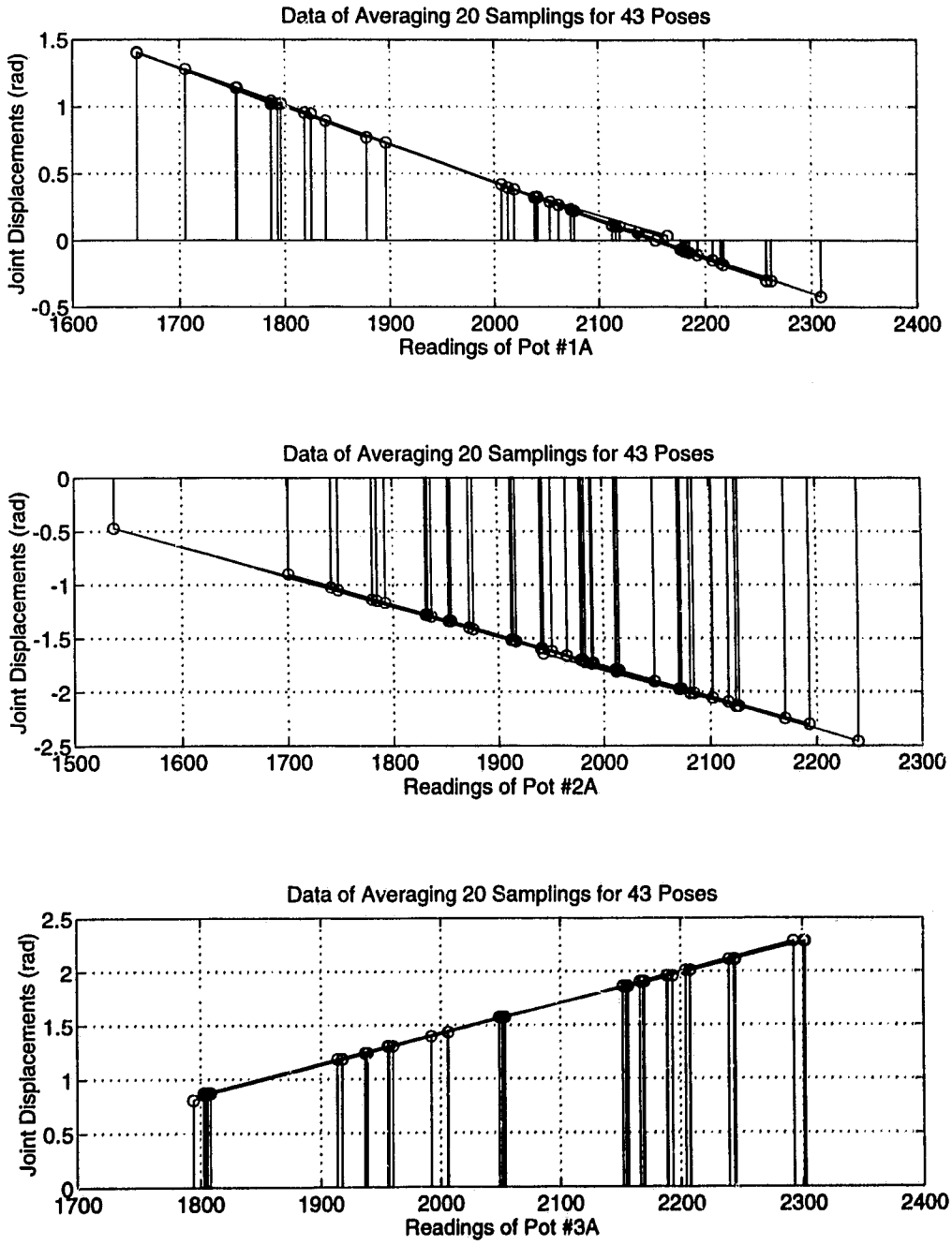

Figure 5.3: Potentiometer readings vs joint displacements of first branch (joint level calibration).

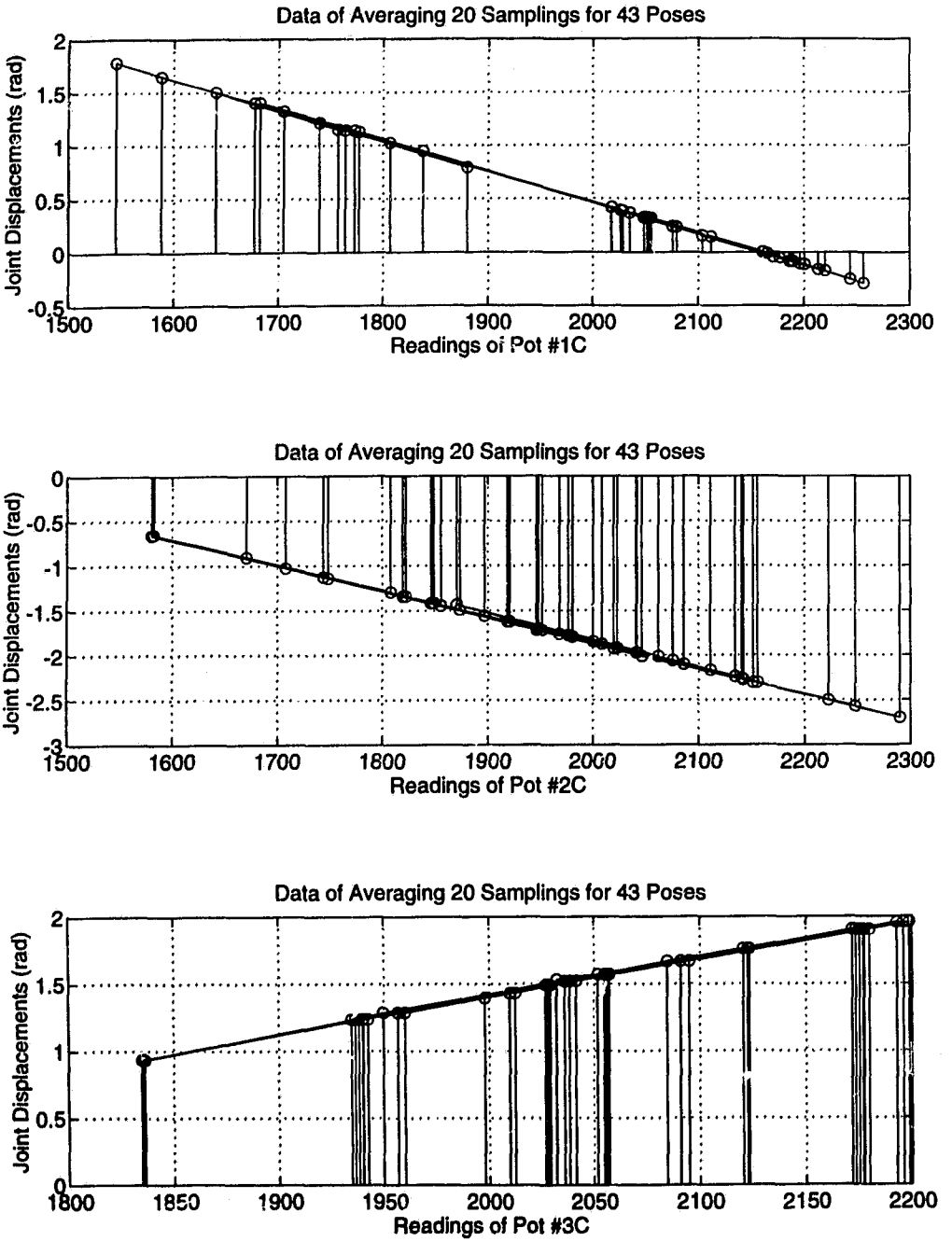

Figure 5.4: Potentiometer readings vs joint displacements of second branch (joint level calibration).

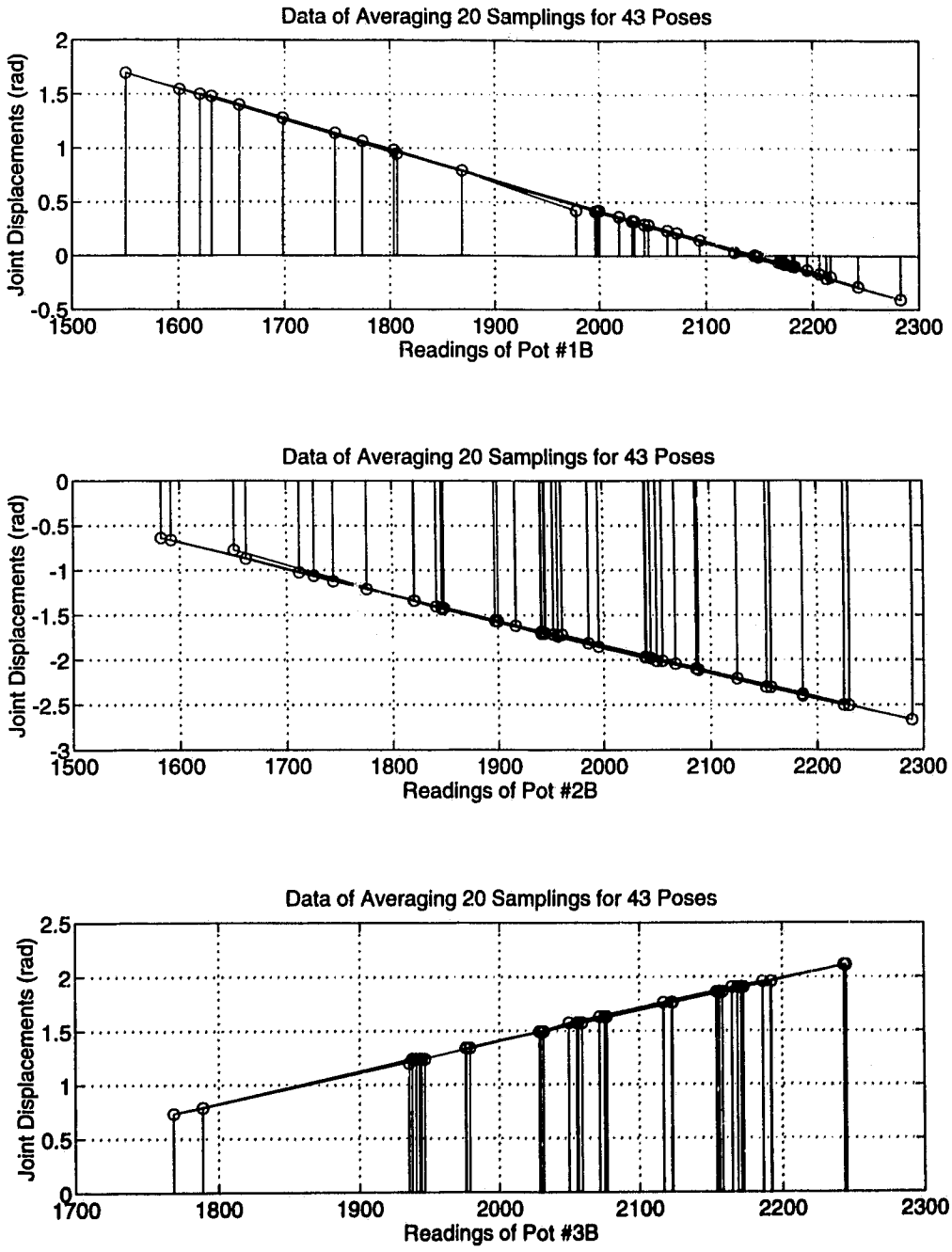

Figure 5.5: Potentiometer readings vs joint displacements of third branch (joint level calibration).

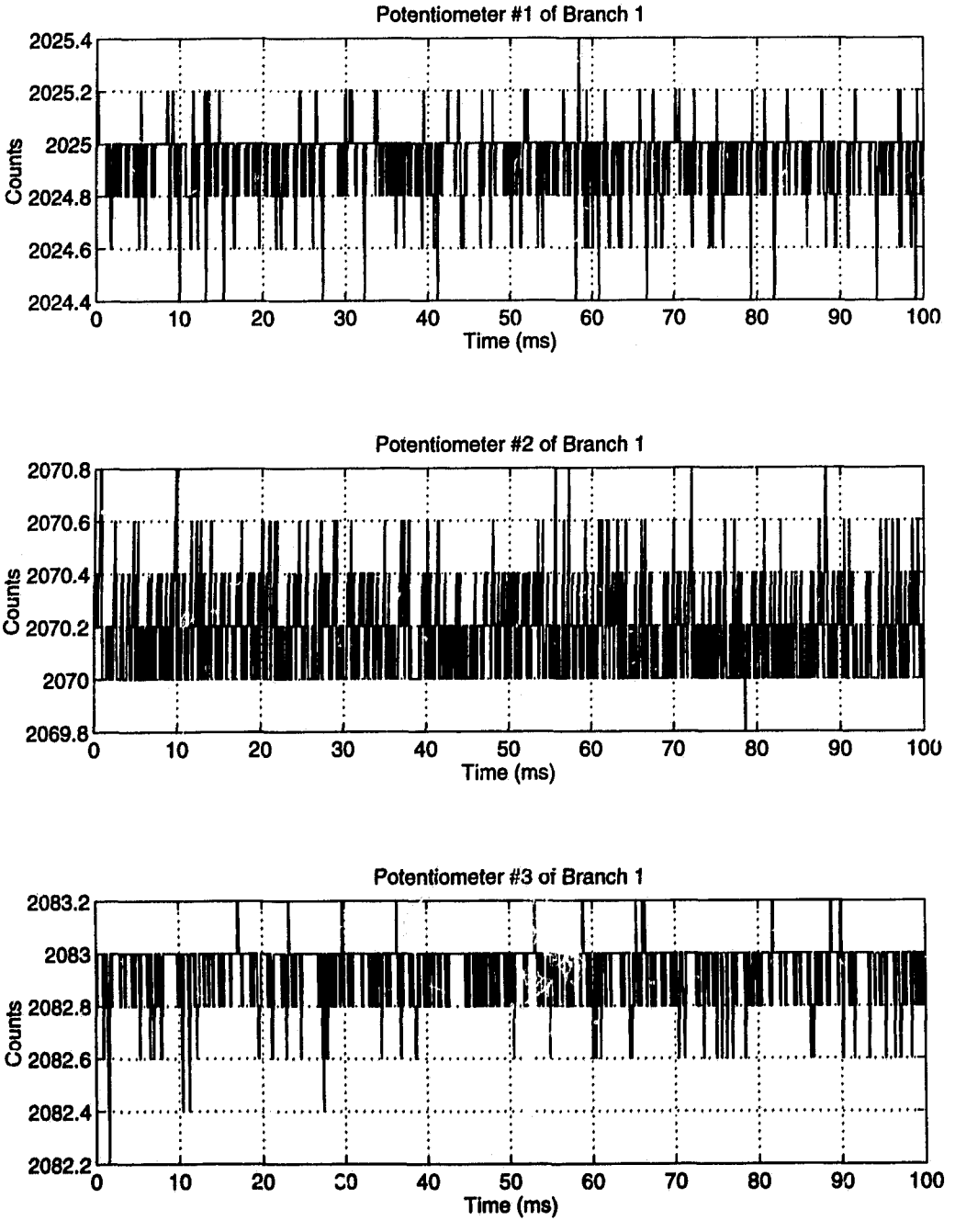

Figure 5.6: Potentiometer readings of first branch (sensor noise investigation).

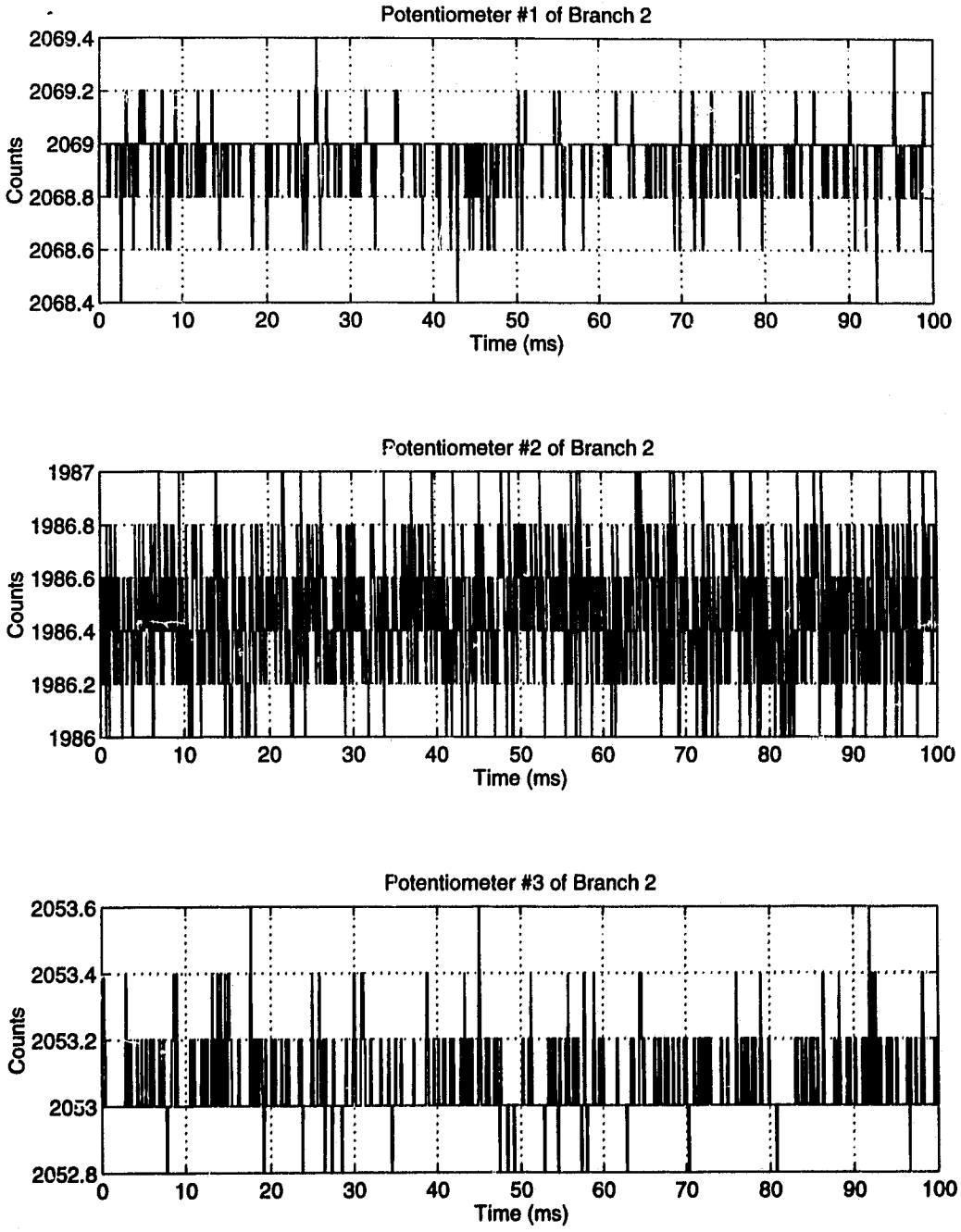

Figure 5.7: Potentiometer readings of second branch (sensor noise investigation).

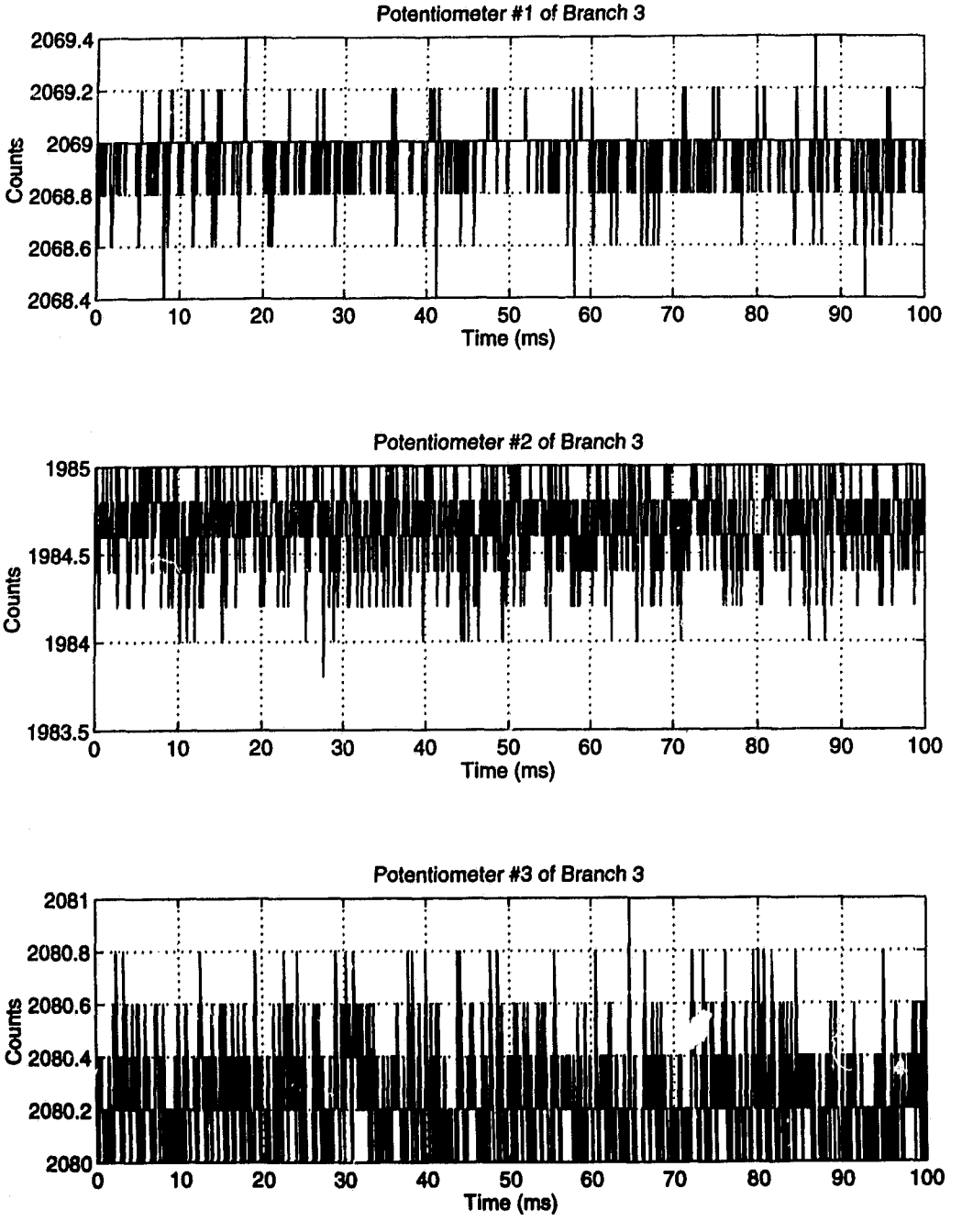

Figure 5.8: Potentiometer readings of third branch (sensor noise investigation).

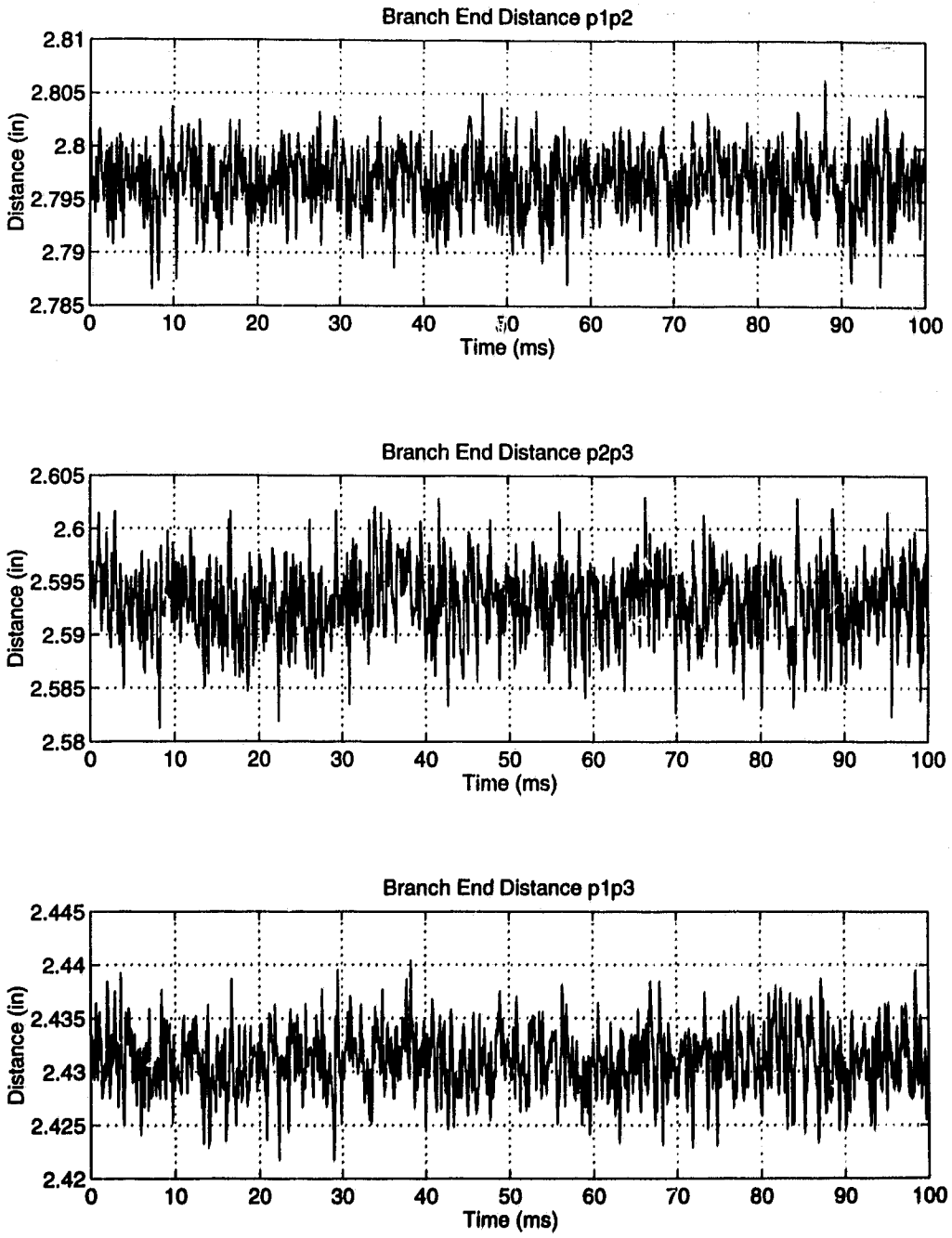

Figure 5.9: Calculated branch end distances (sensor noise investigation - original model).

5.3.2 Kinematic Calibration of Hand Controller

Calibrations were performed considering the original model, the improved model, and the complete model presented in Section 5.2 for 100 data taken over the workspace. The first 43 data out of 100 were obtained using the calibration fixture and they were also used for the initial joint level calibration. Each data was captured by averaging twenty samplings of each pose. The calibrated parameters of the original model, the improved model, and the complete model are summarized in Tables 5.3 & 5.4, 5.6 & 5.7 , and 5.9 & 5.10 for the considered combinations of the calibration parameters and also calibration data. In addition, minimum, maximum, mean, and standard deviation of the error of the branch end distances, and the final value of the χ^2 for the three models are tabulated in Tables 5.5, 5.8, and 5.11.

Comparison of the calibration results tabulated in the third and the fifth columns of Table 5.9, corresponding to the calibration of 59 parameters using 100 and 80 data points (with the initial values given in the second column) shows that the identified values of z_{b_i} (about 0.5 inches) are much larger than the null nominal values, and also the identified α_{b_2} is slightly higher than one might expect. It can be seen from Table 5.11 that the value of χ^2_f is much smaller for the considered number of data for 59 parameters. It seems that the calibration has converged to a set of parameter values that do not correspond to the physical device. To obtain a more realistic parameters the calibration termination tolerance on χ^2 was increased to 0.2 for 100 data and to 0.05 for 80 data from 0.001. In addition, for 100 data points the initial value of z_{b_i} was increased to 0.05 inches (from 0.0). The stopping condition on $\Delta\chi^2$ for the other results remained at 0.001. The results are tabulated in the fourth and the sixth columns of Table 5.9. To study the cause of this behavior the calibration was performed assuming that the positions of the branch bases on the base platform are coplanar, i.e., assuming $z_{b_i} = 0$, and for $\Delta\chi^2 \leq 0.001$ for 100 data and 80 data

points. It can be seen from Table 5.11 that the 56 calibrated parameters are more acceptable for 100 data. However, for the case of using 80 data some parameters do not correspond to the physical device. A further reduction in the number of identification parameters or an increase in the number of data points seems to be necessary to obtain a reasonable result.

Figure 5.10 represents the error of the distances between the three branch ends for the initial parameter values. Figure 5.11 depicts the error of the branch end distances when only potentiometer parameters, i.e, potentiometers' offsets and gains, are identified. It can be seen that the calibration of only potentiometers reduces the error of the branch end distances compared to the nominal values of Figure 5.10. The error of the distance between the three branch ends including parameters of the original model, the improved model, and the complete model used in the calibration procedure are given in Figures 5.12, 5.15, and 5.19. Figure 5.23 depicts the error of the branch end distances of the complete model with initial $z_{b_i} = 0.05$ inches and $\Delta\chi^2 \leq 0.2$. Figures 5.25 and 5.26 show the error for 56 parameters (excluding z_{b_i}) for 100 and 80 data, respectively. It can be seen from Figures 5.19, 5.23 and 5.26 that the error level of each figure is close to the potentiometer noise level of 0.03 inches.

In the next step the first 60 and the last 20 data of the initial 100 data (totally 80 data) were considered to investigate the effect of different data combinations, refer to Figures 5.13, 5.16, and 5.20. Figure 5.24 depicts the error of the branch end distances of the complete model with $\Delta\chi^2 \leq 0.05$. Although Figure 5.24 does not show any deterioration compared to Figure 5.20, the identified parameters corresponding to Figure 5.24 are more realistic. In addition, the error level of Figure 5.24 is very close to the potentiometer noise level of 0.03 inches.

Figures 5.14, 5.17, and 5.21 give the error of the branch end distances for the three kinematic models where only geometric parameters are identified and the po-

tentiometers' gain and offset are considered to be constant and equal to their nominal values. From these figures it is clear that the calibration has been slightly improved for both the improved and complete models but it is slightly deteriorated for the original model. Later, the identified potentiometers' parameters corresponding to Figure 5.11 were used to calibrate the improved and complete models. The results are shown in Figures 5.18 and 5.22. It can be seen by comparison with the results of Figures 5.15 and 5.19 that the error of the branch end distances depends on the initial values of the potentiometers' parameters and that the errors might not get improved by calibrating the hand controller's parameters in two steps.

5.4 Summary

Methodology allowing the kinematic calibration of parallel manipulators was discussed in this chapter. Identification objectives based on measured end effector displacements and on errors in branch end distances were presented. It was concluded that using branch end distance errors was beneficial since branch end location errors are not directly averaged and since the need for a calibration fixture is eliminated.

Calibration results were discussed in detail for the hand controller comparing the results for different levels of model detail. It was shown that results accurate and close to noise related errors can be achieved by the most complete model. It was also demonstrated that convergence to false results is possible if there is insufficient redundancy in sampled data. The calibrated hand controller will be used for the sensor fault diagnostic investigations in the next chapter (Chapter 6).

Although it is not practicable to include all the possible error sources in the kinematic model of the manipulator or to completely eliminate the measurement errors, "completeness" of the error model is essential for the improvement of manipulator

Table 5.3: Geometric parameters of hand controller (original model).

Parameters	Initial Data (Fig. 5.10)	Number of Parameters, Number of Data			
		18, 100 (Fig. 5.11)	29, 100 (Fig. 5.12)	29, 80 (Fig. 5.13)	11, 100 (Fig. 5.14)
g_1	3.2	3.2	3.173461	3.193645	3.205298
h_1	3.971	3.971	4.034977	3.975852	3.955817
r_{b_1}	4.5	4.5	4.509096	4.502355	4.511641
ϕ_1	-1.570796	-1.570796	-1.570796	-1.570796	-1.570796
g_2	3.2	3.2	3.201645	3.217218	3.160177
h_2	3.971	3.971	3.950613	3.954373	3.926413
r_{b_2}	4.5	4.5	4.544460	4.505825	4.453908
ϕ_2	2.617994	2.617994	2.621135	2.612856	2.610249
g_3	3.2	3.2	3.201614	3.206642	3.194134
h_3	3.971	3.971	3.956404	3.929489	3.961013
r_{b_3}	4.5	4.5	4.479113	4.481008	4.500263
ϕ_3	0.523599	0.523599	0.527184	0.526348	0.515576

calibration accuracy. Investigation of the calibration results of the three kinematic models of the hand controller, i.e., original model, improved model, and complete model, have verified this fact.

Table 5.4: Potentiometer parameters of hand controller (original model).

Pots		Initial Data (Fig. 5.10)	Number of Parameters, Number of Data			
			18, 100 (Fig. 5.11)	29, 100 (Fig. 5.12)	29, 80 (Fig. 5.13)	11, 100 (Fig. 5.14)
A1	Gain	-0.002835	-0.002858	-0.002834	-0.002835	-0.002835
	Offset	6.107738	6.158165	6.117719	6.110929	6.107738
A2	Gain	-0.002854	-0.002855	-0.002851	-0.002851	-0.002854
	Offset	3.941238	3.947740	3.946684	3.944997	3.941238
A3	Gain	0.002866	0.002889	0.002858	0.002865	0.002866
	Offset	-4.312349	-4.362966	-4.311623	-4.315299	-4.312349
B1	Gain	-0.002862	-0.002857	-0.002862	-0.002862	-0.002862
	Offset	6.137053	6.130026	6.135088	6.135751	6.137053
B2	Gain	-0.002897	-0.002898	-0.002898	-0.002898	-0.002897
	Offset	3.938330	3.936331	3.940422	3.937272	3.938330
B3	Gain	0.002916	0.002899	0.002916	0.002917	0.002916
	Offset	-4.426159	-4.391466	-4.420654	-4.423707	-4.426159
C1	Gain	-0.002900	-0.002901	-0.002903	-0.002904	-0.002900
	Offset	6.264743	6.255185	6.258089	6.255867	6.264743
C2	Gain	-0.002877	-0.002865	-0.002875	-0.002876	-0.002877
	Offset	3.899044	3.881351	3.899519	3.899149	3.899044
C3	Gain	0.002916	0.002831	0.002829	0.002831	0.002834
	Offset	-4.257495	-4.258658	-4.267133	-4.261753	-4.257495

Table 5.5: Error of branch end distances of hand controller (original model).

Error		Initial Data (Fig. 5.10)	Number of Parameters, Number of Data 18, 100 (Fig. 5.11)	29, 100 (Fig. 5.12)	29, 80 (Fig. 5.13)	11, 100 (Fig. 5.14)
Min	p_0p_1	-0.0872	-0.0817	-0.0810	-0.0672	-0.0880
	p_1p_2	-0.1860	-0.1522	-0.1444	-0.0813	-0.1871
	p_0p_2	-0.3424	-0.2338	-0.2352	-0.0937	-0.3324
Max	p_0p_1	0.1129	0.1224	0.1244	0.0590	0.1198
	p_1p_2	0.1775	0.1254	0.1341	0.1004	0.1471
	p_0p_2	0.1853	0.1435	0.1039	0.1173	0.2009
Mean	p_0p_1	-0.0006	0.0018	0.0026	0.0001	-0.0003
	p_1p_2	0.0086	0.0010	0.0042	0.0041	-0.0001
	p_0p_2	-0.0073	0.0049	0.0018	0.0006	-0.0028
Stand Dev.	p_0p_1	0.0338	0.0331	0.0317	0.0248	0.0311
	p_1p_2	0.0479	0.0450	0.0444	0.0340	0.0439
	p_0p_2	0.0632	0.0465	0.0560	0.0396	0.0609
χ^2_f		–	14.1648	16.3414	7.1795	17.2745

Table 5.6: Geometric parameters of hand controller (improved model).

Parameters	Initial Data (Fig. 5.10)	Number of Parameters, Number of Data			
		44, 100 (Fig. 5.15)	44, 80 (Fig. 5.16)	26, 100 (Fig. 5.17)	44_{18}, 100 (Fig. 5.18)
g_1	3.2	3.198939	3.204473	3.195337	3.200154
h_1	3.971	3.994961	3.962060	3.968702	3.973587
r_{b_1}	4.5	4.489938	4.500802	4.475262	4.499897
ϕ_1	-1.570796	-1.570796	-1.570796	-1.570796	-1.570796
z_{b_1}	0.0	0.028670	0.025817	0.079756	0.002675
α_{b_1}	1.570796	1.580345	1.576226	1.584075	1.571908
l_1	0.0	0.003646	0.006262	0.019153	0.000115
k_1	0.0	0.075962	0.006200	0.054152	-0.000021
n_1	0.0	0.023181	-0.006451	0.056426	0.000364
g_2	3.2	3.173473	3.191265	3.154044	3.200205
h_2	3.971	3.951916	3.958156	3.949510	3.966436
r_{b_2}	4.5	4.539535	4.498916	4.472097	4.500251
ϕ_2	2.617994	2.617776	2.610990	2.609287	2.617651
z_{b_2}	0.0	-0.023297	0.002522	0.093480	-0.004963
α_{b_2}	1.570796	1.570448	1.567791	1.555079	1.571872
l_2	0.0	0.016592	0.000667	-0.055221	0.000093
k_2	0.0	0.021555	0.000934	0.068111	-0.000306
n_2	0.0	0.016396	0.002703	0.101155	0.000350
g_3	3.2	3.222696	3.191572	3.243870	3.200309
h_3	3.971	3.958969	3.943982	3.935360	3.968735
r_{b_3}	4.5	4.484903	4.496587	4.486140	4.499916
ϕ_3	0.523599	0.525337	0.521728	0.523271	0.523026
z_{b_3}	0.0	-0.010246	-0.026376	-0.011842	0.001141
α_{b_3}	1.570796	1.574667	1.571328	1.559703	1.570849
l_3	0.0	-0.021468	0.005784	-0.029549	0.000088
k_3	0.0	-0.018821	0.005532	0.060557	-0.000639
n_3	0.0	-0.023665	-0.007306	0.012834	0.000476

Table 5.7: Potentiometer parameters of hand controller (improved model).

Pots		Initial Data (Fig. 5.10)	# of Parameters, # of Data			
			44, 100 (Fig. 5.15)	44, 80 (Fig. 5.16)	26, 100 (Fig. 5.17)	44_{13}, 100 (Fig. 5.18)
A1	Gain	-0.002835	-0.002834	-0.002836	-0.002835	-0.002858
	Offset	6.107738	6.107747	6.107362	6.107738	6.158169
A2	Gain	-0.002854	-0.002855	-0.002853	-0.002854	-0.002855
	Offset	3.941238	3.944797	3.942741	3.941238	3.947760
A3	Gain	0.002866	0.002868	0.002865	0.002866	0.002889
	Offset	-4.312349	-4.306538	-4.313974	-4.312349	-4.362874
B1	Gain	-0.002862	-0.002863	-0.002862	-0.002862	-0.002857
	Offset	6.137053	6.135610	6.136637	6.137053	6.130223
B2	Gain	-0.002897	-0.002895	-0.002897	-0.002897	-0.002898
	Offset	3.938330	3.944482	3.938431	3.938330	3.936376
B3	Gain	0.002916	0.002916	0.002916	0.002916	0.002899
	Offset	-4.426159	-4.421999	-4.425478	-4.426159	-4.391378
C1	Gain	-0.002900	-0.002902	-0.002902	-0.002900	-0.002901
	Offset	6.264743	6.260374	6.260436	6.264743	6.255294
C2	Gain	-0.002877	-0.002876	-0.002876	-0.002877	-0.002865
	Offset	3.899044	3.899363	3.900643	3.899044	3.881379
C3	Gain	0.002916	0.002831	0.002833	0.002834	0.002831
	Offset	-4.257495	-4.263451	-4.259335	-4.257495	-4.258538

Table 5.8: Error of branch end distances of hand controller (improved model).

Error		Initial Data (Fig. 5.10)	Number of Parameters, Number of Data 44, 100 (Fig. 5.15)	44, 80 (Fig. 5.16)	26, 100 (Fig. 5.17)	44_{18}, 100 (Fig. 5.18)
Min	p_0p_1	-0.0872	-0.0781	-0.0683	-0.0653	-0.0840
	p_1p_2	-0.1860	-0.1419	-0.0742	-0.1050	-0.1529
	p_0p_2	-0.3424	-0.1813	-0.0888	-0.1775	-0.2291
Max	p_0p_1	0.1129	0.0899	0.0505	0.1121	0.1286
	p_1p_2	0.1775	0.1459	0.1098	0.1142	0.1247
	p_0p_2	0.1853	0.0991	0.1278	0.1261	0.1401
Mean	p_0p_1	-0.0006	0.0045	0.0005	-0.0006	0.0019
	p_1p_2	0.0086	0.0051	0.0040	0.0044	0.0008
	p_0p_2	-0.0073	-0.0026	0.0004	0.0006	0.0046
Stand Dev.	p_0p_1	0.0338	0.0303	0.0255	0.0286	0.0339
	p_1p_2	0.0479	0.0407	0.0337	0.0361	0.0441
	p_0p_2	0.0632	0.0548	0.0393	0.0431	0.0465
χ^2_f		–	14.9734	7.1639	10.6616	14.0879

Table 5.9: Geometric parameters of hand controller (complete model).

Parameters	Initial Data (Fig. 5.10)	Number of Parameters, Number of Data			
		59, 100 (Fig. 5.19)	59, $100_{0.2}$ (Fig. 5.23)	59, 80 (Fig. 5.20)	59, $80_{0.05}$ (Fig. 5.24)
g_1	3.2	3.201677	3.196779	3.180462	3.174734
h_1	3.971	3.980657	3.948663	3.912004	3.943473
r_{b_1}	4.5	4.484326	4.476707	4.469152	4.459386
ϕ_1	-1.570796	-1.570796	-1.570796	-1.570796	-1.570796
z_{b_1}	0.0	-0.253739	-0.181910	-0.075457	-0.079220
α_{b_1}	1.570796	1.408146	1.540430	1.449548	1.534335
l_1	0.0	-0.046741	0.000776	-0.041177	-0.042421
k_1	0.0	0.206070	0.133073	0.045082	0.017519
n_1	0.0	0.111697	0.030779	-0.171876	-0.057928
m_1	0.0	-0.079359	-0.003821	0.027653	0.011542
α_{1_1}	0.0	0.003522	0.006745	-0.003959	-0.002523
β_{1_1}	0.0	-0.003426	0.011272	-0.021061	-0.009648
α_{2_1}	-1.570796	-1.556652	-1.558325	-1.566367	-1.565149
α_{3_1}	1.570796	1.582672	1.571933	1.581121	1.581499
g_2	3.2	3.233133	3.154209	3.215394	3.154711
h_2	3.971	3.871653	3.875785	4.035625	3.954465
r_{b_2}	4.5	4.531589	4.534385	4.439414	4.440300
ϕ_2	2.617994	2.596396	2.607532	2.598488	2.610607
z_{b_2}	0.0	-0.447782	0.081690	-0.461685	-0.123631
α_{b_2}	1.570796	1.701556	1.624495	1.648200	1.604560
l_2	0.0	-0.065930	-0.096596	-0.079408	-0.081270
k_2	0.0	-0.052670	0.038128	-0.114281	-0.061973
n_2	0.0	-0.070113	-0.000887	0.338391	0.073101
m_2	0.0	0.147122	0.110902	-0.084096	-0.010319
α_{1_2}	0.0	0.003750	-0.001670	-0.007889	-0.011354
β_{1_2}	0.0	0.009342	0.004741	-0.008360	-0.011714
α_{2_2}	-1.570796	-1.569271	-1.568406	-1.568257	-1.567518
α_{3_2}	1.570796	1.587570	1.596707	1.590874	1.591419
g_3	3.2	3.126609	3.207265	3.133018	3.188008
h_3	3.971	3.883792	3.955714	3.929351	3.941367
r_{b_3}	4.5	4.369064	4.455846	4.348294	4.396894
ϕ_3	0.523599	0.526255	0.555894	0.499090	0.520648
z_{b_3}	0.0	0.741390	0.260741	0.473243	0.161409
α_{b_3}	1.570796	1.603927	1.546546	1.620837	1.580094
l_3	0.0	-0.129416	-0.181397	-0.098159	-0.113427
k_3	0.0	0.018939	0.007684	-0.001590	0.000505
n_3	0.0	-0.175227	-0.047112	-0.068016	-0.027991
m_3	0.0	0.029977	-0.055642	-0.090313	-0.062222
α_{1_3}	0.0	-0.002501	-0.009972	-0.007320	-0.010068
β_{1_3}	0.0	-0.020675	-0.031328	-0.015953	-0.022725
α_{2_3}	-1.570796	-1.571467	-1.570890	-1.576535	-1.576941
α_{3_3}	1.570796	1.603206	1.617549	1.595095	1.599463

Table 5.9: Geometric parameters of hand controller (complete model, cont'd).

Parameters	Initial Data (Fig. 5.10)	Number of Parameters, Number of Data			
		41, 100 (Fig. 5.21)	59_{18}, 100 (Fig. 5.22)	56, 100 (Fig. 5.25)	56, 80 (Fig. 5.26)
g_1	3.2	3.166298	3.199961	3.206883	3.178817
h_1	3.971	3.969441	3.972887	3.962485	3.900298
r_{b_1}	4.5	4.498939	4.500050	4.499735	4.459970
ϕ_1	-1.570796	-1.570796	-1.570796	-1.570796	-1.570796
z_{b_1}	0.0	0.106566	0.001934	0.000000	0.000000
α_{b_1}	1.570796	1.581603	1.572279	1.582442	1.571821
l_1	0.0	0.013839	-0.000085	0.006967	-0.038138
k_1	0.0	0.005318	0.000139	0.011460	0.038580
n_1	0.0	-0.006932	0.000628	-0.000608	-0.206182
m_1	0.0	0.017767	0.000507	-0.030772	0.036304
α_{1_1}	0.0	0.001697	0.000330	-0.000063	-0.003808
β_{1_1}	0.0	-0.003710	0.001157	-0.001202	-0.020723
α_{2_1}	-1.570796	-1.565148	-1.567451	-1.562314	-1.566726
α_{3_1}	1.570796	1.567311	1.570818	1.569042	1.580595
g_2	3.2	3.170404	3.199887	3.183573	3.213425
h_2	3.971	3.894649	3.964915	3.965694	4.042111
r_{b_2}	4.5	4.487260	4.500438	4.503227	4.463572
ϕ_2	2.617994	2.615472	2.616480	2.614738	2.594595
z_{b_2}	0.0	0.073004	-0.004893	0.000000	0.000000
α_{b_2}	1.570796	1.557946	1.572234	1.580631	1.574415
l_2	0.0	-0.007904	0.000144	-0.000025	-0.079378
k_2	0.0	-0.005677	-0.000400	0.008296	-0.087384
n_2	0.0	-0.005006	0.000273	-0.002596	0.370343
m_2	0.0	0.054427	-0.000366	-0.002699	-0.095957
α_{1_2}	0.0	0.006302	0.000111	-0.001078	-0.007880
β_{1_2}	0.0	-0.010280	0.000948	-0.011598	-0.008544
α_{2_2}	-1.570796	-1.561383	-1.564004	-1.556247	-1.568165
α_{3_2}	1.570796	1.572787	1.570760	1.570803	1.591115
g_3	3.2	3.216336	3.200365	3.201291	3.133641
h_3	3.971	3.940308	3.972648	3.994966	3.924615
r_{b_3}	4.5	4.486705	4.499946	4.499963	4.381387
ϕ_3	0.523599	0.526730	0.522610	0.512284	0.502431
z_{b_3}	0.0	-0.025099	0.001858	0.000000	0.000000
α_{b_3}	1.570796	1.580581	1.571399	1.572435	1.572624
l_3	0.0	-0.003391	-0.000050	0.001394	-0.097188
k_3	0.0	0.014350	-0.000649	0.004939	-0.023888
n_3	0.0	-0.004681	0.000327	-0.008500	-0.085930
m_3	0.0	-0.017060	-0.002139	-0.002093	-0.088252
α_{1_3}	0.0	-0.010552	0.000208	-0.002159	-0.007380
β_{1_3}	0.0	-0.024835	-0.002442	-0.003740	-0.016212
α_{2_3}	-1.570796	-1.584733	-1.560380	-1.592950	-1.576357
α_{3_3}	1.570796	1.571650	1.570809	1.570445	1.595464

Table 5.10: Potentiometer parameters of hand controller (complete model).

Pots		Initial Data (Fig. 5.10)	Number of Parameters, Number of Data			
			59, 100 (Fig. 5.19)	59, $100_{0.2}$ (Fig. 5.23)	59, 80 (Fig. 5.20)	59, $80_{0.05}$ (Fig. 5.24)
A1	Gain	-0.002835	-0.002808	-0.002805	-0.002852	-0.002848
	Offset	6.107738	6.087789	6.083789	6.157558	6.155365
A2	Gain	-0.002854	-0.002897	-0.002874	-0.002862	-0.002851
	Offset	3.941238	4.093814	4.015475	3.982734	3.960423
A3	Gain	0.002866	0.002840	0.002869	0.002899	0.002876
	Offset	-4.312349	-4.284238	-4.305869	-4.356167	-4.326979
B1	Gain	-0.002862	-0.002784	-0.002862	-0.002807	-0.002861
	Offset	6.137053	6.087782	6.143600	6.128576	6.169469
B2	Gain	-0.002897	-0.002821	-0.002864	-0.002851	-0.002881
	Offset	3.938330	3.842957	3.930491	3.897352	3.942937
B3	Gain	0.002916	0.002951	0.002935	0.002837	0.002902
	Offset	-4.426159	-4.444318	-4.427705	-4.340879	-4.407587
C1	Gain	-0.002900	-0.003014	-0.002937	-0.003007	-0.002951
	Offset	6.264743	6.354885	6.293872	6.367300	6.329081
C2	Gain	-0.002877	-0.002855	-0.002845	-0.002911	-0.002866
	Offset	3.899044	3.860956	3.898775	3.978671	3.901511
C3	Gain	0.002916	0.002875	0.002840	0.002853	0.002841
	Offset	-4.257495	-4.301989	-4.270619	-4.274745	-4.264591

Table 5.10: Potentiometer parameters of hand controller (complete model, cont'd).

Pots		Initial Data (Fig. 5.10)	Number of Parameters, Number of Data			
			41, 100 (Fig. 5.21)	59_{18}, 100 (Fig. 5.22)	56, 100 (Fig. 5.25)	56, 80 (Fig. 5.26)
A1	Gain	-0.002835	-0.002835	-0.002858	-0.002836	-0.002853
	Offset	6.107738	6.107738	6.158168	6.107876	6.146364
A2	Gain	-0.002854	-0.002854	-0.002855	-0.002853	-0.002863
	Offset	3.941238	3.941238	3.947708	3.942984	3.984732
A3	Gain	0.002866	0.002866	0.002889	0.002866	0.002907
	Offset	-4.312349	-4.312349	-4.362808	-4.312502	-4.364679
B1	Gain	-0.002862	-0.002862	-0.002857	-0.002862	-0.002809
	Offset	6.137053	6.137053	6.130165	6.136581	6.034040
B2	Gain	-0.002897	-0.002897	-0.002898	-0.002897	-0.002854
	Offset	3.938330	3.938330	3.936406	3.938517	3.902186
B3	Gain	0.002916	0.002916	0.002899	0.002916	0.002829
	Offset	-4.426159	-4.426159	-4.391397	-4.426813	-4.333076
C1	Gain	-0.002900	-0.002900	-0.002901	-0.002902	-0.003005
	Offset	6.264743	6.264743	6.255295	6.261793	6.474375
C2	Gain	-0.002877	-0.002877	-0.002865	-0.002876	-0.002913
	Offset	3.899044	3.899044	3.881349	3.899558	3.982803
C3	Gain	0.002916	0.002834	0.002831	0.002833	0.002857
	Offset	-4.257495	-4.257495	-4.258576	-4.259635	-4.279379

Table 5.11: Error of branch end distances of hand controller (complete model).

Error		Initial Data (Fig. 5.10)	Number of Parameters, Number of Data			
			59, 100 (Fig. 5.19)	59, $100_{0.2}$ (Fig. 5.23)	59, 80 (Fig. 5.20)	59, $80_{0.05}$ (Fig. 5.24)
Min	p_0p_1	-0.0872	-0.0631	-0.0575	-0.0441	-0.0351
	p_1p_2	-0.1860	-0.0611	-0.0481	-0.0492	-0.0474
	p_0p_2	-0.3424	-0.1281	-0.1444	-0.0352	-0.0427
Max	p_0p_1	0.1129	0.0641	0.0930	0.0344	0.0415
	p_1p_2	0.1775	0.0645	0.0690	0.0501	0.0716
	p_0p_2	0.1853	0.0650	0.0615	0.0406	0.0409
Mean	p_0p_1	-0.0006	-0.0035	-0.0034	-0.0015	-0.0017
	p_1p_2	0.0086	0.0012	0.0015	0.0014	0.0008
	p_0p_2	-0.0073	-0.0008	0.0055	0.0009	0.0003
Stand	p_0p_1	0.0338	0.0237	0.0258	0.0166	0.0159
Dev.	p_1p_2	0.0479	0.0208	0.0218	0.0179	0.0197
	p_0p_2	0.0632	0.0310	0.0329	0.0167	0.0180
χ^2_f		–	5.2404	6.0492	1.8776	2.0718

Table 5.11: Error of branch end distances of hand controller (complete model, cont'd).

Error		Initial Data (Fig. 5.10)	Number of Parameters, Number of Data			
			41, 100 (Fig. 5.21)	59_{18}, 100 (Fig. 5.22)	56, 100 (Fig. 5.25)	56, 80 (Fig. 5.26)
Min	p_0p_1	-0.0872	-0.0584	-0.0694	-0.0777	-0.0449
	p_1p_2	-0.1860	-0.1354	-0.1532	-0.1636	-0.0502
	p_0p_2	-0.3424	-0.2200	-0.2277	-0.2597	-0.0357
Max	p_0p_1	0.1129	0.0948	0.1274	0.1174	0.0351
	p_1p_2	0.1775	0.0929	0.1398	0.1326	0.0495
	p_0p_2	0.1853	0.0833	0.1156	0.2118	0.0389
Mean	p_0p_1	-0.0006	-0.0024	0.0037	0.0091	-0.0015
	p_1p_2	0.0086	-0.0035	0.0011	0.0017	0.0014
	p_0p_2	-0.0073	0.0011	0.0041	0.0014	0.0008
Stand	p_0p_1	0.0338	0.0243	0.0332	0.0385	0.0168
Dev.	p_1p_2	0.0479	0.0339	0.0460	0.0459	0.0178
	p_0p_2	0.0632	0.0373	0.0454	0.0581	0.0167
χ^2_f		–	8.2986	14.1544	18.8764	1.8829

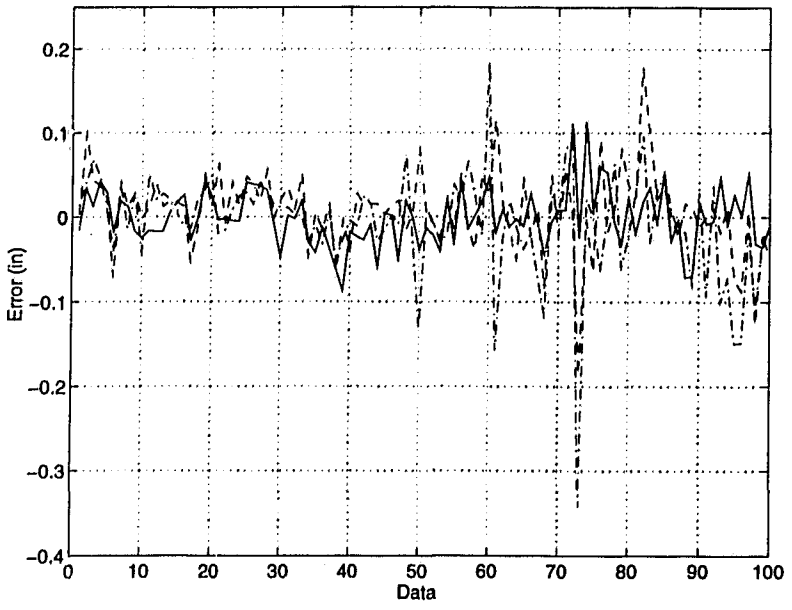

Figure 5.10: Error of initial branch end distances.

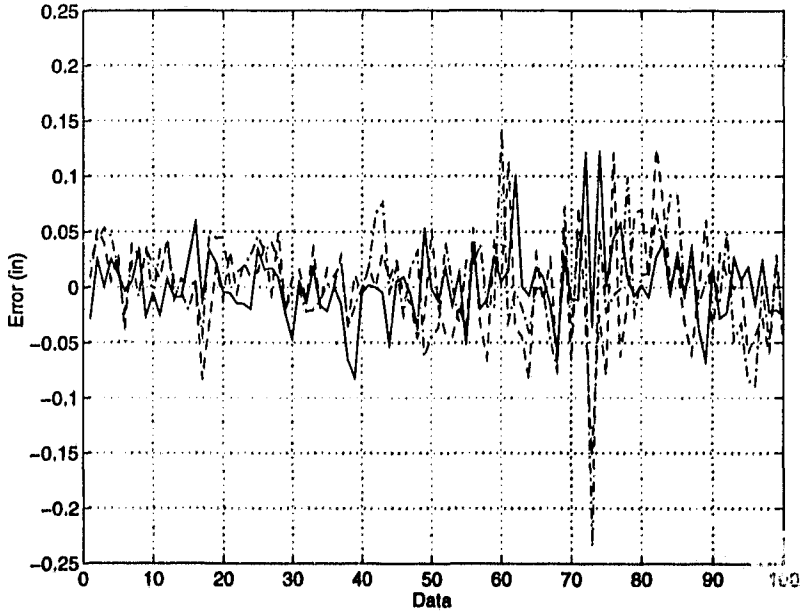

Figure 5.11: Error of branch end distances considering potentiometers only (18 parameters).

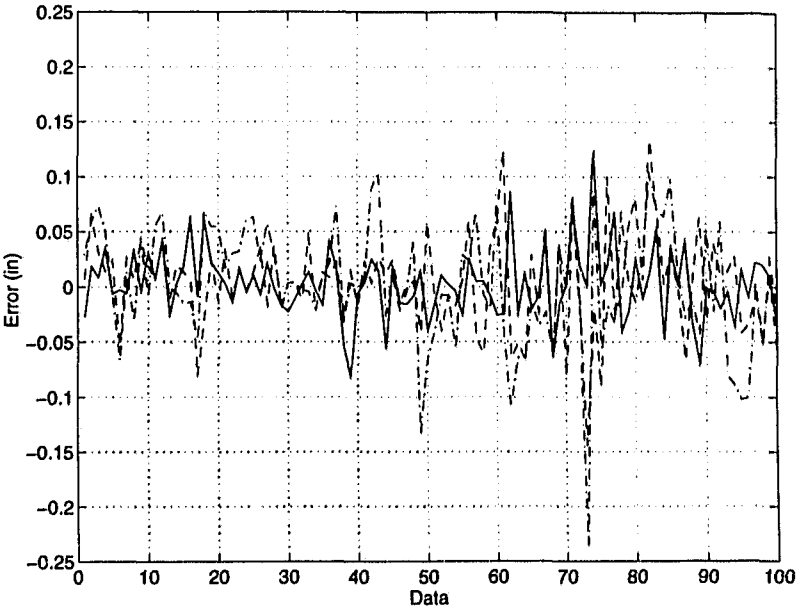

Figure 5.12: Error of branch end distances for original model (29 parameters).

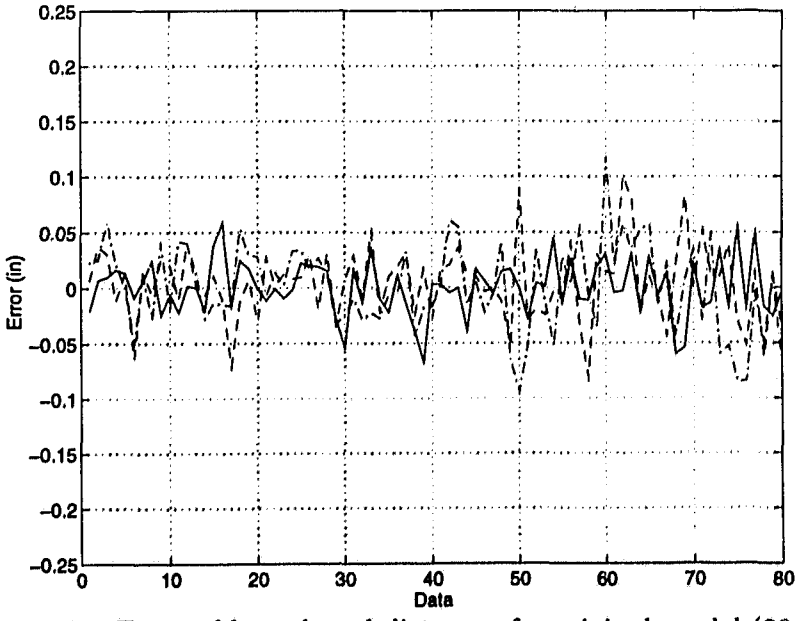

Figure 5.13: Error of branch end distances for original model (29 parameters).

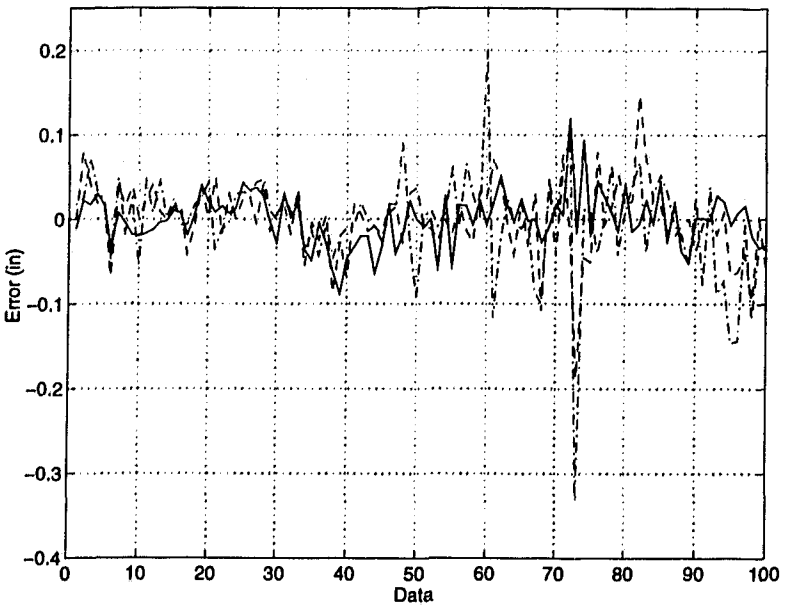

Figure 5.14: Error of branch end distances for original model (11 parameters).

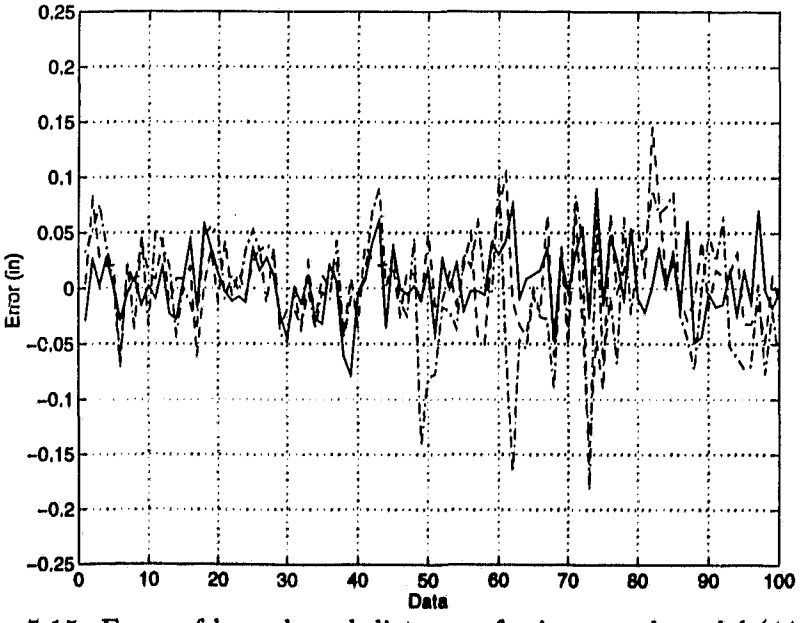

Figure 5.15: Error of branch end distances for improved model (44 parameters).

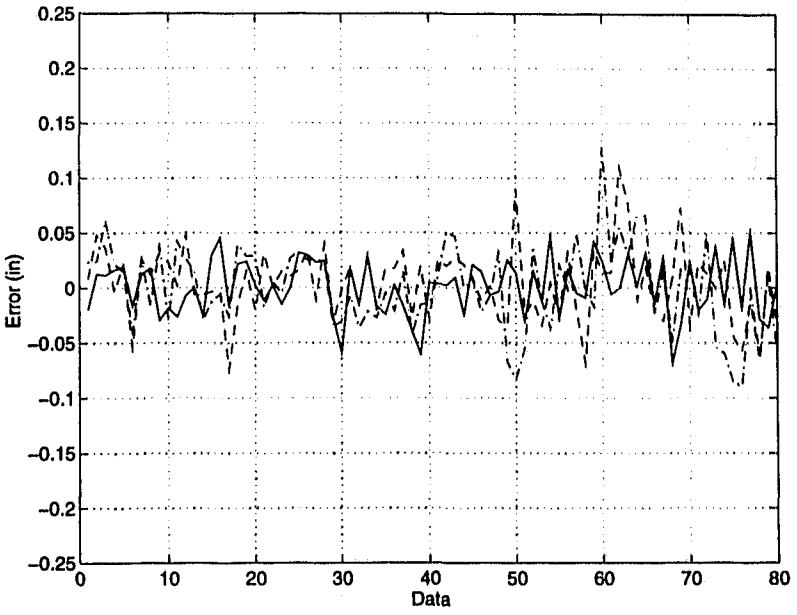

Figure 5.16: Error of branch end distances for improved model (44 parameters).

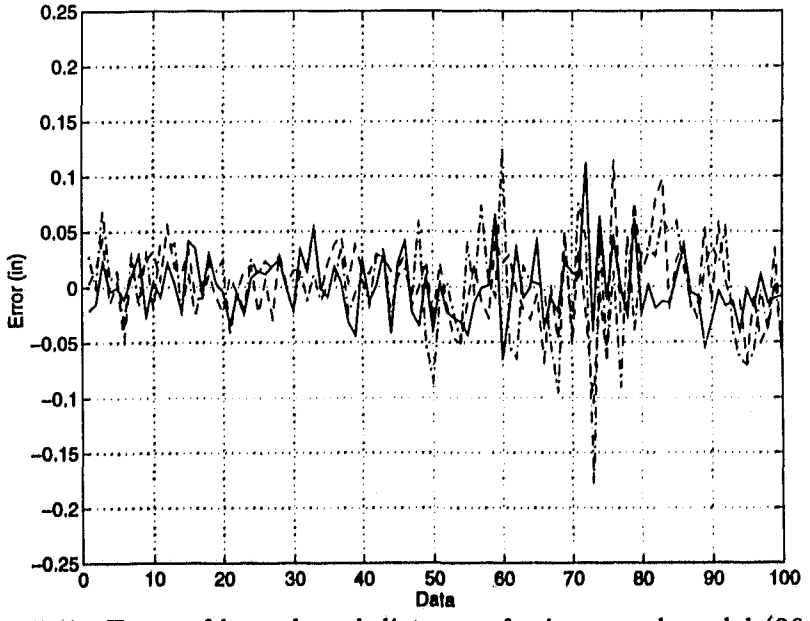

Figure 5.17: Error of branch end distances for improved model (26 parameters).

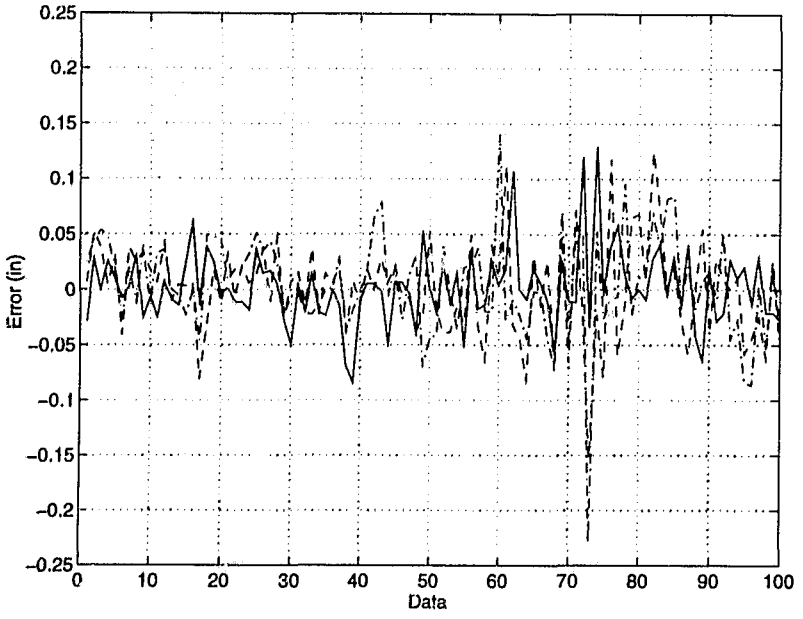

Figure 5.18: Error of branch end distances for improved model (44_{18} parameters).

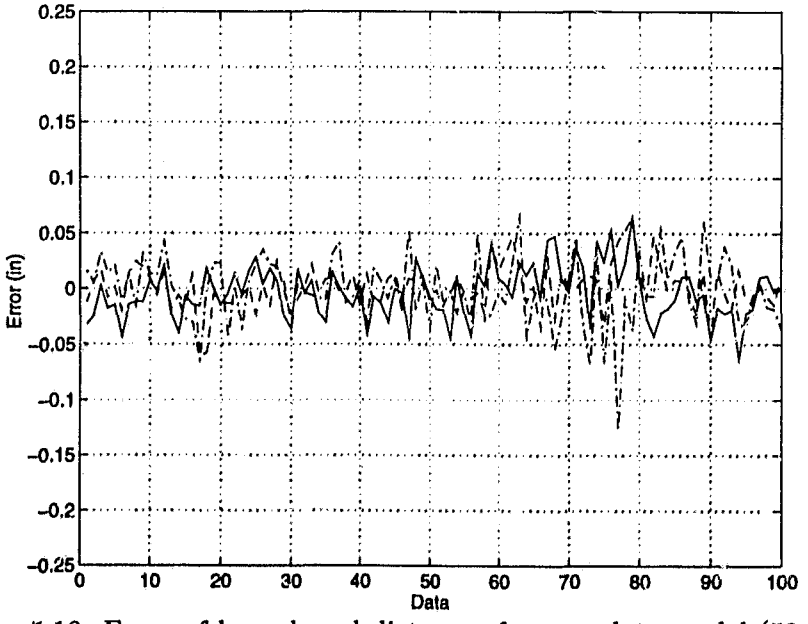

Figure 5.19: Error of branch end distances for complete model (59 parameters).

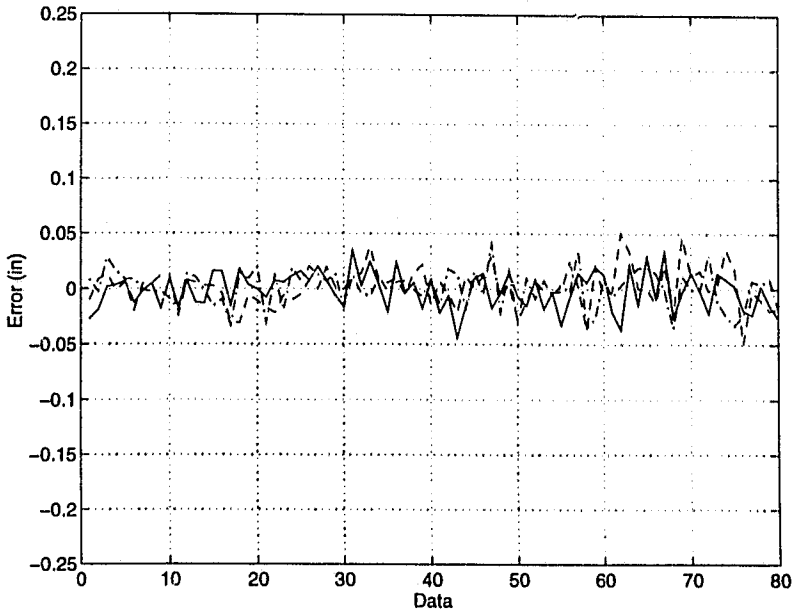

Figure 5.20: Error of branch end distances for complete model (59 parameters).

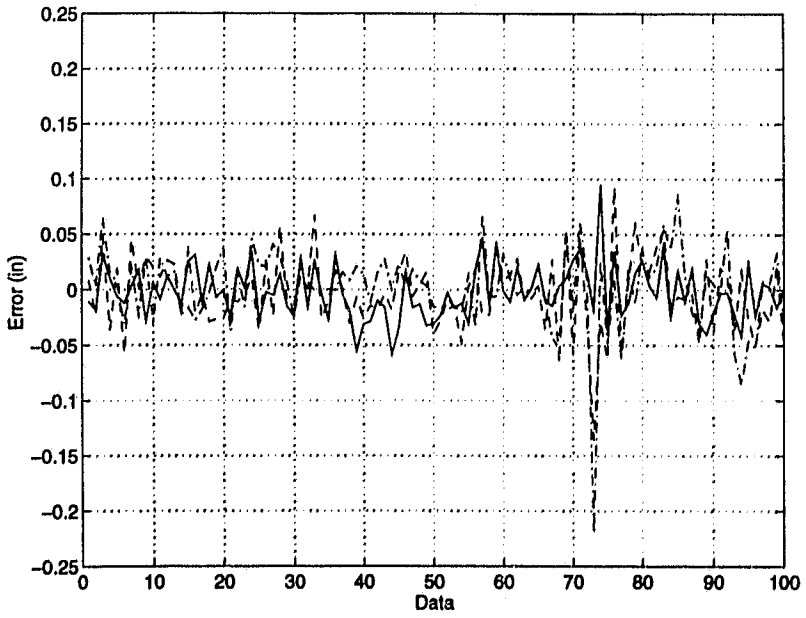

Figure 5.21: Error of branch end distances for complete model (41 parameters).

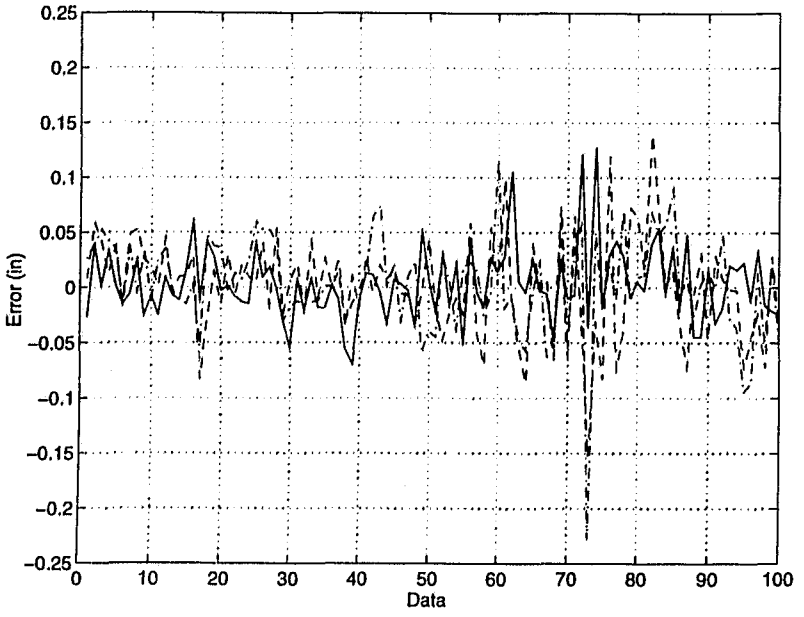

Figure 5.22: Error of branch end distances for complete model (59_{18} parameters).

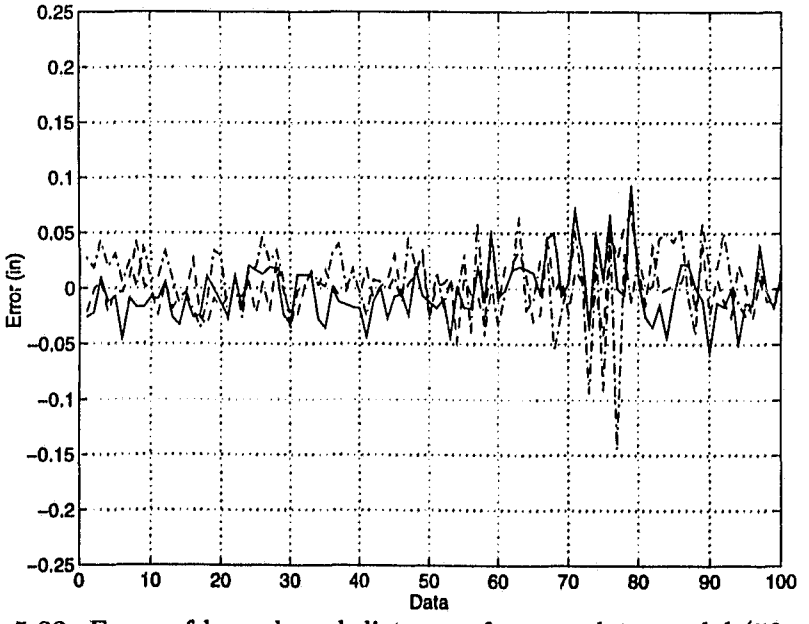

Figure 5.23: Error of branch end distances for complete model ($59_{0.2}$ parameters).

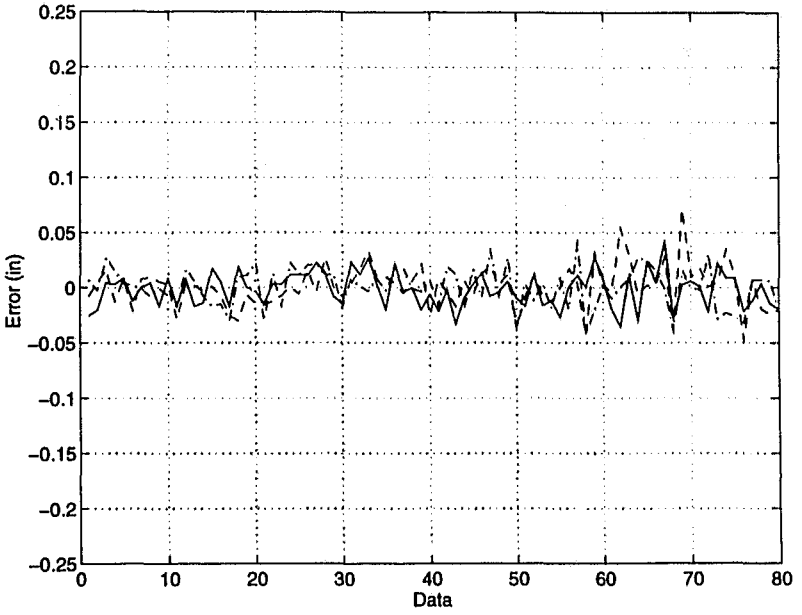

Figure 5.24: Error of branch end distances for complete model ($59_{0.05}$ parameters).

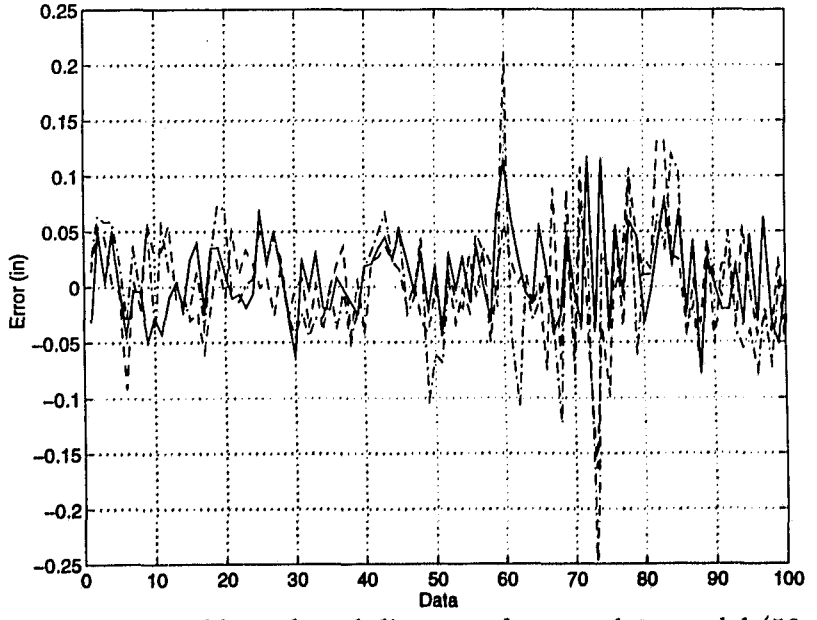

Figure 5.25: Error of branch end distances for complete model (56_z parameters).

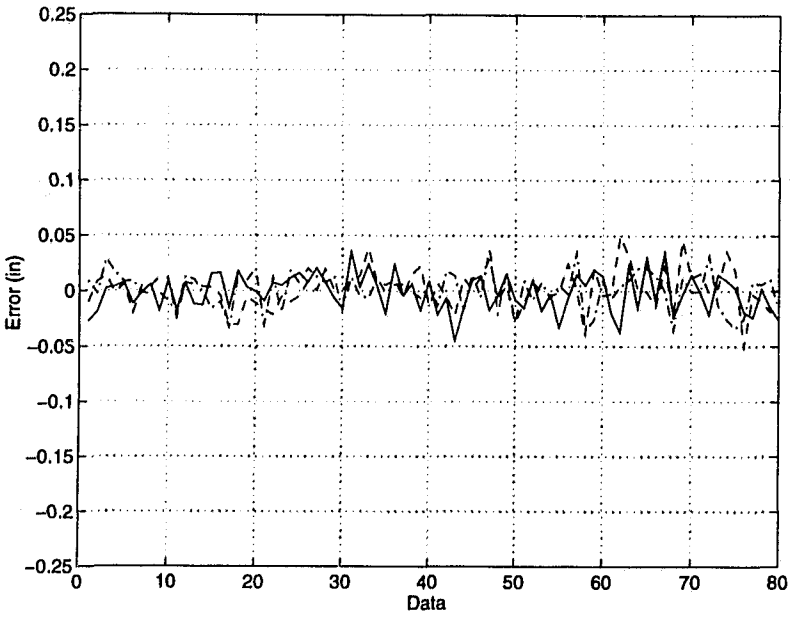

Figure 5.26: Error of branch end distances for complete model (56_z parameters).

Chapter 6

Fault Detection and Fault Tolerant Operation

Fault detection and fault tolerance are of great importance in the design of autonomous systems. The ability to detect and tolerate component failure within manipulators, e.g., joint sensors and actuators, enables the manipulators to finish their task successfully without any interruptions. Continuous operation of manipulators is more critical for remote applications and in hazardous environments where high reliability and safety are required. Redundant sensing and/or actuation of parallel manipulators can be employed to improve reliability of manipulators and to enhance their robustness and performance.

Sensor failure detection methods for the considered class of three-branch parallel manipulators of Section 1.5 are investigated in this chapter. These methods are based on the forward displacement solutions discussed in Chapter 2 and further geometric considerations. Redundant sensing of all main-arm joints for all feasible combinations of revolute and prismatic joints is considered. The sensor failure detection scheme is combined with a full set of solutions for various sensing combinations to allow fault

tolerant operation after a failure detection.

6.1 Sensor Fault Detection Scheme

The solutions presented in Chapter 2 can be utilized to diagnose the failed sensor(s) of a redundantly sensed (actuated) three-branch parallel manipulator. Sensing all three main-arm joints of a branch i allows the location of the center point p_i of the passive spherical branch end to be determined as a function of the sensed joint displacements. When all main-arm joints are sensed and all of the sensors are perfect - perfect in the sense of negligible reading error - the exact locations of p_i, $i = 1, 2, 3$, are known (assuming accurately identified link parameters). Since the passive spherical joints are attached to the platform, p_i, $i = 1, 2, 3$, they can also be considered to be three points on the mobile platform. For all perfect joint sensors $\|\mathbf{p}_i - \mathbf{p}_j\| = p_ip_j$, $i, j = 1, 2, 3$ and $i \neq j$, where $\mathbf{p}_i$ represents the location of i-th branch end and the distance p_ip_j is the platform edge length and is a constant value.

Section 6.1.1 considers the potential of using combinations of two branches to identify the existence of failed sensors. Section 6.1.2 considers failed sensor identification using all three branches at the same time. Cases of more than one failed sensor are examined in Section 6.1.3 and a sensor fault detection summary and algorithm are presented in Section 6.1.4.

6.1.1 Combinations of Two Branches

When all of the sensors of branch i are perfect the exact location of the branch end p_i can be calculated. The location of branch end p_j is constrained by branch i to be on a sphere SP_{j_i} with center at p_i and radius p_ip_j equal to the distance between these

two branch ends. If main-arm joint l of branch j has a failed sensor (or the reading of sensor l is unknown) the location of branch end point p_j is also constrained to be on a circle C_{l_j}, if the failed sensor corresponds to a revolute joint l, with a center on the axis of the joint with failed sensor. If the sensor of a prismatic joint l is failed, due to the constraints of branch j, the branch end p_j must lie on a line L_{l_j} in the direction of the prismatic joint with a starting point at the branch j-th end location corresponding to zero joint displacement.

The first approach to identify the failed sensor of a branch can be characterized by considering only two branches, assuming one of the branches has perfect sensors and the other branch has one failed sensor. There will be up to two intersection points between a sphere and a circle and also between a sphere and a line. Considering two main-arm joint sensors at a time for a branch there are three different combinations. Thus, there will be three circles/lines corresponding to branch j and there will be three solution sets for p_j. Two of the three solution sets are obtained utilizing the reading of the failed sensor. The three solution sets in general will not have identical solutions, i.e., within acceptable tolerance corresponding to a negligible error in sensors' readings. If the failed sensor has a small drift there is a chance that all three solution sets have one close solution. However, it is not possible to distinguish the accurate solution set, i.e., to identify the failed sensor, unless the reading of failed sensor does not result in an intersection point.

If one of the sensors of branch i was failed and branch j did not have a failed sensor, the three solution sets obtained by the combinations of two sensors of branch j would not have a common solution. If there are no intersections between SP_{j_i} and $\mathsf{C}_{l_j}/\mathsf{L}_{l_j}$, $l = 1, 2, 3$, either branch i has at least one failed sensor or branch j has a minimum of two failed sensors. If there is one faulty sensor reading on each of the branches i and j, combinations of branches $i\&k$ and $j\&k$ can be utilized to identify the case

where more than one branch contains failed sensors. However, neither the branches with failed sensors nor the failed sensor of these branches can be marked using this approach. The first approach can be summarized as follows. (a) If the three solution sets of $\mathsf{SP}_{j_k} \cap (\mathsf{C}_{l_j}/\mathsf{L}_{l_j})$ have one identical solution, the sensors of branches j and k are accurate. Sensors of branch i can be checked from $\mathsf{SP}_{i_j} \cap (\mathsf{C}_{l_i}/\mathsf{L}_{l_i})$ knowing the exact location of p_j (center of SP_{i_j}). (b) If there is no common solution for $\mathsf{SP}_{j_i} \cap (\mathsf{C}_{l_j}/\mathsf{L}_{l_j})$ there are three possible cases: (1) branch i has at least one faulty joint displacement reading which can be identified using $\mathsf{SP}_{i_{j,k}} \cap (\mathsf{C}_{l_i}/\mathsf{L}_{l_i})$; (2) branch j has a minimum of one faulty reading which can be identified considering $\mathsf{SP}_{j_{i,k}} \cap (\mathsf{C}_{l_j}/\mathsf{L}_{l_j})$; or (3) both branches i and j have at least one inaccurate sensor each. Thus, all of the three branches should be examined - two at a time - to identify the branch with failed sensor(s). This procedure is applicable to 3-3-2 and 3-3-1 (number of perfect sensors of branch i, $i = 1, 2, 3$) configurations. It can also be used to determine if more than one branch has failed sensor, i.e., 3-2-2 and 3-2-1 cases.

6.1.2 Combinations of Three Branches

Another approach (second approach) to diagnose this problem exists for the 3-3-2 case where the exact location of two branch ends are known. Let branch end points p_i and p_j correspond to the branches with perfect sensors and branch k have a failed sensor.

The location of branch end point p_k is constrained by branches i and j to lie on a circle $\mathsf{C}_{i,j}$ with center at the projection of branch end p_k on the line defined by p_i and p_j. Considering one main-arm joint l of branch k, p_k is also constrained to be on a spatial surface SS_{l_k} depending on the layout and the type of main-arm joints of branch k. The intersection of this spatial surface and $\mathsf{C}_{i,j}$ will correspond to feasible p_k locations. Considering in turn all three main-arm joints of branch k generates

three sets of solutions. Two of these solution sets are obtained from the readings of accurate sensors and they will have one identical solution. The other set is obtained from the reading of the failed sensor which can be marked. Discarding the uncommon solution corresponding to the failed sensor the common solution will give the correct location of branch end p_k. If the sensors of branch k are accurate and either branch i or j has a faulty reading there will be no common solution, i.e., there will be different solutions potentially including no intersection cases. Other combination of branches should be considered as well to check for all of the sensors.

If only one sensor of a parallel manipulator is failed, utilizing this approach the branch k containing the faulty reading can be isolated. Also the failed sensor can be marked from the intersections of $\mathsf{C}_{i,j}$, $i, j \neq k$ and the spatial surface SS_{l_k} corresponding to the loci of potential branch end p_k locations.

6.1.3 Case of More than One Failed Sensor

To diagnose the faulty sensors of a branch with more than one failed sensor let branch end points p_i and p_j correspond to the branches with perfect sensors and let branch k have two failed sensors. The location of branch end p_k is constrained by branches i and j to lie on a circle $\mathsf{C}_{i,j}$ with center at the projection of branch end p_k on the line passing through p_i and p_j. p_k is also constrained to be on a spatial surface. In this case, there will be three sets of solutions for p_k corresponding to each main-arm joint displacement of branch k - one of them representing the correct location (if the other branches do not have failed sensors). Therefore, the failed sensors cannot be identified unless the false reading(s) produces no intersection point (real point).

Knowledge of having a branch with at least two failed sensors gives a chance to replace/recalibrate one of the sensors. If the replaced/recalibrated sensor is one of the

failed ones there will remain only one failed sensor which can be identified applying the procedure discussed above. If the replaced sensor was the only accurate one or if all of the three sensors were failed there will still remain two failed sensors that are known. It should be noted that in general two sensors of a branch do not fail at the same time. Therefore, the first sensor of a branch which fails can be identified (and recalibrated) and then the second one can be marked when it fails. Note that when the failed sensor of a branch is identified, if before recalibrating that sensor a sensor of another branch fails the second failed sensor can also be identified (after calculating the correct location of the branch with the already known failed sensor from the intersections of sphere and circle/line as discussed in Chapter 2) and hence both of the failed sensors can be identified.

6.1.4 Fault Detection Summary

If only one branch possesses a failed sensor the first and the second approaches can be utilized to identify the branch with the failed sensor. The failed sensor of the branch can be marked employing the second approach. The first approach can also be used to identify if there exist more than one failed sensor on a branch or if more than one branch has a failed sensor, whereas these two cases cannot be distinguished by the second approach. When two branches of a parallel manipulator have failed sensors simultaneously, i.e., 3-2-2 case, neither of these approaches are applicable to mark the branches and the corresponding joints with failed sensors.

Sensor Fault Detection Algorithm

Step 1a. Check if any sensor is failed by calculating $\|\mathbf{p}_i - \mathbf{p}_j\|$, $i, j = 1, 2, 3$ and $i \neq j$.

If these values are equal to the fixed lengths $p_i p_j$ within a specified tolerance,

the sensors of the branches can be considered accurate.

- If $(\|\mathbf{p}_i - \mathbf{p}_k\| - p_i p_k)$ and $(\|\mathbf{p}_j - \mathbf{p}_k\| - p_j p_k)$ are larger than the tolerance $\Rightarrow$ branch k has at least one failed sensor.
- The branch with a failed sensor cannot be identified if only $(\|\mathbf{p}_i - \mathbf{p}_k\| - p_i p_k)$ is larger than the tolerance, if all of the branch end distances satisfy the tolerance, or if none of the branch end distances satisfy the tolerance.

Step 1b. Use two branches at a time to mark the branch with failed sensor(s).

- If $\mathsf{SP}_{j_i} \cap (\mathsf{C}_{l_j}/\mathsf{L}_{l_j})$, $l = 1, 2, 3$, have a common solution $\Rightarrow$ sensors of branches i and j are accurate.
- If $(\mathsf{SP}_{j_i} \& \mathsf{SP}_{j_k}) \cap (\mathsf{C}_{l_j}/\mathsf{L}_{l_j})$, $l = 1, 2, 3$, do not have associated common solutions but $\mathsf{SP}_{i_k} \cap (\mathsf{C}_{l_i}/\mathsf{L}_{l_i})$, $l = 1, 2, 3$, have one common solution $\Rightarrow$ branch j has a failed sensor(s).
- If both $\mathsf{SP}_{j_i} \cap (\mathsf{C}_{l_j}/\mathsf{L}_{l_j})$ and $\mathsf{SP}_{k_i} \cap (\mathsf{C}_{l_k}/\mathsf{L}_{l_k})$, $l = 1, 2, 3$, do not have associated common solutions and also there is either no common solution or no solution for any of both $(\mathsf{SP}_{i_j} \& \mathsf{SP}_{i_k}) \cap (\mathsf{C}_{l_i}/\mathsf{L}_{l_i})$, $l = 1, 2, 3 \Rightarrow$ at least two branches have failed sensors.

Step 2. Use all three branches to mark joint(s) with failed sensor.

- If there is only one branch k with a faulty joint displacement reading,
  - If two of $\mathsf{C}_{i,j} \cap \mathsf{SS}_{l_k}$, $l = 1, 2, 3$, have a common solution they correspond to the joints with accurate sensors and the other joint has a failed sensor.
  - If no pairs of $\mathsf{C}_{i,j} \cap \mathsf{SS}_{l_k}$, $l = 1, 2, 3$, have a common solution $\Rightarrow$ at least two joint sensors are failed. If there only exists a solution for one l, then joint l_k has an accurate sensor.

- If two branches j and k have failed sensors,
  - If the sensors fail simultaneously, the branches with failed sensors cannot be identified and neither can be the corresponding joints.
  - If before calibrating one known failed sensor of branch j a sensor of another branch fails, the second sensor with faulty reading can be identified from $\mathsf{C}_{i,j} \cap \mathsf{SS}_{l_k}$, $l = 1, 2, 3$ after calculating the correct location of branch end p_j considering the two branches i and j.
  - If before calibrating one known failed sensor of branch j, two sensors of another branch fail, the second branch with faulty sensor readings would be identified considering two branches at a time (step 1b) after calculating the correct location of branch end p_j. However, since the correct location of p_j cannot be judged, the branch with failed sensors cannot be identified (unless p_j is brought to a known position).

6.2 Example Manipulator

The proposed sensor failure detection algorithm has been implemented in a computer simulation of the three-branch parallel manipulator depicted in Figure 2.4. The example manipulator is modeled using two levels of kinematic parameters, referred to as the original model and the improved model (Figure 6.1). The values of the parameters have been calculated from the kinematic calibration of the hand controller (Chapter 5) considering the two models. The original model is a calibrated version of the model of the RSI hand controller that is specified by the manufacturer. Further potential machining tolerances and assembly inaccuracies are considered in the improved model. The assumptions made for the improved model of a branch are that the first and the second joint axes are parallel, that the second and the third joint

axes are intersecting and perpendicular, and that the last three joints of each branch define a spherical joint group with center at the intersection of the forth joint with the fifth joint.

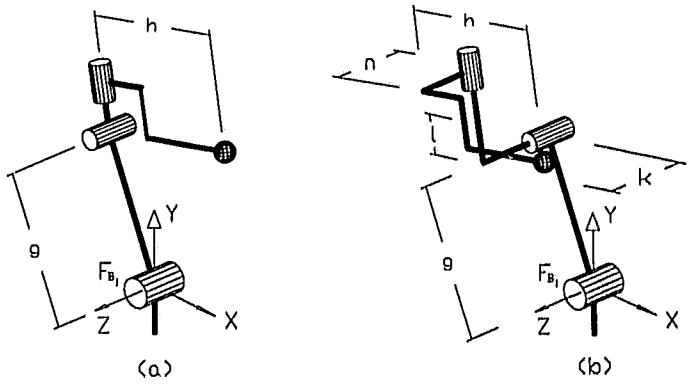

Figure 6.1: Branch layout: (a) Original model; (b) Improved model.

Detailed description of the example three-branch manipulator is given in the previous chapters. In particular, the original and the improved models, including the reference frames adopted for the models and branch displacement solutions, are discussed in Sections 5.2.1 and 5.2.2. The link parameters associated with the models are reproduceed in Figure 6.1 for reference.

6.2.1 Displacement Solutions Used in Failed Sensor Identification

In the following discussion the point coordinates and the directions will be defined with respect to the branch reference frame F_{B_i} unless otherwise specified.

Combinations of two branches

If all main-arm joints of branch i are sensed the location of p_i can be evaluated. The potential locations of the end of branch j can be evaluated by considering the intersection of a sphere SP_{j_i} and the circle C_{l_j}, where C_{l_j} is obtained excluding readings of the l-th joint sensor of branch j. The sphere SP_{j_i} will be centered at p_i and will have a radius equal to $p_i p_j = 2r_p \cos(\frac{\pi}{3})$. The potential circles for C_{l_j} are as follows.

Original model

- If the sensor reading of the first joint of branch j is excluded in the analysis, C_{1_j} has a center q_j having coordinates of $\{0, 0, hC_3\}_j^T$ and a radius $q_j p_j = \left(|g^2 + h^2 {S_3}^2 + 2ghC_2S_3|_j\right)^{\frac{1}{2}}$. The normal to the plane of C_{1_j} is $\{0, 0, 1\}_j^T$, i.e., in the direction of the first joint.

- If the sensor reading of the second joint of branch j is excluded, C_{2_j} has a center q_j having coordinates of $\{gC_1, gS_1, hC_3\}_j^T$ and a radius $q_j p_j = |hS_3|_j$. The normal to the plane of C_{2_j} is $\{0, 0, 1\}_j^T$, i.e., in the direction of the second joint.

- If the sensor reading of the third joint of branch j is excluded, C_{3_j} has a center q_j having coordinates of $\{gC_1, gS_1, 0\}_j^T$ and a radius $q_j p_j = h_j$. The normal to the plane of C_{3_j} is $\{-S_{12}, C_{12}, 0\}_j^T$, i.e., in the direction of the third joint.

Improved model

- If the sensor reading of the first joint of branch j is excluded in the analysis, C_{1_j} has a radius of $q_j p_j = \left(|g^2 + (hS_3 + nC_3)^2 + l^2 + 2g(hC_2S_3 - lS_2 + nC_2C_3)|_j\right)^{\frac{1}{2}}$

and a center q_j having coordinates of $\{0, 0, hC_3 + k - nS_3\}_j^T$. The normal to the plane of C_{1_j} is $\{0, 0, 1\}_j^T$, i.e., in the direction of the first joint.

- If the sensor reading of the second joint of branch j is excluded, C_{2_j} has a center q_j having coordinates of $\{gC_1, gS_1, hC_3 + k - nS_3\}_j^T$ and a radius $q_jp_j = \left((hS_3 + nC_3)^2 + l^2\right)_j^{\frac{1}{2}}$. The normal to the plane of C_{2_j} is $\{0, 0, 1\}_j^T$, i.e., in the direction of the second joint.

- If the sensor reading of the third joint of branch j is excluded, C_{3_j} has a center q_j having coordinates of $\{gC_1 - lS_{12}, gS_1 + lC_{12}, k\}_j^T$ and a radius $q_jp_j = (h^2 + n^2)_j^{\frac{1}{2}}$. The normal to the plane of C_{3_j} is $\{-S_{12}, C_{12}, 0\}_j^T$, i.e., in the direction of the third joint.

Combinations of three branches

If all main-arm joints of branches i and j, $i, j = 1, 2$, or 3, $j \neq i$ are sensed the locations ${}^0\mathbf{p}_i$ and ${}^0\mathbf{p}_j$ can be evaluated. The location of the k-th branch end, ${}^0\mathbf{p}_k$, $k \neq i, j$, will be located on a circle, $C_{i,j}$, with center at ${}^0\mathbf{m} = \frac{1}{2}({}^0\mathbf{p}_i + {}^0\mathbf{p}_j)$ and radius $mp_k = 1.5r_p$. The plane of circle $C_{i,j}$ is normal to the platform edge p_ip_j, i.e., $C_{i,j}$ has a unit normal vector parallel to $\mathbf{u}_{ij} = ({}^0\mathbf{p}_j - {}^0\mathbf{p}_i)/\|\mathbf{p}_j - \mathbf{p}_i\|$. The location of p_k will correspond to the common solution of the intersection of $C_{i,j}$ with at least two out of three spatial surfaces generated utilizing the readings of one sensor of branch k at a time. Considering the readings of the first, the second, or the third main-arm joint sensor of branch k, the loci of branch end p_k will be a sphere, a torus, or a ring, respectively.

Original model

- If the first joint sensor of branch k is considered sensed, intersection of $\mathsf{C}_{i,j}$ and a sphere SP_k having a center at $\{gC_1, gS_1, 0\}_k^T$ and a radius equal to h, defines the potential p_k locations.

- If the second joint sensor of branch k is considered sensed, intersection of $\mathsf{C}_{i,j}$ and a torus TR_k having a center at $\{0,0,0\}_k^T$ with an offset of $|gS_2|_k$ and primary and secondary radii of $|gC_2|_k$ and h, yields the potential p_k locations.

- If the third joint sensor of branch k is considered sensed, intersection of $\mathsf{C}_{i,j}$ and a ring RG_k having a center at $\{0,0,hC_3\}_k^T$, an axis direction of $\{0,0,1\}_k^T$, and smaller and larger radii of $|g - hS_3|_k$ and $|g + hS_3|_k$, defines the potential p_k locations.

Improved model

- If the first joint sensor of branch k is considered sensed, intersection of $\mathsf{C}_{i,j}$ and a sphere SP_k having a center at $\{gC_1, gS_1, k\}_k^T$ and a radius equal to $(h^2 + l^2 + n^2)_k^{\frac{1}{2}}$, defines the potential p_k locations.

- If the second joint sensor of branch k is considered sensed, intersection of $\mathsf{C}_{i,j}$ and a torus TR_k having a center at $\{0,0,k\}_k^T$ with an offset of $|l - gS_2|_k$ and primary and secondary radii of $|gC_2|_k$ and $(h^2 + n^2)_k^{\frac{1}{2}}$, yields the potential p_k locations.

- If the third joint sensor of branch k is considered sensed, intersection of $\mathsf{C}_{i,j}$ and a ring RG_k having a center at $\{0,0,hC_3 + k - nS_3\}_k^T$, an axis direction of $\{0,0,1\}_k^T$, and smaller and larger radii of $|g - lS_{12} - (hS_3 + nC_3)|_k$ and $|g - lS_{12} + (hS_3 + nC_3)|_k$, defines the potential p_k locations.

6.3 Simulation and Implementation

The proposed sensor fault detection algorithm has been implemented in the computer simulation developed for the two kinematic models of the three-branch parallel manipulator of Section 6.2 (refer to Figures 2.4 and 6.1). In addition, the algorithm has been implemented for actual measurements on a RSI hand controller.

6.3.1 Simulation

The end positions of the branches with accurate sensors are calculated as discussed in Section 5.2. The branch with the failed sensor (branch k) is identified either considering the error of the branch end distances or considering permutations of three branches. If there exists an error in the sensors of a branch, the branch end distances that are calculated using the readings of the failed sensor(s) will have non-zero error and the branch end distance that is calculated using the readings of the sensors of the other two branches will have zero error. Permutations of three branches can be employed by assuming that two of the three branches have perfect readings and looking for the common solution of the position of the third branch, thus identifying the branch with failed sensor.

The failed sensors are identified considering the three branches as discussed in Section 6.2.1. The two common solutions corresponding to the end position of the branch with the failed sensor give the position of that branch end. The position of the branch with a failed sensor can also be identified considering the remaining eight accurate sensors and calculating the intersections of two circles ($C_{i,j}$ & C_k).

In simulation, the algorithm always identifies the failed sensor and the corresponding branch. The only exception occurs when the first or the second joints of a branch k has a failed sensor and the direction of the line connecting branch ends p_i and p_j is

parallel to the first (second) joint axis of branch k (e.g., when the mobile platform has zero orientation). In these configurations there exist an infinite number of solutions for the intersection of the circle $\mathsf{C}_{i,j}$ and the ring RG_k, i.e., the circle and ring are coplanar.

6.3.2 Implementation

The algorithm was implemented on a RSI hand controller. The implementation results were not as successful as the simulation results. Some of the problems that were observed were overcome during implementation procedure. However, detailed analysis of the hand controller's data was required to investigate the cause of the algorithmic failure. Some of these problems are as follows.

Tolerances

In the implementation of the algorithm, tolerances on common solutions had to be redefined. The tolerance on the common solution of the intersection point(s) of the circles $\mathsf{C}_{i,j}$ and the spatial surfaces SP_k, TR_k, and RG_k, is different for each branch k. These tolerances are used to compensate for remaining inaccuracies in the kinematic model and for the noise of the potentiometers. Because the effect of model and sensor inaccuracies depend on the manipulator configuration and it varies as the device moves, the tolerances need to be dynamic to maintain an optimal bound for sensing real failures at each configuration. This would require a through analysis of the hand controller's workspace to define the tolerances.

Identification of the branch with a failed sensor

Due to the modeling error and noise in sensor readings in some configurations none of the branch end distance errors satisfy the tolerance, and in some other configurations none of the branch end distance errors violate the tolerance. In addition, in some configurations two branch end distance errors satisfy the specified tolerance. In these cases the branch with the failed sensor cannot be identified.

The branch end distance errors might not satisfy a very small tolerance even if there is no faulty readings, or they might satisfy a "large" tolerance even in the presence of faulty readings, i.e., due to "large" thresholds some failures might be undetected. The tolerance on the branch end distances can be chosen from the calibration plots of each model reported in Chapter 5.

Identification of the failed sensor

In some cases there was no solution for circle and spatial surface intersection. This disables the ability to isolate a failed sensor within a branch.

End location calculation of the branch with failed sensor

After identifying the branch with a failed sensor and isolating the failed sensor, in the implementation it was found that there could be no solution for the intersection of two circles utilized in the algorithm. This was because none of the two solutions corresponding to the intersection of the circles with the common line of their planes satisfied the tolerance specified on the identical solutions, although they corresponded to the correct identification of the failed sensor. The tolerance cannot be increased because with "large" tolerance the faulty reading might be taken as the correct one.

For the levels of inaccuracies and noise present different values of the tolerance would have to be defined for each joint.

The above problem would not arise if the end position of the branch with the failed sensor is calculated by taking the average of the branch end positions which correspond to the common solutions and avoiding the solution of intersecting two circles. In addition, the branch end location can be calculated as the common solution of the intersection of one of the circles and a sphere having a cross-section of the other circle.

Due to the real time implementation problems mentioned above the proposed algorithm was investigated for the set of 100 data used in the calibration of the hand controller. These data were analyzed assuming that there was no drift in the potentiometers and examining the potential error cases which might cause algorithmic failure. Results of the analysis of the data are included as Section 6.4.

6.4 Data Analysis

The 100 data points used in the calibration process of the hand controller (Chapter 5) were analyzed for the fault diagnosis and the fault tolerant operation issues. The improved kinematic model of the hand controller was considered. The complete model would give a better result, but complete formulation of the geometric shapes (spatial curves and surfaces) and their characteristics (center points, radii, axes, etc.) had not been formulated in time for use in the real-time operation of the parallel device. In any case, the results of the calibration of the complete model did not show much improvement over the improved model. The parameters estimated from the calibration procedure utilizing 80 data points were employed. This is because the estimated parameters utilizing 80 data points give better response than the 100

data. However, in the fault detection implementation all of the 100 data points were investigated.

6.4.1 Fault Detection

The failed sensor of a branch can be identified by comparing the three solutions of the branch end locations employing readings of one joint sensor of the branch at a time (employing seven joint readings). This will correspond to the intersection of a circle $C_{i,j}$ and: a sphere; a torus; or a ring. Some of the data points correspond to the zero orientation of the mobile platform (within the specified tolerance). At these configurations there is an infinite solution for the intersection of the circle and the ring, i.e., they correspond to a singular configuration for the forward displacement problem (FDP) for seven sensed (3-3-1) joints. Table 6.1 summarizes the data analysis for the joint sensor fault detection. For the chosen tolerances a failed sensor within the first, the second, and the third branch would not have been identified for a total of 37, 33, and 43 data points, respectively. This failure to identify is due to the nonexistence of intersection point(s) between $C_{i,j}$ and the spatial surfaces. Combining all of the failures leads to a total of 74 data that did not work for fault detection. In addition, it should be noted that not all of the remaining 26 data will satisfy the tolerance on the identical solutions. It was found that there exists a common solution for a total of 11, 10, and 15 data points (out of remaining 26) for the first, the second, and the third branches, respectively. If the common solution cases are intersected it is found that a failed sensor can be identified for only three data points (data 4, 83, and 84) if we assume that any sensor on any branch may fail.

The failed sensor of a branch can also be identified utilizing eight joint readings. Eight out of the nine combinations of eight sensors will use the faulty sensor reading and may result in a large branch end distance error. The remaining combination will

only include the correct sensor readings. The 100 data were analyzed using eight sensor readings. The location of the branch end with a failed sensor corresponds to the intersection point(s) of two circles. The investigation also considers intersection of any one of the circles and a sphere having a cross-section of the other circle. This was done since a small error in a joint reading may change the plane of the circle which in turn will alter the intersection. The program also checks for the common solution of two circle-sphere solutions and assigns the average of common solution to the corresponding branch end location. If there is no common solution the intersection of two circles is investigated. The program will check the solution of only one of the circle-sphere intersections if there is no solution for the other circle-sphere, if there is no intersection for the two circles, or if the calculated branch end locations do not satisfy the tolerance on the error of branch end distances.

Table 6.2 summarizes the 62 data numbers that do not give a common solution for the branch end location (without any added sensor error) using the methodology discussed above. In Table 6.2 the data which do not have an intersection point or the ones that result in a large branch end distance error of the branch are excluded for that branch joint. The data that result in a branch end distance error excluding a main-arm joint reading of the branch (Table 6.3) and that do not give a common branch end solution excluding a joint reading of other branches (Table 6.2) are marked in Table 6.2. The tolerance for the common solution is taken to be 0.100 inches to investigate and illustrate the error of the common solution for the majority of data. It can be seen that although there are 71 data which give an intersection point that does satisfy the tolerance of 0.080 inches on the branch end distance error (Tables 6.3 and 6.4) 64 data (62 data of Table 6.2 and data 72 and 73 which are not listed in this table) result in no common solution for at least one branch. Therefore, "small" branch end distance error does not necessarily guarantee a common solution for a branch end location.

It can be concluded that the hand controller is not a good candidate to implement the sensor fault detection algorithm. A precisely manufactured and calibrated device with noise free joint displacement sensing is important for the implementation and real-time examination of the algorithm.

6.4.2 Fault Tolerant Operation - FDP Solution Using Eight Sensors

To test the suitability of the hand controller for fault tolerant operation the FDP of the hand controller was solved utilizing readings of eight out of nine sensors of the hand controller. The location of the branch end with a failed sensor corresponds to the intersection point(s) of two circles. To increase the robustness of the solution the investigation also considered intersection of any one of the circles and a sphere having a cross-section of the other circle. If there is no intersection for the two circles or if the calculated branch end locations do not satisfy the tolerance on the error of branch end distances the program will check for the common solution of two circle-sphere solutions. The program checks the solution of one of circle-sphere if the common solution does not satisfy the branch end distance error, if there is no common solution, or if there is no solution for one of the circle-sphere. It should be noted that this procedure is similar to the sensor fault diagnosis using eight sensors. The only difference is that the program first checks for the intersection of circles and then for the solution of circle-spheres.

The results of the analysis for 100 data are summarized in Table 6.3. Investigations show that when the first joint sensor of a branch is excluded more data numbers give no solution for the FDP. Whereas there are more solutions for the FDP when either the second or the third joint sensor is not considered, i.e., including the readings of

the first joint sensor. This is because the position and the orientation of the first joint axes have been modeled and the corresponding parameters have been calculated from the calibration of the hand controller (Chapter 5). The second joint axis of each branch is modeled to be parallel to the first joint axis and the second and the third joint axes are assumed to be intersecting and perpendicular. These assumptions along with the assumption of having a spherical branch end joint and the potentiometer noise could be the main source of the error which causes either no intersection between the spatial curves and surfaces or large errors in the branch end distances. It should be noted that the tolerance on the error of the branch end distances was chosen to be 0.080 inches based on the plot of this error for the improved model (Figure 5.15).

It can be seen from Tables 6.3 and 6.4 that there exist no solution for the FDP of 29 data points either because of no intersection between the circles or the circle-sphere (15 data) or because of large branch end distance error (14 data). 8, 3, or 7 out of 100 data points might result in no intersection for the FDP if a main-arm joint of the first, the second, or the third branch is failed, respectively. Precisely, 21 out of 29 data may not give intersection point and 14 data will not satisfy the chosen tolerance on the branch end distance error and 6 data (data 50, 54, 61, 72, 74, 80) may not give intersection and may not satisfy the branch end tolerance. This number car be increased or reduced by changing the tolerance on the branch end distance error. The maximum error occurs for data 73 where the error is 0.174 and 0.262 inches for the first and the third branches. It should be noted that the maximum branch end distance error (0.262 inches) for nine sensors corresponds to data 73 as well. If the tolerance on the error of the branch end distances is increased to 0.204 inches this number can be reduced to 15 (data corresponding to no intersection between circles and also circle-spheres) from 21. For a tolerance of 0.174 inches the number of data without solution can be reduced to 18 (including data numbers 54 and 73 with errors

of 0.203 and 0.262 inches respectively, and data corresponding to no intersection between circles and circle-spheres) from 29.

As it can be seen from Table 6.4, 13 out of 100 data points do not satisfy the tolerance on the branch end error for the case of using nine main-arm joint sensors. These 13 data also correspond to the data which result in a large branch end distance error for eight sensor case (except data number 54 which satisfies the tolerance when all nine sensors are used). Table 6.4 also summarizes the data numbers resulting in no solution for the eight sensor case excluding the 13 data which give a poor result using the nine sensor readings. It can be seen that there will remain 16 data that cannot be used in the fault tolerant operation of the hand controller using the FDP for eight sensors. These 16 data correspond to 20 different sensor failure cases. Considering 87 data (excluding the 13 poor data for nine sensors) there exist a total of $87 \times 9 = 783$ cases where 20 out of 783 cases have no solution, i.e., the algorithm failure rate is $20/783 = 2.6\%$. This failure must be due to the remaining inaccuracies in the kinematic model and the potentiometer noise. Therefore, it can be concluded that this algorithm is sensitive to the uncertainties in the kinematic model and also to the potentiometer noise. For implementation a device manufactured with improved tolerances and noise free methods of sensing would be preferred.

It should be noted that for many data points there are two solutions for the branch end location and both solutions satisfy the tolerance on the branch end distance error. In the simulation and data analysis it is not possible to identify the "correct" solution (except while choosing the common solution). However, in the real-time operation the "correct" solution can be easily identified from the previous location of that branch end.

6.5 Summary

A sensor failure detection scheme for fault tolerant operation of a class of three-branch parallel manipulators was presented. The algorithm is applicable for branches with a passive spherical branch end joint and can diagnose the failure of any linear or rotary main-arm joint sensor. The algorithm is based on considering potential loci of a branch end location and further geometric considerations and can be applied to a broad family of parallel manipulators.

It was presented that the algorithm works well in the simulation. The implementation of the algorithm for the real-time operation of an existing parallel device (a three-branch parallel hand controller) was not as successful. This was concluded (after analysis of results) to be due to the remaining inaccuracies in the kinematic model of the hand controller and potentiometer noise. The effect of these inaccuracies on the failure of proposed algorithm was investigated. It was presented that the algorithm can be very sensitive to these error sources. Tolerances were used to attempt to accommodate the effect of modeling errors. It was discussed that the tolerances should be large enough to compensate for the uncertainties and that the tolerances should not be too large otherwise the sensor failure might not be detected. In addition, it was verified that the effect of the inaccuracies in the kinematic model depends on the configuration of the device. Therefore, the tolerances should be dynamic to conform with the different poses of the parallel device. In addition, the fault detection and fault tolerance schemes are recommended to be implemented on the precisely manufactured and calibrated devises only. It is also recommended to employ low noise joint displacement sensors.

Table 6.1: Data analysis for fault detection of hand controller using seven sensors.

Branch #	Data Numbers Resulting in No Solution	
Branch 1	Sphere-Circle:	52, 61, 69, 89, 97
	Torus-Circle:	32, 42, 44, 55, 66, 76, 77, 97, 99
	Ring-Circle:	1*, 5*, 7*, 9, 15, 16, 17, 18, 19, 20, 22, 24, 25, 26, 27, 28, 40, 41, 42, 43, 45, 48, 54, 68, 92
Branch 2	Sphere-Circle:	72
	Torus-Circle:	44, 50
	Ring-Circle:	1*, 2, 3*, 5*, 7*, 9*, 13, 17, 18, 19, 21, 22, 23, 24, 25, 26, 28, 30, 31, 33, 39, 42, 43, 44, 47, 52, 53, 62, 67, 81, 87
Branch 3	Sphere-Circle:	47, 54, 62, 71, 80, 87, 88, 91
	Torus-Circle:	33, 43, 62, 65, 76
	Ring-Circle:	2, 8, 9, 10, 12, 19, 21, 22, 25, 26, 27, 35, 36, 37, 39, 41, 42, 43, 44, 45, 49, 56, 57*, 58, 63, 64, 68, 75, 81, 82, 85, 97
Remaining Data		
4, 6, 11, 14, 29, 34, 38, 46, 51, 59, 60, 70, 73, 74, 78, 79, 83, 84, 86, 90, 93, 94, 95, 96, 98, 100		
Data Numbers with Common Solutions		
Branch 1	4, 6, 34, 70, 73, 74, 83, 84, 90, 96, 100	
Branch 2	4, 46, 73, 78, 83, 84, 86, 95, 96, 98	
Branch 3	4, 38, 59, 70, 78, 79, 83, 84, 86, 90, 93, 94, 95, 98, 100	

*Infinite solution: coplanar ring and circle.

Table 6.2: Data analysis for fault detection of hand controller using eight sensors.

Data Numbers with No Common Solution* (Tolerance = 0.100 in)					
Data #	Branch #(s)	p_i location error (in)	Data #	Branch #(s)	p_i location error (in)
14	1, 2	0.302, 0.541	60†	1, 2	0.108, 0.454
15†	2	0.141	61†	2, 3	0.131, 0.165
16†	1	0.226	62†	1	0.295
17	2, 3	0.307, 0.327	63	2, 3	0.156, 0.115
18†	2, 3	0.222, 0.106	64	2	0.127
20	3	0.105	65	1	0.117
23	1	0.105	66	1	0.158
25	1	0.102	68	2	0.131
26	2	0.102	70	1, 2, 3	0.151, 0.113, 0.100
27	1	0.154	71†	1	0.106
28	2	0.136	74†	3	0.116
29	1, 2, 3	0.305, 0.227, 0.313	75†	2	0.106
30	1, 3	0.436, 0.269	76†	2, 3	0.117, 0.159
32	1, 2	0.289, 0.372	77	1, 3	0.235, 0.145
39	1	0.113	78†	2	0.140
41†	3	0.188	79	1, 2, 3	0.159, 0.261, 0.120
42†	2	0.109	80†	3	0.118
43†	2, 3	0.540, 0.274	81	2	0.129
44†	1	0.230	82†	2, 3	0.228, 0.127
45†	1	0.201	83	3	0.105
46	1	0.517	85	3	0.112
47	1	0.157	86	1	0.198
49	1	0.122	87	3	0.204
50†	2	0.135	88	2, 3	0.242, 0.248
51	1, 2, 3	0.363, 0.300. 0.176	89	1	0.106
54†	1, 2	0.122, 0.139	90	1, 3	0.131, 0.116
55†	1, 2	0.287, 0.131	95†	1	0.231
56	1, 2, 3	0.135, 0.403, 0.112	96†	1, 2	0.143, 0.112
57	3	0.128	98	1	0.115
58	3	0.142	99	1	0.166
59	1, 2	0.294, 0.176	100	2	0.624

*Excluding the branch joint for data which give no intersection or result in a large branch end distance error as listed in Table 6.3.

†Data with no solution for more than one branch (Table 6.3).

Table 6.3: Data analysis for fault tolerant operation of hand controller.

Excluded Joint #	Data Numbers Resulting No Solution	
Joint 1 of Branch 1	No Intersection:	13, 15, 18, 41, 42, 43, 55, 80(0.086)*
	Large p_ip_j Error:†	50, 61, 73, 75, 76, 82
	p_ip_j error (in):	0.093, 0.157, 0.174, 0.094, 0.107, 0.107
Joint 2 of Branch 1	No Intersection:	69, 74(0.140)‡
	Large p_ip_j Error:	50, 61, 73, 75, 76, 80, 82
	p_ip_j error (in):	0.093, 0.157, 0.174, 0.094, 0.107, 0.086, 0.107
Joint 3 of Branch 1	No Intersection:	61(0.157)*
	Large p_ip_j Error:	50, 73, 75, 76, 80, 82
	p_ip_j error (in):	0.093, 0.174, 0.094, 0.107, 0.086, 0.107
Joint 1 of Branch 2	No Intersection:	13, 41, 44
	Large p_ip_j Error:	72, 74
	p_ip_j error (in):	0.094, 0.136
Joint 2 of Branch 2	No Intersection:	72(0.094)*
	Large p_ip_j Error:	74
	p_ip_j error (in):	0.136
Joint 3 of Branch 2	No Intersection:	72(0.094)*
	Large p_ip_j Error:	74
	p_ip_j error (in):	0.136
Joint 1 of Branch 3	No Intersection:	15, 16, 31, 33, 45, 62
	Large p_ip_j Error:	50, 60, 73, 78, 95, 96
	p_ip_j error (in):	0.086, 0.129, 0.262, 0.103, 0.089, 0.089
Joint 2 of Branch 3	No Intersection:	50(0.086)§, 54(0.203)‡, 62, 71
	Large p_ip_j Error:	60, 73, 78, 95, 96
	p_ip_j error (in):	0.129, 0.262, 0.103, 0.089, 0.089
Joint 3 of Branch 3	No Intersection:	–
	Large p_ip_j Error:	50, 60, 73, 78, 95, 96
	p_ip_j error (in):	0.086, 0.129, 0.262, 0.103, 0.089, 0.089

*Large p_ip_j error for circle-circle and one circle-sphere intersection and no intersection for the other circle-sphere.

†Maximum tolerance on the error of the branch end distances p_ip_j is 0.080 inches.

‡No intersection for circle-circle (large error between the intersection of circles with the common line of circles' planes) and one circle-sphere and large p_ip_j error for the other circle-sphere.

§Large p_ip_j error for circle-circle intersection and no intersection for both circle-spheres.

Table 6.4: Data analysis for fault tolerant operation of hand controller excluding 13 data of nine sensor case with large branch end distance error.

Total Data Numbers Resulting No Solution	
Eight Sensors	13, 15, 16, 18, 31, 33, 41, 42, 43, 44, 45, 50, 54, 55, 60, 61, 62, 69, 71, 72, 73, 74, 75, 76, 78, 80, 82, 95, 96
Nine Sensors (Large p_ip_j error)	50, 60, 61, 72, 73, 74, 75, 76, 78, 80, 82, 95, 96 0.093, 0.129, 0.157, 0.094, 0.262, 0.136, 0.094, 0.107, 0.103, 0.086, 0.107, 0.089, 0.089
Excluded Joint #	Data Numbers Resulting No Intersection
Joint 1 of Branch 1	13, 15, 18, 41, 42, 43, 55
Joint 2 of Branch 1	69
Joint 3 of Branch 1	–
Joint 1 of Branch 2	13, 41, 44
Joint 2 of Branch 2	–
Joint 3 of Branch 2	–
Joint 1 of Branch 3	15, 16, 31, 33, 45, 62
Joint 2 of Branch 3	54(0.203)*, 62, 71
Joint 3 of Branch 3	–
Total	13, 15, 16, 18, 31, 33, 41, 42, 43, 44, 45, 54, 55, 62, 69, 71

*No intersection for circle-circle (large error between the intersection of circles with the common line of circles' planes) and one circle-sphere and large p_ip_j error for the other circle-sphere.

Chapter 7

Discussion

7.1 Redundant Joint Sensing and Actuation

7.1.1 Assets of Joint Sensing Redundancy

Redundant joint displacement sensing has been shown to be effective in reducing the number of potential assembly modes of a parallel manipulator and in allowing analytical solutions for the forward displacement problem (FDP) to be found (Chapter 2). Both of these assets are important considerations for implementation of parallel manipulation devices. The advantages of including redundancy in main-arm joint sensing suggest that appropriate redundancy is an important consideration in the design of parallel manipulators.

A further benefit of redundant displacement sensing can be realized through the development of solutions with robustness to partial failure of displacement sensors. The key to such failure-safe solutions is sensor failure-detection schemes combined with the full set of solutions for various sensing combinations. Sensor failure-detection

methods have been developed for the considered class of three-branch parallel manipulators and implemented on a hand controller, based on the forward displacement solutions (Chapter 6). As discussed in Section 7.4 the success of the attempt to implement these detection methods was limited due to device precision and tolerances.

7.1.2 Minimum Sensors for a Unique Solution of FDP

One danger inherent in the use of devices with multiple forward displacement solutions is the possibility of false switching between assembly modes, i.e., an assembly mode switching (or lack of appropriate switching) in the control related software that does not correspond to the actual assembly mode of the physical device. Such a false switch will lead to unsuccessful task completion and can be extremely dangerous. The danger of false switching becomes extremely relevant for manipulators with multiple forward displacement solutions that are capable of operating near or passing through end effector poses where assembly modes coexist. Appropriate schemes for management of multiple solutions and prevention of false mode switching must be implemented for such manipulators. Manipulators with a unique forward displacement solution or easily managed multiple solutions are preferred.

To have a unique forward displacement solution for the considered class of three-branch manipulators, regardless of the choice of branches and regardless of the location of the end effector in its workspace, 3-3-3 sensing (nine sensors) of the main-arm joints was shown to be required.

In the simulation of 3-3-2 solutions for example manipulator it has been found that normally one solution exists. As outlined in Section 2.2.2 special conditions (e.g., intersecting circle centerlines for an unsensed revolute joint) are necessary for the existence of two solutions. False switching could only be a potential issue if

the manipulator tracked a path that maintained the special condition and brought the two assembly modes into (near) coexistence. This extremely special case is easy to handle since as soon as the special condition is no longer true only one solution exists. Also it is easy to develop software to monitor for the existence of the special conditions.

7.1.3 Potential Uncertainty Cases and Elimination via Actuation Redundancy

Redundant joint actuation is effective in eliminating the uncertainty configurations of parallel manipulators, and furthermore allows actuator loads to be optimally shared.

Potential uncertainties for the different actuation cases of three-branch parallel manipulators can be summarized as follows (Chapter 3). **Cases 3a**, **4a**, and **4c** do not exist for the considered class of parallel manipulators. It was shown that **Case 1** will not cause an uncertainty problem if one branch is redundantly actuated, e.g., 3-2-2 actuation.

Case 2b can not exist with 3-3-2 and 3-3-3 actuations.

Case 3b will not cause an uncertainty configuration with at least one redundant actuated joint, i.e., 3-2-2, 3-3-1, 3-3-2, and 3-3-3 actuations. **Case 3c** might result from four or five concurrent wrenches. Therefore, at least two redundant actuated joints are required to eliminate potential uncertainty configurations arising from it, i.e., 3-3-2 or 3-3-3 actuation. Since four or more coplanar wrenches will belong to a variety of **Case 3d** and a maximum of six wrenches of the class of parallel manipulator can be coplanar, the order of reciprocal wrenches will not be less than six with 3-3-3 actuation.

In general **Case 4b** will not be a problem with a minimum of one redundant

actuated joint, i.e., with 3-2-2, 3-3-1, 3-3-2, and 3-3-3 actuations. **Case 4d** can exist among the six wrenches of 2-2-2 or 3-2-1 actuation. Redundant actuation of at least two joints (3-3-2 actuation) is required to completely eliminate the potential uncertainty configurations arising from this dependency case.

Redundant actuation of one joint is required to maintain the order of reciprocal wrenches at six when six of the wrenches belong to the variety of **Case 5a**. It should be noted that the wrenches of 3-2-1 and 3-3-1 actuations do not belong to a general complex. With 3-2-1 and 3-3-1 actuations if the only wrench of the branch with one actuator lies on the mobile platform plane **Case 5b** will result. **Case 5b** cannot occur with 3-3-3 actuation.

7.1.4 Preferred Redundant Joint Actuation and Sensing

For the 3-2-1 actuation of the considered class of manipulators, when the wrench associated with the branch with one actuated joint lies on the mobile platform the six wrenches will belong to a special complex (Case 5b). This wrench can lie on the mobile platform in a significant part of the work space. If that branch had two actuators, in most configurations the two associated wrenches would not lie on the mobile platform simultaneously. Therefore considering uncertainties, 2-2-2 actuation is more attractive compared to 3-2-1 actuation, although 2-2-2 actuation is less preferred considering finite forward kinematics. 3-2-1 sensing allows a closed-form solution for the FDP of parallel manipulators where as with 2-2-2 sensing the FDP can only be resolved by iteration. Similarly, 3-2-2 actuation is more attractive compared to 3-3-1 actuation considering uncertainties. The FDP of 3-2-2 sensing is also preferred (simpler) to 3-3-1 sensing.

It was shown that 3-3-2 actuation eliminates all of the potential uncertainty cases

for the considered class of parallel manipulators except Case 5b. With 3-3-2 actuation Case 5b is achieved if both wrenches of the branch with two actuators lie on the mobile platform plane. Uncertainties correspond to the configurations where different solutions of the FDP of a parallel manipulator meet. It was presented in Chapter 2 that there can exist in special cases up to two solutions for the FDP of the considered class of parallel manipulators with 3-3-2 sensing. The manipulator configurations representing the cases where two forward displacement solutions coalesce, also correspond to the only uncertainty case of the 3-3-2 actuation. Again, it would be simple in this case to monitor in software the closeness to a potential uncertainty configuration.

7.2 Redundant Branch

7.2.1 Assembly Modes

The maximum number of assembly modes of the 3-4 form of four-branch symmetrically sensed parallel manipulators (2-2-2-2 sensing) with all revolute and all prismatic unsensed main-arm joints was shown to be eight and four, respectively (Chapter 4). It was also shown that there is up to eight and up to four assembly modes when the unsensed main-arm joint of one of the concurrent branches is prismatic and when the unsensed joints of both concurrent branches are prismatic joints, respectively. In general due to the manipulator geometry, position of the actuated joints, and the unsensed joints' limits, the number of assembly configurations will be less.

The maximum number of solutions for the FDP of the 3-4 form of four-branch parallel manipulators can be further reduced employing asymmetric sensing of eight main-arm joints. For example, if all of the main-arm joints of the two non-concurrent

branches are sensed and the two concurrent branches each has one sensed main-arm joint (3-3-1-1 sensing) the loci of potential concurrent branch end location is either a circle (for unsensed revolute joints) or a line (for unsensed prismatic joints). There will be a maximum of two solutions, corresponding to the intersection of two circles or a circle and a line, for the location of the concurrent branch ends, i.e., there will be up to two solutions for the FDP.

The maximum number of assembly configurations of the four-branch parallel manipulators can be further reduced employing redundant sensing of main-arm joints. The effect of redundant main-arm joint sensing on the reduction of the number of potential assembly modes of the three-branch parallel manipulators has been discussed in Chapter 2. It can be shown that by employing a redundant main-arm joint sensor on any branch (concurrent or non-concurrent) of the 3-4 form of four-branch parallel manipulators, the maximum number of assembly configurations can be reduced by half. When three main-arm joints of a branch are sensed the location of the corresponding branch end is known. If this branch is one of the concurrent branches, then the location of $p_{1,2}$ is unique. Similarly, if three main-arm joints of a non-concurrent branch are sensed there is a unique solution for that branch end location. In this case, nine main-arm joints of the four-branch parallel manipulators are sensed and there will be up to four and up to two solutions for the FDP if the unsensed main-arm joint of at least one of the concurrent branches is revolute and if the unsensed joints of both concurrent branches are prismatic joints, respectively. Whereas sensing of all main-arm joints of the three-branch parallel manipulators (nine sensors) provides a unique solution for the FDP. However, with proper design of the branches and sensing of three main-arm joints of a non-concurrent branch it would be possible to obtain a unique solution for the FDP of the four-branch class of manipulators.

Employing redundant main-arm joint sensing on two branches (at least one of

them being either of the non-concurrent branches) the maximum number of assembly modes will be reduced to two regardless of the type of the unsensed main-arm joints. In this case, a total of ten sensors will be used and the maximum number of forward displacement solution will be the same as the case where eight main-arm joints of the class of three-branch parallel manipulators are sensed. Again, appropriate design could allow a unique solution to be assumed.

For the general 2-2-2-2 symmetric sensing layout of the class of four-branch parallel manipulators (4-4 form) the FDP can be investigated following the analysis presented by Parenti-Castelli and Innocenti (1992) (employing loop closure equations). Considering combinations of three branches at a time, there will be three independent sets of closure equations, e.g., 1&2&3, 1&4&3, and 1&2&4. For all revolute unsensed main-arm joints these three closure equations will be represented by three 16-th order polynomials in terms of one unknown. The maximum number of assembly configurations of the 4-4 all-revolute-jointed parallel manipulator must be less than or equal to the order of the greatest common divisor of the three 16-th order polynomials. Unless the 16-th order polynomials are identical or equivalent, the order of greatest common divisor will always be less than or equal to fourteen. Applying the same procedure an upper bound on the number of assembly modes of the 4-4 parallel manipulators with all prismatic unsensed joints can be shown to be equal to the order of the greatest common divisor of three 8-th order polynomials, i.e., less than or equal to six. The upper bound on the number of assembly configurations of the 4-4 parallel manipulators with one prismatic unsensed main-arm joint must be less than or equal to the order of the greatest common divisor of three 16-th order polynomials. Similarly, the upper bound on the number of assembly modes of the 4-4 parallel manipulators with two (three) unsensed prismatic main-arm joints can be shown to be less than or equal to the order of the greatest common divisor of one 16-th order and two 12-th order

polynomials (one 8-th order and two 12-th order polynomials).

While an upper bound can be defined as discussed above, it is likely that the maximum number of assembly modes are less. Uncertainties of a parallel manipulator correspond to configurations where different solutions of the direct kinematic problem (assembly modes) meet. The 3-4 form of four-branch parallel manipulators possesses more dependency cases which can potentially result in the uncertainty configurations compared to the 4-4 form, refer to Table 4.1. Therefore, it may be expected that the maximum number of assembly modes of the 4-4 form manipulators will be less than the 3-4 form.

7.2.2 Uncertainty Cases

It was presented that addition of a redundant branch does not fundamentally eliminate all of the uncertainty configurations associated with a "three-branch" 2-2-2 actuated parallel manipulator completely. Although some of the uncertainties can be eliminated, uncertainties resulting from **Cases 3c, 3d, 4b, 4d, 5a** and **5b** and also uncertainties resulting from some multiple dependencies can still potentially occur. Some of these potential uncertainties require several conditions to be satisfied and some of them require only a few conditions.

It was presented in Chapter 3 that redundant actuation of all main-arm joints (nine joints) of the three-branch parallel manipulators eliminates all uncertainty configurations. It was also presented that actuation of a total of eight main-arm joints eliminates all of the potential uncertainties for the considered class of parallel manipulators except those corresponding to Case 5b (a case that can be effectively eliminated at the design stage). The four-branch (3-4) parallel manipulators have more potential uncertainty cases compared to the redundant actuation of eight main-arm joints

(3-3-2 actuation) of the class of three-branch manipulators even though both possess eight actuated joints. A summary of potential uncertainty cases that exist for the symmetric actuations of the 3-4 form and the general form (4-4 form) of the four-branch manipulators (2-2-2-2 actuation), and also for the non-redundant symmetric and asymmetric actuations (2-2-2 and 3-2-1) and redundant actuations (3-2-2, 3-3-1, 3-3-2, 3-3-3) of three-branch parallel manipulators is given in Table 4.1.

The four-branch two-actuated joints per branch configuration is advantageous over a three-branch three-actuated joints per branch device since base (or base proximal) mounting of the drives will be easier. At the design stage of a four-branch two actuated-joints per branch manipulator, particular attention should be paid to the potential uncertainty configurations. It is possible that through appropriate design many uncertainty cases, if not all, could be eliminated by ensuring that the multiple conditions required for uncertainty configurations cannot coexist or correspond to configurations that the device cannot attain.

7.3 Calibration of Manipulators

Kinematic calibration of parallel manipulators has been discussed in Chapter 5. The methodology has been applied on a three-branch parallel manipulator based hand controller. It was shown that results close to being as accurate as the noise levels of the sensing of the potentiometers can be achieved by the most complete of the models introduced. It was also demonstrated that convergence to false results is possible if insufficient redundancy in sampled data is present. The calibrated hand controller was used for the sensor fault detection investigations in Chapter 6.

When three main-arm joints of each branch are sensed (3-3-3 sensing) the location of the branch ends are known. The loop closure equations can be written consider-

ing any two branches and the joint displacement readings to calculate the distance between the corresponding branch ends. The distance between the branch end locations on the mobile platform is constant and known. The error of these branch end distances can be used in the objective function of the calibration. This objective function only requires measurement of main-arm joint displacements and it eliminates the need for a calibration fixture. With two or one redundant main-arm joint sensing (3-3-2, 3-2-2, and 3-3-1 sensings) and asymmetric non-redundant sensing (3-2-1) there exists more than one solution for the branch end positions of the branches with at least one unsensed main-arm joint. That is, there exists multiple solutions for the branch end distance error, where only one of these solutions correspond to the actual configuration of the branch. Unless the parallel device is in a known assembly configuration, the actual position of the branch ends cannot be distinguished.

The calibration may be improved by increasing the number of data. This was attempted by capturing 20 more data and using the 120 data in the calibration. Combinations of the initial 100 data and the additional 20 data points were analyzed. However, a few combination cases did not converge and the others did not follow the expected trend and converged to a different result with larger error. Since the two sets of data were captured several months apart, the device might have been mishandled within this period leading to the acquired data being incompatible. Future researchers may wish to acquire further data to verify this hypothesis.

The calibration results can be further improved by increasing the precision of the potentiometers. The potentiometers can be supplied with regulated voltage of ± 10 volts (instead of current ± 5 volts). This will double the precision from 11 to 12 bits.

The base distal joints of each of the branches of the hand controller were designed such that they nominally would form a spherical joint group. These joints were modeled as a spherical joint in the kinematic models of the hand controller. This

potentially is not an adequate assumption. If the hand controller was manufactured and assembled precisely, specifically if the three distal joints of each branch formed a "perfect" spherical joint, the calibration result of the complete model could potentially be improved. This is because the only assumption for the complete model was the spherical branch end joint and the rest of the potential inaccuracies were modeled. This assumption was required to obtain a unique solution for the FDP. Otherwise, a calibration fixture would be necessary.

7.4 Sensor Fault Detection for Fault Tolerant Manipulators

A sensor failure detection scheme for fault tolerance operation of the considered class of three-branch parallel manipulators was presented in Chapter 6. The algorithm is applicable for branches with a passive spherical branch end joint and can diagnose the failure of any linear or rotary main-arm joint sensor. The algorithm is based on considering the potential loci of a branch end location (as discussed in Chapter 2) and can be applied to a broad family of parallel manipulators.

Although the algorithm works well in simulation, the implementation of the algorithm for the real-time operation of the three-branch parallel hand controller was not as successful. This was due to the uncertainties in the kinematic model of the hand controller and potentiometer noise. It was presented that the algorithm can be very sensitive to these uncertainties. Tolerances were used to attempt to accommodate the effect of modeling errors. It was discussed that the tolerances should be large enough to compensate for the uncertainties and that the tolerances should not be too large otherwise the sensor failure might not be detected. In addition, it was verified that the effect of the inaccuracies in the kinematic model depends on the configuration of

the device. Therefore, the tolerances should be dynamic to conform with the different poses of the parallel device. The fault detection and fault tolerance schemes are recommended to be implemented on precisely manufactured and calibrated devices only. It is also recommended to employ low noise joint displacement sensors.

Chapter 8

Conclusions and Recommendations for Further Work

8.1 Conclusions

This work contributes to the implementation issues of parallel manipulators by addressing problems which arise from the kinematics of the associated serial and parallel chains. Specifically, the work provides: complete solutions to the forward displacement problem for a broad class of three-branch devices; knowledge of uncertainty configurations of the manipulators and approaches to reduce/eliminate special configurations; and on-line methods for calibration, sensor failure detection, and failure safe operation, a base for failure-safe implementations. The conclusions can be summarized as follows in this section.

Redundant main-arm joint sensing is an effective means of allowing closed-form

solutions to be found (Chapter 2). For three-branch parallel manipulators, composed of three joints in the main-arm and a passive spherical branch-end joint, closed-form forward displacement solutions can be found for all cases of redundant main-arm joint sensing (3-3-3, 3-3-2, 3-2-2, 3-3-1 sensing) and for asymmetrical nonredundant sensing (3-2-1). Closed-form solutions can also be found for the forward displacement problem (FDP) of three-branch parallel manipulators by adding a redundant branch having passive spherical joint center concurrency with one of the three branches and symmetric 2-2-2-2 sensing or asymmetric 3-3-1-1 sensing.

Actuation redundancy is an effective means of uncertainty reduction/elimination. Similarly, main-arm joint sensing redundancy is an effective means of reducing potential assembly modes. Sensing and actuation redundancy should be carefully considered in the design of parallel manipulators (Chapters 2 and 3).

For redundant sensing and actuation of all main-arm joints of the considered class of manipulators a unique solution of the FDP exists and uncertainty configurations can be completely eliminated (3-3-3 sensing and actuation). With 3-3-3 actuation the screw system spanned by the reciprocal screws associated with the actuated joints of the branches and also by the structural wrenches corresponding to degenerate branch configurations, will always have an order of six.

A maximum of two forward displacement solutions exist for the case of redundant sensing and actuation of two main-arm joints (3-3-2 sensing and actuation) and all uncertainties are eliminated except for uncertainty cases resulting from the line dependency Case 5b. Normally only one forward displacement solution exists for 3-3-2 sensing, the existence of two solutions requiring the satisfaction of special conditions. For an unsensed revolute main-arm joint S_R, intersection of the line collinear with S_R and the line passing through the centers of the passive spherical end joints of the two branches with all main-arm joints sensed is necessary to have up to two solutions.

For an unsensed prismatic main-arm joint S_P, the direction of S_P must lie on a plane normal to the line passing through the centers of the passive spherical end joints of the branches with all main-arm joints sensed.

For a single redundant sensor and actuator (3-2-2 and 3-3-1 sensing and actuation cases) 3-2-2 redundant sensing and actuation is the preferred sensing and actuation layout. This is due to the FDP of 3-2-2 sensing being simpler than 3-3-1 sensing and that uncertainties can potentially occur more frequently and in a more significant part of the task space for 3-3-1 actuation compared to 3-2-2 actuation.

For non-redundant actuation 2-2-2 actuation is the preferred actuation layout for uncertainty configuration considerations, although 3-2-1 sensing provides closed-form solution for the FDP.

The feasible assembly modes of the 3-4 form of four-branch parallel manipulators with symmetric sensing can be limited to two through appropriate design. However, it is not possible to get a unique solution for the FDP with one redundant branch and symmetric 2-2-2-2 sensing. Utilizing a redundant branch and 2-2-2-2 actuation, not all of the potential wrench dependencies leading to the uncertainty configurations of three-branch parallel manipulators with spherical branch-end joints can be eliminated. In addition, a redundant branch will limit the workspace due to branch interference, will increase overall weight and cost of the device, and will increase motion singularities due to branch degeneracies. Therefore, in-parallel redundant sensing and actuation is not as efficient and practical of a solution for FDP and uncertainty considerations as compared to serial redundant sensing and actuation and it should only be employed when redundant serial sensing and actuation of the main-arm joints is undesirable (Chapter 4).

Kinematic calibration of the considered class of parallel manipulators can be achieved without using a calibration fixture when the main-arm joints of all of the

branches are redundantly sensed (3-3-3 sensing) (Chapter 5).

The developed fault detection scheme has been shown to be a feasible way of diagnosing a failed displacement sensor. The fault tolerance operation of the manipulators can be achieved by providing the solutions of the FDP for various sensing combinations. However, the scheme requires a very precise device with low noise displacement sensors (Chapter 6).

In summary, redundant sensing of main-arm joint displacements provides an ability to have closed-form forward displacement solutions, an inherent reduction in potential assembly modes for known joint displacements, and the potential for the consideration of sensor-failure-safe implementations. Furthermore, redundant joint actuation is effective for the elimination of uncertainty configurations. Therefore, appropriate redundancy in joint displacement sensing and actuation are important considerations for the effective implementation of parallel manipulators and should be considered during the design of parallel manipulation devices.

8.2 Recommendations for Future Work

This work has addressed implementation issues of parallel manipulators and has provided solutions for the kinematic problems of a class of manipulators. Problems that have not been addressed in this work and are recommended for future research include:

1. Development of actuator fault detection schemes for parallel manipulators, specifically for the considered class of three-branch parallel manipulators.

2. Exploitation of degeneracies of parallel manipulators: i.e., exploitation of branch degeneracies to increase the payload capacity of the manipulators; and exploita-

tion of uncertainty configurations, e.g., for assembly mode switching in path planning applications of manipulators.

3. Prototyping of more appropriate test devices, specifically ones with "perfect" passive spherical branch end joints and low noise displacement sensors, allowing further implementations of the developed solutions for the calibration, FDP, sensor fault detection, and failure tolerance operation of the devices.

References

[1] E. W. Aboaf and R. P Paul. Living with the singularity of robot wrists. In *Proc. of IEEE Int. Conf. on Robotics and Automation*, pages 1713–1717, 1987.

[2] J. Angeles, K. Anderson, X. Cyril, and B. Chen. The kinematic inversion of robot manipulators in the presence of singularities. *J. Dynamic Systems, Measurement, and Control*, 110:246–254, September 1988.

[3] K. C. Cheok, J. L. Overholt, and R. R. Beck. Exact method for determining the kinematics of a Stewart platform using additional displacement sensors. *J. Robotic Systems*, 10(5):689–707, 1993.

[4] A. Cheung and H. Crapo. A combinatorial perspective on algebraic geometry. *Advances in Mathematics*, 20:388–414, 1976.

[5] J. T. Chladek. Fault tolerance for space manipulator mechanisms and control systems. In *Proc. of First Int. Symposium on Measurement and Control in Robotics, ISMCR'90*, page D3.3, 1990.

[6] K. Cleary and T. Arai. A prototype parallel manipulator: Kinematics, construction, software, workspace results, and singularity analysis. In *Proc. of IEEE Int. Conf. on Robotics and Automation*, pages 566–571, April 1991.

[7] K. Cleary and T. Brooks. Kinematic analysis of a novel 6-dof parallel manipulator. In *Proc. of IEEE Int. Conf. on Robotics and Automation*, pages 708–713, 1993.

[8] R. Colbaugh and M. Jamshidi. Robot manipulator control for hazardous waste-handling applications. *J. Robotic Systems*, 9(2):215–250, 1992.

[9] A. Dandurand. The rigidity of compound spatial grids. *Structural Topology*, 10:41–56, 1984.

[10] J. Dieudonne, R. Parrish, and R. Rardusch. An actuator extension transform for a motion-simulator and an inverse transformation applying Newton-Raphson method. Technical report, NASA Report D-7067, 1972.

[11] E. F. Fichter. A Stewart platform-based manipulator: General theory and practical construction. *Int. J. Robotics Research*, 5(2):157–182, 1986.

[12] E. F. Fichter and K. H. Hunt. The fecund torus, its bitangent-circles and derived linkages. *J. Mech. Mach. Theory*, 10(2):167–176, 1975.

[13] C. Gosselin and J. Angeles. Singularity analysis of closed-loop kinematic chains. *IEEE Trans. Robotics and Automation*, 6(3):281–290, 1990.

[14] M. Griffis and J. Duffy. A forward displacement analysis of a class of Stewart platform. *J. Robotic Systems*, 6(6):703–720, 1989.

[15] S. Hayati and M. Mirmiraui. Improving the absolute positioning accuracy of robot manipulators. *J. Robotic Systems*, 2(4):397–413, 1985.

[16] S. Hayati, K. Tso, and G. Roston. Robot geometry calibration. In *Proc. of IEEE Int. Conf. on Robotics and Automation*, pages 947–951, 1988.

[17] S. A. Hayati. Robot arm geometric link parameter estimation. In *Proc. of 22nd IEEE Conf. on Decision and Control*, pages 1477–1483, 1983.

[18] V. Hayward and R. Kurtz. Kinematic modeling of a parallel wrist mechanism with actuator redundancy. *J. Laboratory, Robotics and Automation*, 4:69–76, 1992.

[19] J. M. Hollerbach. Optimum kinematic design for a seven degree of freedom manipulator. In *Proc. of the Second Int. Symposium on Robotics Research*, chapter 4, pages 215–222. 1984.

[20] J. M. Hollerbach and D. M. Lokhorst. Closed-loop kinematic calibration of the RSI 6-dof hand controller. In *Proc. of IEEE Int. Conf. on Robotics and Automation*, pages 142–148, 1993.

[21] K. H. Hunt. *Kinematic Geometry of Mechanisms.* Oxford University Press, Oxford, UK, 1978 and 1990.

[22] K. H. Hunt. Structural kinematics of in-parallel actuated robot-arms. *J. Mech. Trans. and Automation in Design*, 105:705–712, 1983.

[23] K. H. Hunt. Special configurations of robot-arms via screw theory, Part 1: The Jacobian and its matrix of cofactors. *J. Robotica*, 4:171–179, 1986.

[24] K. H. Hunt and E. J. F. Primrose. Assembly configurations of some in-parallel-actuated manipulators. *J. Mech. Mach. Theory*, 28(1):31–42, 1993.

[25] K. H. Hunt, A. E. Samuel, and P. R. McAree. Special configurations of multi-freedom grippers - A kinematic study. *Int. J. Robotics Research*, 10(2):123–134, April 1991.

[26] M. Husain and K. J. Waldron. Position kinematics of a mixed mechanism. In *Proc. of ASME 22nd Biennial Mechanisms Conf.*, volume DE-45, pages 41–48, September 1992.

[27] C. Innocenti and V. Parenti-Castelli. Direct position analysis of the Stewart platform mechanisms:. *J. Mech. Mach. Theory*, 25(6):611–621, 1990.

[28] H. Inoue, Y. Tsusaka, and T. Fukuizumi. Parallel manipulator. In *Robotics Research The Third Int. Symposium*, pages 321–327, 1986.

[29] Borm J.-H and C.-H. Meng. Determination of optimal measurement configurations for robot calibration based on observability measure. *J. Robotics Research*, 10(1):51–63, 1991.

[30] J. Kieffer. Bifurcations and isolated singularities in the inverse kinematics of linkages and manipulators. In *Proc. of IEEE Conf. on Robotics and Automation*, pages 428–433, 1992.

[31] J. Kieffer and J. Lenarcic. On the exploitation of mechanical advantage near robot singularities. *3rd Int. Workshop on Advances in Robot Kinematics*, pages 65–72, September 1992.

[32] M. V. Kircanski and T. M. Petrovic. Inverse kinematic solution for a 7 dof robot with minimal computational complexity and singularity avoidance. In *Proc. of IEEE Int. Conf. on Robotics and Automation*, pages 2664–2669, 1991.

[33] C. A. Klein and C.-H. Huang. Review of pseudoinverse control for use with kinematically redundant manipulators. *IEEE Trans. Sys. Man, Cyber.*, SMC-13(3):245–250, 1983.

[34] V. Kumar and J. F. Gardner. Kinematics of redundantly actuated closed chains. *IEEE Trans. Robotics and Automation*, 6(2):269–274, April 1990.

[35] Z. C Lai and D. C. H Yang. An efficient motion control algorithm for robots with wrist singularities. *IEEE Trans. Robotics and Automaton*, 6(1):113–117, 1990.

[36] F. L. Litvin, Z. Yi, V. P. Castelli, and C. Innocenti. Singularities, configurations, and displacement functions for manipulators. *Int. J. Robotics Research*, 5(2):52–65, 1986.

[37] O. Ma and J. Angeles. Architecture singularities of platform manipulators. In *Proc. of IEEE Int. Conf. on Robotics and Automation*, pages 1542–1547, April 1991.

[38] A. A. Maciejewski. Fault tolerant properties of kinematically redundant manipulators. In *Proc. of IEEE Int. Conf. on Robotics and Automation*, pages 638–642, 1990.

[39] A. A. Maciejewski and C. A. Klein. Numerical filtering for the operation of robotic manipulators through kinematically singular configurations. *J. Robotic Systems*, 5(6):527–552, 1988.

[40] A. A. Maciejewski and C. L. Lewis. An example of failure tolerant operation of a kinematically redundant manipulator. In *Proc. of IEEE Int. Conf. on Robotics and Automation*, pages 1380–1387, 1994.

[41] O. Masory, J. Wang, and H. Zhuang. On the accuracy of a Stewart platform-Part II: Kinematic calibration and compensation. In *Proc. of IEEE Int. Conf. on Robotics and Automation*, pages 725–731, 1993.

[42] R. V. Mayorga and A. K. C. Wong. A singularities avoidance method for the trajectory planning of redundant and nonredundant robot manipulators. In *Proc. of IEEE Int. Conf. on Robotics and Automation*, pages 1707–1712, 1987.

[43] C.-H. Meng, J.-H. Borm, and J. Z. Lai. Identification and observability measure of a basis set of error parameters in robot calibration. *J. Mech. Trans. and Automation in Design*, 111:513–518, 1989.

[44] J.-P. Merlet. Parallel manipulator: Kinematics, singular configurations and compliance. In *Proc. of 3rd Int. Conf. on Advanced Robotics ICAR'87*, October 1987.

[45] J.-P. Merlet. Parallel manipulators, Part 2: Theory, singular configurations and grassmann geometry. Technical Report 791, INRIA Research Report, February 1988.

[46] J.-P. Merlet. Singular configurations of parallel manipulators and grassmann geometry. *J. Robotics Research*, 8(5):45–56, 1989.

[47] J.-P. Merlet. On the infinitesimal motion of a parallel manipulator in singular configurations. In *Proc. of IEEE Int. Conf. on Robotics and Automation*, pages 320–325, May 1992.

[48] J.-P. Merlet. Closed-form resolution of the direct kinematics of parallel manipulators using extra sensors data. In *Proc. of IEEE Int. Conf. on Robotics and Automation*, pages 200–204, 1993.

[49] M. G. Mohamed and J. Duffy. A direct determination of the instantaneous kinematics of fully parallel robot manipulators. *J. Mechanisms, Transmission, and Automation in Design*, 107:226–229, June 1985.

[50] B. W. Mooring, Z. S. Roth, and M. R. Driels. *Fundamentals of Manipulator Calibration.* John Wiley and Sons, INC., 1991. TJ211.M65.

[51] Y. Nakamura and H. Hanafusa. Inverse kinematic solutions with singularity robustness for robot manipulator control. *ASME J. Dynamic Systems, Measurement, and Control*, 108:163–171, 1986.

[52] P. Nanua, K. J. Waldron, and V. Murthy. Direct kinematic solution of a Stewart platform. *IEEE Trans. Robotics and Automation*, 6(4):438–444, August 1990.

[53] L. Notash and R. P. Podhorodeski. Complete forward displacement solutions for a class of three-branch parallel manipulators. *J. Robotic Systems*, 11(6):471–485, 1994a.

[54] L. Notash and R. P. Podhorodeski. Uncertainty configurations of three-branch parallel manipulators - Identification and elimination. In *Proc. of ASME 23rd Biennial Mechanisms Conf.*, volume DE-Vol. 72, pages 459–466, 1994b.

[55] L. Notash and R. P. Podhorodeski. Forward displacement analysis and assembly configurations of parallel manipulators with a redundant branch. submitted to *J. Robotic Systems*, October 1994c.

[56] L. Notash and R. P. Podhorodeski. On the forward displacement problem of three-branch parallel manipulators. *J. Mech. Mach. Theory*, 30(3):391–404, 1995a.

[57] L. Notash and R. P. Podhorodeski. Kinematic calibration of a parallel manipulator based hand controller. In *Proc. of 15th CANCAM Conf.*, pages 872–873, 1995b.

[58] L. Notash and R. P. Podhorodeski. Sensor fault detection for fault tolerant operation of parallel manipulators. In *Proc. of IEEE Int. Conf. on Sys., Man and Cyber.*, 1995c.

[59] Z. R. Novakovic and B. Nemec. A solution of the inverse kinematics problem using the sliding mode. *IEEE Trans. Robotics and Automaton*, 6(2):247–252, 1990.

[60] V. Parenti-Castelli and C. Innocenti. Direct displacement analysis for some classes of parallel mechanisms. In *RoManSy '90, the 8th CISM-IFTOMM Symposium on Theory and Practice of Robots and Manipulators*, pages 126–133, 1990.

[61] V. Parenti-Castelli and C. Innocenti. Forward displacement analysis of parallel mechanisms: Closed form solution of PRR-3S and PPR-3S structures. *J. of Mechanical Design*, 114:68–73, March 1992.

[62] R. P. Paul. *Robot Manipulators: Mathematics, Programming, and Control.* MIT Press, Cambridge, MA, 1981.

[63] R. P. Podhorodeski. A screw theory based forward displacement solution for hybrid manipulators. In *Proc. of 2nd National Conf. on Applied Mechanic and Robotics*, page IIIc.2, 1991.

[64] R. P. Podhorodeski. An approach for ensuring manipulator tip accuracy near singularities. *J. Mech. Mach. Theory*, 28(5):641–650, 1993.

[65] W. H. Press, S. A. Teukolsky, W. T. Vetterling, and B. P. Flannery. *Numerical Recipes in C - The Art of Scientific Computing.* Cambrifge University Press, 2nd edition, 1992.

[66] M. Raghavan and B. Roth. Inverse kinematics of the general 6R manipulators and related linkages. In *Proc. of ASME 21st Biennial Mechanisms Conf.*, volume DE-25, pages 59–65, 1990.

[67] Z. S. Roth, B. W. Mooring, and B. Ravani. An overview of robot calibration. *IEEE J. Robotics and Automation*, RA-3(5):377–385, October 1987.

[68] M Sampei and K. Furuta. Robot control in the neighborhood of singular points. In *Proc. of IEEE Int. Conf. on Robotics and Automation*, volume 3, pages 1696–1700, 1987.

[69] T. Shamir. The singularities of redundant robot arms. *Int. J. Robotics Research*, 9(1):113–121, 1990.

[70] M. Sklar and D. Tesar. Dynamic analysis of hybrid serial manipulator systems containing parallel modules. *J. Mechanisms, Transmissions, and Automation in Design*, 110:109–115, June 1988.

[71] E. S. Smith, M. Salkover, and H. K. Justice. *Analytic Geometry.* John Wiley & Sons, Inc., 1943.

[72] P. F. Smith and A. S. Gale. *The Elements of Analytic Geometry.* Ginn & Company, 1904.

[73] M. M. Stanisic and O. Duta. Symmetrically actuated double pointing systems: The basis of singularity-free robot wrists. *IEEE Trans. Robotics and Automaton*, 6(5):562–569, 1990.

[74] M. M. Stanisic and G. R. Pennock. A nondegenerate kinematic solution of a seven-jointed robot manipulator. *Int. J. Robotics Research*, 4(2):10–20, 1985.

[75] D. Stewart. A platform with six degrees of freedom. In *Proc. of Inst. Mech. Engr.*, volume 180, pages 371–378, London, 1965-66.

[76] J. P. Trevelyan, P. D. Kovesi, M. Ong, and D. Elford. Et: A wrist mechanism without singular position. *Int. J. Robotics Research*, 4(4):71–85, 1986.

[77] O. Veblen and J. W. Young. *Projective Geometry*, volume 1. Ginn and Company, 1910.

[78] K. J. Waldron, M. Raghavan, and B Roth. Kinematics of a hybrid series-parallel manipulation system. *J. Dynamic System, Measurement, and Control*, 111:211–221, June 1989.

[79] C. W. Wampler. Manipulator inverse kinematic solutions based on vector formulations and damped least-squares methods. *IEEE Trans. Sys. Man, Cyber.*, SMC-16(1):93–101, 1986.

[80] J. Wang and O. Masory. On the accuracy of a Stewart platform- Part I: The effect of manufacturing tolerances. In *Proc. of IEEE Int. Conf. on Robotics and Automation*, pages 114–120, 1993.

[81] S.-L. Wang and K. J. Waldron. A study of the singular configurations of serial manipulators. *J. Mechanisms, Transmissions and Automation in Design*, 109:14–20, 1987.

[82] E. Wu, M. Diftler, J. Hwang, and J. Chladek. A fault tolerant joint drive system for the space shuttle remote manipulator system. In *Proc. of IEEE Int. Conf. on Robotics and Automation*, pages 2504–2509, 1991.

[83] C. Zhang and S.-M. Song. Forward position analysis of nearly general Stewart platforms. In *Proc. of ASME 22nd Biennial Mechanisms Conf.*, volume DE-45, pages 81–87, September 1992.

[84] H. Zhuang and Z. S. Roth. Method for kinematic calibration of Stewart platforms. *J. Robotic Systems*, 10(3):391–405, 1993.

[85] D. Zlatanov, M.Q. Dai, R.G. Fenton, and B. Benhabib. Mechanical design and kinematic analysis of a three-legged six degree-of-freedom parallel manipulator. In *Proc. of ASME 22nd Biennial Mechanisms Conf.*, volume DE-45, pages 529–536, 1992.

Appendix A

Theorems

A.1 Cayley's Theorems

A.1.1 Theorem I

If two points p_i and p_j a fixed distance apart on a line are constrained to lie respectively on two curves C_i and C_j, where the two curves either are planar and lie on non-parallel planes or are spatial, curve C_i having order n_i and circularity[1] s_i and curve C_j having order n_j and circularity s_j, then the line p_ip_j generates a ruled surface whose degree is given by $2n_i(n_j - s_j) + 2n_j(n_i - s_i)$, Hunt (1990).

[1]The equation of a spatial curve/surface can be written in the *homogeneous coordinates* by substituting x/w, y/w, and z/w for x, y, and z, respectively. When $w = 1$, $x/w = x$, and so on. As w increases the curve gets smaller and as w decreases the curve gets larger. When $w = 0$ the curve is infinitely enlarged ($w = 0$ is called the line at infinity, Hunt (1990)). A spatial circle $(x-a)^2 + (y-b)^2 + (z-c)^2 = r^2$ can be written in the homogeneous coordinates as $(x-aw)^2 + (y-bw)^2 + (z-cw)^2 - r^2w^2 = 0$. The intersection of this circle and the line at infinity ($w = 0$) is the equation of the imaginary spherical circle $x^2+y^2+z^2 = 0$. That is, the line at infinity intersects the circle at two imaginary points ($w = 0, x = \pm i\sqrt{y^2+z^2}$). These two imaginary points are called the *imaginary circular points*. Any circle contains the two imaginary circular points once and a circle is said to have a circularity of one. A curve which has these two points as double (triple) is said to have circularity of two (three).

A.1.2 Theorem II

If two points p_i and p_j a fixed distance apart on a line are constrained to lie respectively on two curves C_i and C_j lying in parallel planes, and n_i, n_j, s_i, and s_j satisfying the curves' orders and circularities as in Cayley's theorem **I**, then the line p_ip_j traces a line series whose feather (order) is given by $2n_i(n_j - s_j) + 2n_j(n_i - s_i) - 2s_is_j$, Hunt (1990).

A.2 Bezout's Theorem

The order of a complete curve of intersection of two distinct algebraic surfaces of orders n_i and n_j is n_in_j and an algebraic surface of order n_i has n_in_j points in common with an algebraic curve of order n_j. The curve or points of intersection may in part be imaginary. The order of the real curve of intersection will be n_in_j, and there will be n_in_j real points of intersection between two curves provided that the surfaces and curves have circularity zero. If the circularities of the two intersecting surfaces (or of a surface and a curve) are respectively s_i and s_j, then the maximum order of the real curve of intersection is $n_in_j - 2s_is_j$ (the number of real points in common between the surface and the curve cannot exceed $n_in_j - 2s_is_j$), Hunt (1990), and Hunt and Primrose (1993).

Appendix B

Curves, Surfaces and Intersections

B.1 Curves and Surfaces

A sphere with center at $\{a, b, c\}^T$ and radius r can be represented in Cartesian coordinates as

$$\mathsf{SP} \ : \ (x-a)^2 + (y-b)^2 + (z-c)^2 = r^2 \tag{B.1}$$

The point-equations of a spatial circle are

$$\mathsf{C} \ : \ \begin{cases} (x-a)^2 + (y-b)^2 + (z-c)^2 = r^2 \\ Lx + My + Nz + P = 0 \end{cases} \tag{B.2}$$

where the first equation is the equation of a sphere with center at the center point, $\{a, b, c\}^T$, of the circle and radius equal to the circle radius, r, and the second equation represents the plane of the circle with unit normal of $\{L, M, N\}^T$ which in fact is the axis of the circle. P represents the normal distance of the plane from the origin of a

reference frame, i.e., $P = -(L\,a + M\,b + N\,c)$. The two equations together represent the intersection of a sphere with a plane which is a circle.

The equation of a ring can be expressed as

$$\mathsf{RG}\ :\ \begin{cases} s^2 \leq (x-a)^2 + (y-b)^2 + (z-c)^2 \leq r^2 \\ Lx + My + Nz + P = 0 \end{cases} \tag{B.3}$$

where $\{a, b, c\}^T$ is the coordinates of the ring center, s and r are the inner and outer radii of the ring, and $\{L, M, N\}^T$ and P define the plane of the ring and the distance of the plane from the reference frame origin.

The equation of a torus is

$$\mathsf{TR}\ :\ \{(x^2+y^2+z^2) - ({r_p}^2 + {r_s}^2 + f^2)\}^2 = 4{r_p}^2 \left\{ {r_s}^2 - \left(\frac{z - f cos\beta}{sin\beta} \right)^2 \right\} \tag{B.4}$$

where r_p and r_s represent the primary and secondary radii of the torus respectively, f is the joint offset between R-pairs (revolute joints) and the two R-pairs are inclined at an angle β, (Fichter and Hunt (1975)). Note that this expression is with respect to a torus reference frame located at the torus center with z-axis of the frame normal to the plane of torus and x, y-axes in the plane of the torus.

When $\beta = 90°$ and $f = 0$ this equation simplifies to the equation of a right circular torus

$$\mathsf{TR}\ :\ \{(x^2+y^2+z^2) - (r_p^2 + r_s^2)\}^2 = 4r_p^2(r_s^2 - z^2) \tag{B.5}$$

This equation can be derived from the surface equation of a torus generated when a circle of radius r_s with its center located at a distance r_p from z-axis, is revolved

about z-axis if the axis of revolution (z-axis) lies in the plane of circle, Smith et al. (1943) and Smith and Gale (1904), as

$$\mathsf{TR} \ : \ \left(\sqrt{x^2+y^2}-r_p\right)^2+z^2=r_s^2 \tag{B.6}$$

B.2 Intersection of Two Circles

The two circles C_1 and C_2 can be expressed as

$$\mathsf{C}_1 \ : \ \begin{cases} (x_1-a_1)^2+(y_1-b_1)^2+(z_1-c_1)^2=r_1^2 \\ L_1x_1+M_1y_1+N_1z_1+P_1=0 \end{cases} \tag{B.7}$$

$$\mathsf{C}_2 \ : \ \begin{cases} (x_2-a_2)^2+(y_2-b_2)^2+(z_2-c_2)^2=r_2^2 \\ L_2x_2+M_2y_2+N_2z_2+P_2=0 \end{cases} \tag{B.8}$$

where L_i, M_i, and N_i are the components of the unit vector normal to the plane P_i of the circle C_i. P_i represents the normal distance of the plane P_i from the reference frame origin and can be calculated by substituting coordinates of a point on P_i into the equation of the corresponding plane. $\{a_i, b_i, c_i\}^T$ are the coordinates of the center of C_i, and r_i is the radius of C_i, $i=1,2$.

When two circles intersect

$$\begin{aligned} x_1 &= x_2 \equiv x \\ y_1 &= y_2 \equiv y \\ z_1 &= z_2 \equiv z \end{aligned} \tag{B.9}$$

Intersection of planes P_1 and P_2 yields a line l. (unless the two planes are parallel or identical) which can be represented as

$$\mathsf{L} : \begin{cases} x = -\frac{N_2M_1 - N_1M_2}{N_2L_1 - N_1L_2}y - \frac{N_2P_1 - N_1P_2}{N_2L_1 - N_1L_2} \\ z = \frac{L_2M_1 - L_1M_2}{N_2L_1 - N_1L_2}y + \frac{L_2P_1 - L_1P_2}{N_2L_1 - N_1L_2} \end{cases} \tag{B.10}$$

Substituting the expressions for the x and z coordinates of the intersection line into the equations for the circles results in two quadratic equation in one unknown, each equation representing the intersection of one circle and the line.[1] For each equation there will be two real solutions if the expression under radical sign (discriminant) of the solution of the quadratic equation is positive, one solution if the expression is zero, or no solution when the expression is negative. The common solution(s) from the L and C_i, $i = 1, 2$ intersections is the intersection point(s) of the two circles C_1 and C_2.

B.3 Intersection of Circle and Sphere

The expressions for a circle C and a sphere SP are

$$\mathsf{C} : \begin{cases} (x_1 - a_1)^2 + (y_1 - b_1)^2 + (z_1 - c_1)^2 = r_1^2 \\ L_1x_1 + M_1y_1 + N_1z_1 + P_1 = 0 \end{cases} \tag{B.11}$$

$$\mathsf{SP} : (x_2 - a_2)^2 + (y_2 - b_2)^2 + (z_2 - c_2)^2 = r_2^2 \tag{B.12}$$

At the intersection point(s)

$$\begin{aligned} x_1 = x_2 &\equiv x \\ y_1 = y_2 &\equiv y \\ z_1 = z_2 &\equiv z \end{aligned} \tag{B.13}$$

[1] The maximum number of real intersection points between a line (order one and circularity zero) and a circle (order two and circularity one) is two, refer to Section A.2.

The relationship between x_1, y_1, and z_1 of the plane of C, can be expressed by the equation of the plane P as

$$x_1 = \frac{-M_1}{L_1} y_1 + \frac{-N_1}{L_1} z_1 + \frac{-P_1}{L_1} \tag{B.14}$$

This equation should be satisfied at the intersection point(s), as well as the two quadratic equations corresponding to circle C and sphere SP. Substituting the expression of P for x, (y, or z) of the quadratic equations and eliminating one of the remaining y or z from the two quadratic equations results in a quadratic equation in one unknown[2] which can be solved easily.

B.4 Intersection of Circle and Ring

The expressions for a circle C and a ring RG are

$$\mathsf{C} : \begin{cases} (x_1 - a_1)^2 + (y_1 - b_1)^2 + (z_1 - c_1)^2 = r_1^2 \\ L_1 x_1 + M_1 y_1 + N_1 z_1 + P_1 = 0 \end{cases} \tag{B.15}$$

$$\mathsf{RG} : \begin{cases} s_2^2 \leq (x_2 - a_2)^2 + (y_2 - b_2)^2 + (z_2 - c_2)^2 \leq r_2^2 \\ L_2 x_2 + M_2 y_2 + N_2 z_2 + P_2 = 0 \end{cases} \tag{B.16}$$

The intersection line L of the planes of C and RG can be expressed as

$$\mathsf{L} : \begin{cases} x = -\frac{N_2 M_1 - N_1 M_2}{N_2 L_1 - N_1 L_2} y - \frac{N_2 P_1 - N_1 P_2}{N_2 L_1 - N_1 L_2} \\ z = \frac{L_2 M_1 - L_1 M_2}{N_2 L_1 - N_1 L_2} y + \frac{L_2 P_1 - L_1 P_2}{N_2 L_1 - N_1 L_2} \end{cases} \tag{B.17}$$

[2]The maximum number of real intersection points between a circle (order two and circularity one) and a sphere (order two and circularity one) is two.

The intersection point(s) of the circle and the ring corresponds to the intersection(s) of L and C that satisfy the equation of the ring.

B.5 Intersection of Circle and Torus

The expressions for a circle C and a torus TR are

$$\mathsf{C} \; : \; \begin{cases} (x_1 - a_1)^2 + (y_1 - b_1)^2 + (z_1 - c_1)^2 = r_1^2 \\ L_1 x_1 + M_1 y_1 + N_1 z_1 + P_1 = 0 \end{cases} \tag{B.18}$$

$$\mathsf{TR} \; : \; \{({x_2}^2 + {y_2}^2 + {z_2}^2) - ({r_p}^2 + {r_s}^2 + f^2)\}^2 = 4{r_p}^2 \left\{ {r_s}^2 - \left(\frac{z_2 - f cos\beta}{sin\beta} \right)^2 \right\} \tag{B.19}$$

The intersections of C and TR can be obtained similar to the circle and sphere intersections of Section B.3. That is, based on the plane equation of (B.18) one of the location coordinates can be expressed in terms of the other two. Substitution of this expression into the quadratic equations of (B.18) and (B.19) yields two expressions in terms of two unknowns. Eliminating one of the unknowns yields a quartic expression in terms of one unknown.[3] Up to four intersection points can exist (corresponding to four real distinct roots). It should be noted that if the reference frame is located at some other point (e.g., at point $\{a, b, c\}^T$) rather than torus center, x_2, y_2, and z_2 should be replaced by $x_2 - a$, $y_2 - b$, and $z_2 - c$, respectively.

[3]The maximum number of real intersection points between a circle (order two and circularity one) and a torus (order four and circularity two) is four.

Appendix C

Screw Quantities of Example Manipulator

C.1 Joint Screws

The joint screws of a branch i will be expressed with respect to a frame F_{sph_i} located at the spherical joint center p_i. The orientation of F_{sph_i} is the same as the branch base frame F_{Bi}, i.e., the z-axis is parallel to the first and the second joint axes S_{1i} and S_{2i} with the positive direction in CCW direction about Z_0-axis of the base reference frame F_0, the x-axis of F_{sph_i} is parallel to the line from b_i to the origin of F_0. Figure 3.2 illustrates the main-arm joint axes (screws) and their corresponding reciprocal wrenches for a branch i. The, joint screws in frame F_{sph_i} are

$$^{sph_i}\mathbf{S}_{1_i} = \{0,\ 0,\ 1;\ -(hS_{12}S_3 + gS_1),\ hC_{12}S_3 + gC_1,\ 0\}_i^T \qquad \text{(C.1)}$$

$$^{sph_i}\mathbf{S}_{2_i} = \{0,\ 0,\ 1;\ -hS_{12}S_3,\ hC_{12}S_3,\ 0\}_i^T \qquad \text{(C.2)}$$

$$^{sph_i}\mathbf{S}_{3_i} = \{-S_{12},\ C_{12},\ 0;\ hC_{12}C_3,\ hS_{12}C_3,\ -hS_3\}_i^T \tag{C.3}$$

$$^{sph_i}\mathbf{S}_{4_i} = \{C_{12}S_3,\ S_{12}S_3,\ C_3;\ 0,\ 0,\ 0\}_i^T \tag{C.4}$$

$$^{sph_i}\mathbf{S}_{5_i} = \{-C_{12}C_3S_4 - S_{12}C_4,\ -S_{12}C_3S_4 + C_{12}C_4,\ S_3S_4;\ 0,\ 0,\ 0\}_i^T \tag{C.5}$$

$$\begin{aligned} &^{sph_i}\mathbf{S}_{6_i} = \{a_i,\ b_i,\ c_i;\ 0,\ 0,\ 0\}_i^T \\ &a_i = [(C_{12}C_3C_4 - S_{12}S_4)S_5 + C_{12}S_3C_5]_i \\ &b_i = [(S_{12}C_3C_4 + C_{12}S_4)S_5 + S_{12}S_3C_5]_i \\ &c_i = [-S_3C_4S_5 + C_3C_5]_i \end{aligned} \tag{C.6}$$

C.2 Reciprocal Screws

The reciprocal screws associated with the main-arm joints of a branch i with respect to F_{sph_i} can be expressed as follows.

$$^{sph_i}\mathbf{W}_{1_i} = \{C_{12}S_3,\ S_{12}S_3,\ C_3;\ 0,\ 0,\ 0\}_i^T \tag{C.7}$$

$$^{sph_i}\mathbf{W}_{2_i} = \{(hC_{12}S_3 + gC_1)S_3,\ (hS_{12}S_3 + gS_1)S_3,\ (hS_3 + gC_2)C_3;\ 0,\ 0,\ 0\}_i^T \tag{C.8}$$

$$^{sph_i}\mathbf{W}_{3_i} = \{0,\ 0,\ 1;\ 0,\ 0,\ 0\}_i^T \tag{C.9}$$

where $\mathbf{W}_i\chi\mathbf{S}_j = \{\mathbf{w}_i^T;\ \mathbf{w}_{0_i}^T\}^T\chi\{\mathbf{s}_j^T;\ \mathbf{s}_{0_j}^T\}^T = \mathbf{w}_i^T\mathbf{s}_{0_j} + \mathbf{w}_{0_i}^T\mathbf{s}_j = 0;\ i = 1,2,3,\ j = 1,\ldots,6,$ $j \neq i$, i.e., the reciprocal product of $\mathbf{W}_i$ and $\mathbf{S}_j$ is equal to zero for $j \neq i$.

C.3 Structural Screws

A branch i has a degenerate configuration corresponding to the fully extended or folded back configuration of the branch ($\theta_2 = 0$ or π, and $\theta_3 = \pm\frac{\pi}{2}$).[1] There exists a "structural wrench" which is reciprocal to all of the joints of the branch when the branch is in this degenerate configuration. The screw coordinates of the structural wrench with respect to F_{sph_i} is

$$^{sph_i}\mathbf{W}_{s1_i} = \{C_1,\ S_1,\ 0;\ 0,\ 0,\ 0\}_i^T \tag{C.10}$$

Another branch degeneracy that involves a main-arm joint, occurs when $\theta_3 = 0,\ \pi$. In this configuration the second joint axis is collinear with the fourth joint axis and it passes though the spherical joint center (the last four joints of branch i form a bundle of order three). A zero-pitch wrench acting on a line passing through the bundle center p_i and the intersection of the second and the third joint axes q_i will be parallel to the first joint axis and it will be reciprocal to all of the joints of branch i. The screw coordinates of the structural wrench with respect to F_{sph_i} is

$$^{sph_i}\mathbf{W}_{s2_i} = \{0,\ 0,\ 1;\ 0,\ 0,\ 0\}_i^T \tag{C.11}$$

[1]The wrist degeneracy of a branch i corresponds to the configuration that $\theta_5 = 0,\ \pi$. This results from the dependency of the three branch distal (passive spherical) joints where the fourth and the sixth joint axes become collinear.

C.4 Velocity Analysis

C.4.1 Analysis Methods

In the forward velocity problem the velocity of active joints are known, whereas the inverse velocity problem requires finding the active joint rates which produce a required end effector velocity. Screw quantities and reciprocal products can be applied to calculate the instantaneous kinematics of parallel manipulators (Mohamed and Duffy (1985)). Redundant joint sensing can be taken advantage of in the calculation of the translational and rotational velocities of the end effector. For the considered class of parallel manipulators when all of the branch main-arm joint rates are sensed the translational velocity of the branch ends can be calculated. The end effector twist can be obtained using these translational velocities.

The velocity of the end effector can be described in terms of screw coordinates as $\mathbf{V} = \{\omega^T; \mathbf{v}_0{}^T\}^T$, where ω and $\mathbf{v}_0$ are respectively the vectors of the angular velocity of the end effector and the translational velocity of a point on the end effector instantaneously coincident with the reference origin. The branches of a parallel manipulator act on a common mobile platform. Thus, the motion of the end link of each branch is also $\mathbf{V}$. For a 6 dof branch the velocity of the branch end can be presented as $\sum_{j=1}^{6} \dot{q}_j \mathbf{S}_j = \mathbf{V}$, where $\mathbf{S}_j$ represents the screw of joint j of the branch. For general $\mathbf{V}$ none of the branches can be in a degenerate configuration, i.e., for each branch the joint screws $\mathbf{S}_j$, $j = 1, \ldots, 6$, must be independent. The required active joint rates can be calculated using the reciprocal product of a screw $\mathbf{W}_j$, which is reciprocal to all of the joints of the branch except for the actuated joint j, as

$$\dot{q}_j = \frac{\mathbf{V} \chi \mathbf{W}_j}{\mathbf{S}_j \chi \mathbf{W}_j} \quad , \quad \mathbf{S}_i \chi \mathbf{W}_j = 0 \quad \texttt{for} \quad i \neq j \; , \quad \mathbf{S}_j \chi \mathbf{W}_j \neq 0 \qquad \text{(C.12)}$$

The reciprocal products $\mathbf{V}\chi\mathbf{W}_j$ and $\mathbf{S}_j\chi\mathbf{W}_j$ are scalar quantities and can be calculated in any frame as long as the screws of the product are defined in the same frame. The screw transformation matrix $\mathbf{T}_{l,m}$ required to transfer a screw from frame m to frame l, where frame m is displaced ${}^l\mathbf{r}_{l,m}$ from frame l (expressed with respect to frame l) and its orientation with respect to frame l is defined by the 3×3 rotation matrix $\mathbf{R}_{l,m}$, is

$$\mathbf{T}_{l,m} = \begin{bmatrix} \mathbf{R}_{l,m} & \mathbf{0} \\ {}^l\tilde{\mathbf{r}}_{l,m}\mathbf{R}_{l,m} & \mathbf{R}_{l,m} \end{bmatrix} \tag{C.13}$$

The reciprocal screws can be expressed with respect to a common reference frame and can be rearranged in axis-coordinate order as $\mathbf{W}^* = \{\mathbf{w}^T; \mathbf{w}_0{}^T\}^{*T} = \{\mathbf{w}_0{}^T; \mathbf{w}^T\}^T$. The transformation matrix for each branch can be obtained from the rotation matrix and position of the specified branch frame to the common reference frame. Assembling all of these reciprocal wrenches into a matrix $[\mathbf{W}^*]$ yields

$$diag[(\mathbf{S}_j\chi\mathbf{W}_j)]\dot{\mathbf{q}}_a = [\mathbf{W}^*]^T\mathbf{V} \tag{C.14}$$

where $diag[(\mathbf{S}_j\chi\mathbf{W}_j)]$ is a $d \times r$ diagonal matrix with the diagonal elements of $\mathbf{S}_j\chi\mathbf{W}_j$. If the determinant of the matrix $[\mathbf{W}^*]$ is not zero, the end effector velocity is

$$\mathbf{V} = [\mathbf{W}^*]^{-T} diag[(\mathbf{S}_j\chi\mathbf{W}_j)]\dot{\mathbf{q}}_a \tag{C.15}$$

When $\det[\mathbf{W}^*] = 0$ the manipulator is in an uncertainty configuration.

The velocity problems for parallel manipulators can also be solved by assembling components of branch Jacobian matrices (Kumar and Gardner (1990)). For the i-th serial branch, the $d \times 1$ end effector velocity vector, $\mathbf{V}$, is $\mathbf{V} = [\mathbf{J}]_i\dot{\mathbf{q}}_i$, where $[\mathbf{J}]_i$ is the $d \times m$ dimensional Jacobian matrix of the i-th branch. If the i-th branch is

in a nondegenerate configuration and the m joints in the i-th branch are linearly independent then $m = d$ (e.g., $m = d = 6$ for a spatial non-redundant 6 dof branch). In this situation, the joint rates required for a desired velocity of the end effector can be obtained as $\dot{\mathbf{q}}_i = [\mathbf{J}]_i^{-1}\mathbf{V}$. Equations for the inverse velocity problem of the n branches can be rearranged and assembled into a matrix form

$$\begin{bmatrix} \dot{\mathbf{q}}_1 \\ \dot{\mathbf{q}}_2 \\ \vdots \\ \dot{\mathbf{q}}_n \end{bmatrix} = \begin{bmatrix} [\mathbf{J}]_1^{-1} \\ [\mathbf{J}]_2^{-1} \\ \vdots \\ [\mathbf{J}]_n^{-1} \end{bmatrix} \mathbf{V} \tag{C.16}$$

The velocity of r active joints ($r = n$ a, for symmetric actuation), $\dot{\mathbf{q}}_a$, can be expressed as

$$\dot{\mathbf{q}}_a = [\mathbf{\Gamma}]\mathbf{V} \tag{C.17}$$

where each of the rows of $[\mathbf{\Gamma}]$ are the rows from the (n $m \times d$) $[\mathbf{J}]_i$ inverses. Notice that each row of $[\mathbf{\Gamma}]$ is equivalent to $\frac{\mathbf{W}_j^{*T}}{\mathbf{S}_j \mathbf{X} \mathbf{W}_j}$. If $r = d$, $\det[\mathbf{J}]_i \neq 0$, $i = 1, \ldots, n$, and $\det[\mathbf{\Gamma}] \neq 0$, $[\mathbf{\Gamma}]$ is invertible. The forward velocity solution can be obtained as

$$\mathbf{V} = [\mathbf{\Gamma}]^{-1}\dot{\mathbf{q}}_a \tag{C.18}$$

Considering the equations for the inverse and forward velocity problem it can be seen that inverse velocity problem requires each branch Jacobian, $[\mathbf{J}]_i$, be nonsingular but the forward velocity case requires all the branches as well as the manipulator be in a nondegenerate configuration.

C.4.2 Forward Velocity Solutions

3-3-3 Joint Velocity Sensing

The velocities of the branch end points can be obtained by taking the derivative of the branch end position vectors, equation (2.5), with respect to time, i.e., for a branch i, $i = 1, 2, 3$

$$ {}^{Bi}\mathbf{v}_i = \begin{bmatrix} v_x \\ v_y \\ v_z \end{bmatrix}_i = \begin{bmatrix} -(hS_{12}S_3 + gS_1)\dot{q}_1 - hS_{12}S_3\dot{q}_2 + hC_{12}C_3\dot{q}_3 \\ (hC_{12}S_3 + gC_1)\dot{q}_1 + hC_{12}S_3\dot{q}_2 + hS_{12}C_3\dot{q}_3 \\ -hS_3\dot{q}_3 \end{bmatrix}_i \tag{C.19} $$

These branch end translational velocities can be expressed with respect to the base reference frame by ${}^0\mathbf{v}_i = \mathbf{R}_{0,B_i}{}^{Bi}\mathbf{v}_i$, and averaged to obtain the translational velocity of the end effector (center of the platform)

$$ \mathbf{v}_0 = \frac{1}{3}({}^0\mathbf{v}_1 + {}^0\mathbf{v}_2 + {}^0\mathbf{v}_3) \tag{C.20} $$

The rotational velocity of the mobile platform can be obtained utilizing the translational velocities of the branch ends, i.e.,

$$ \begin{cases} \omega_x = \frac{r_{1,e_x}\Delta v_{2x} + r_{2,e_y}\Delta v_{1y} + r_{2,e_z}\Delta v_{1z}}{-r_{2,e_y}r_{1,e_x} + r_{2,e_z}r_{1,e_y}} \\ \omega_y = \frac{-\Delta v_{1z} + \omega_x r_{1,e_y}}{r_{1,e_x}} \\ \omega_z = \frac{\Delta v_{1y} + \omega_x r_{1,e_z}}{r_{1,e_x}} \end{cases} \tag{C.21} $$

using

$$ \Delta\mathbf{v}_i = \mathbf{v}_0 - {}^0\mathbf{v}_i = \tilde{\omega}\mathbf{r}_{i,e} \tag{C.22} $$

and $\mathbf{r}_{e,i} = -\mathbf{r}_{i,e} = {}^0\mathbf{p} - {}^0\mathbf{p}_i$ and $\tilde{\omega}$ is the skew symmetric matrix of the end effector angular velocities.

Non-Redundant Symmetric Joint Velocity Sensing

The velocity of the end effector can be described by $\mathbf{V} = \{\omega^T; \mathbf{v}_0^T\}^T$

$$\mathbf{V} = [\mathbf{W}^*]^{-T} diag[(\mathbf{S}_j \chi \mathbf{W}_j)]\dot{\mathbf{q}}_a \tag{C.23}$$

where for a branch i

$$\begin{aligned} \mathbf{S}_1 \chi \mathbf{W}_1 &= g S_2 S_3 \\ \mathbf{S}_2 \chi \mathbf{W}_2 &= -g h S_2 {S_3}^2 \\ \mathbf{S}_3 \chi \mathbf{W}_3 &= -h S_3 \end{aligned} \tag{C.24}$$

C.4.3 Inverse Velocity Solutions

The active joint rates can be calculated using the reciprocity as

$$\dot{q}_1 = \frac{\mathbf{V} \chi \mathbf{W}_1}{\mathbf{S}_1 \chi \mathbf{W}_1} = \frac{C_{12} S_3 v_{0x} + S_{12} S_3 v_{0y} + C_3 v_{0z}}{g S_2 S_3} \tag{C.25}$$

$$\dot{q}_2 = \frac{\mathbf{V} \chi \mathbf{W}_2}{\mathbf{S}_2 \chi \mathbf{W}_2} = \frac{(gC_1 + hC_{12}S_3) S_3 v_{0x} + (gS_1 + hS_{12}S_3) S_3 v_{0y} + (gC_2 + hS_3) C_3 v_{0z}}{-g h S_2 {S_3}^2} \tag{C.26}$$

$$\dot{q}_3 = \frac{\mathbf{V} \chi \mathbf{W}_3}{\mathbf{S}_3 \chi \mathbf{W}_3} = \frac{v_{0z}}{-h S_3} \tag{C.27}$$

C.5 Forward and Inverse Force Analyses

Using the conservation of rate of work the $m \times 1$ vector of i-th branch joint torques, τ_i, is $\tau_i = [\mathbf{J}]_i^T \mathbf{F}_i$, where $\mathbf{F}_i$ is the $d \times 1$ vector of forces and moments exerted by the end effector (mobile platform) on the i-th branch end. Since only a actuators are active, $m - a$ joint torques in τ_i must be zero. The vector of joint torques, τ_a, could be calculated using the principle of virtual work

$$\mathbf{F}^T \mathbf{V} = {\tau_a}^T \dot{\mathbf{q}}_a = {\tau_a}^T [\mathbf{\Gamma}] \mathbf{V} \tag{C.28}$$

$$\mathbf{F} = [\mathbf{\Gamma}]^T \tau_a \tag{C.29}$$

where $\mathbf{F} = \sum_{i=1}^{n} \mathbf{F}_i$ is the $d \times 1$ vector of forces and torques applied on the end effector.

Utilizing the screw quantities $\mathbf{F}$ can be obtained as

$$\mathbf{F} = [\mathbf{W}]\mathbf{w} \tag{C.30}$$

where the wrench intensities, $\mathbf{w}$, are

$$w_j = \frac{\tau_j}{\mathbf{S}_j \chi \mathbf{W}_j} \tag{C.31}$$

and τ_j is the input torque of j-th actuator for each branch. Note that the indices corresponding to the branch numbers are omitted for simplicity. Similarly, the required actuator's torques for the end effector wrench are

$$\tau_j = w_j(\mathbf{S}_j \chi \mathbf{W}_j) \quad \texttt{for} \quad j = 1, \ldots, m \tag{C.32}$$

where

$$\mathbf{w} = [\mathbf{W}]^{-1}\mathbf{F} \tag{C.33}$$

Appendix D

RSI Hand Controller Redesign

D.1 Kinematic Specifications

The six degree of freedom hand controller, manufacturered by RSI Research Ltd., is a three-branch parallel mechanism with identical branches (Figure 2.4). Nominally the axes of the first and the second joints are parallel and the third joint axis intersects and is perpendicular to the second joint for each branch. The branch main-arm joints are separated by a link distance between the first and the second joints and a joint offset between the intersection point of the second and the third joint and the spherical branch end joint. The first joints of each branch are nominally tangent to and equally spaced ($\frac{2\pi}{3}$ radians apart) about a base circle. Similarly, the end points of the branches are attached to the common mobile platform such that the three branch ends define an equilateral triangle contained in a platform circle.

The parts of the hand controller are claimed to have been manufactured with a tolerance of ± 0.001 inches. In addition to the manufacturing tolerances, because of the assemblying of multiple parts and potential inaccuracies due to assembly mis-

alignments, the error range of the handle position and orientation is expected to be at least an order of magnitude larger than 0.001.

The branch which is connected to the base platform in between the two stands is referred to as the first branch (branch A) and the remaining two branches are numbered in the CCW direction as the second and the third branches. The second and the third branches are numbered in the CW direction by RSI Research Ltd as branches A, B, and C. It should be noted that the CW numbering (A, B, C order) is used in the calibration routines. However, the CCW numbering is employed in the forward displacement and diagnostic routines.

A reference frame F_0 is located at the center of the base platform (base center) with Z_0 normal to the platform plane and Y_0 in the direction of a line from the center of the base toward the first joint of branch one. The branch i reference frame is chosen at the branch base point b_i with the z-axis being tangent to the base circle and collinear with the first joint axis of branch i. The positive z-axes of the branch reference frames are in the CCW direction about the Z_0-axis of the base reference frame. The x-axis is in the direction of a line from b_i to the origin of the base reference frame (base platform center), and the y-axis is in the direction of the base reference frame's Z_0-axis (normal to the base platform).

The hand controller's rest position corresponds to the end effector position of

$$\{X_0, Y_0, Z_0; \theta_{X_0}, \theta_{Y_0}, \theta_{Z_0}\}^T = \{0, 0, -2.666; 0, 0, 0\}^T$$

The hand controller used to return to the rest position by the spring force after being released. Due to the tightening of the joint clearances in the redesign it does not return to the rest position anymore and it stays where it is released. However, the rest position can be used as the home position for starting up the hand controller. At the rest position the joint displacements (in radians) of branch i, $i = 1, 2, 3$, are

$$\{\theta_1, \theta_2, \theta_3, \theta_4, \theta_5, \theta_6\}^T = \{0.420(24.1°), -1.971(-112.9°), 1.571(90°), 0, 0, 0\}^T$$

These joint rotations are measured with respect to the zero-configuration of the branch. At the zero-configuration of a branch, the branch's lower and upper arm along with the first and the second joint axes would lie on the base platform while the second joint axis would pass through the branch end point (spherical joint center). This configuration is a branch degeneracy. It should be noted that due to the joint limits, this zero-configuration cannot be reached by the branches of hand controller.

The motion range of the end effector of the hand controller with respect to the rest position is about ± 3 inches in the X_0, Y_0, and Z_0 directions and its rotational range is approximately $\pm\frac{\pi}{2}(90°)$ about X_0, Y_0, and Z_0 directions.

The joint limits of hand controller with respect to the zero-configuration of its branches are as follows. For the first joint, the joint displacement range is between $-\frac{\pi}{2}$ to $\frac{2\pi}{3}$ ($-90°$ to $120°$). The second joint's displacement range is approximately between $-\pi$ ($-180°$) to 0. The displacement range of the third joint is less than $\frac{\pi}{6}$ to π ($30°$ to $180°$).

D.2 Additional Potentiometers

The original device had potentiometers on the first and the third joint axes of each branch, i.e., it accommodated a total of six potentiometers. These potentiometers were used to measure displacements of the corresponding joints to allow calculation of the handle pose. An end effector pose can be defined utilizing six sensed joints. However, there is no closed form solution for the handle pose and the solution has to be calculated by an iteration method. To obtain a closed form solution for the

Table D.1: Hand controller connections.

HAND CONTROLLER		BLUE BOX	RTI600 A/D	
	Pin #	Pin #	Pin #	Channel #
POT A1	10	31	31	18
POT A2	5	35	35	19
POT A3	11	37	37	20
POT B1	8	41	41	21
POT B2	6	43	43	22
POT B3	9	47	47	23
POT C1	12	26	26	24
POT C2	7	28	28	25
POT C3	13	32	32	26
TRIGGER IN	15	34	34	27
TRIGGER OUT	16	38	38	28
THUMB RIGHT	17	40	40	29
THUMB LEFT	18	44	44	30
GRIP SWITCH	19	46	46	31
GND	14	50	50	
-5 V (A)	1			
-5 V (B)	2			
-5 V (C)	3			
+5 V (A)	23			
+5 V (B)	24			
+5 V (C)	25			

forward displacement problem of the hand controller three more potentiometers were added to the device, i.e., a potentiometer on the second joint axis of each branch. This resulted in the sensing of all of the branch main-arm joints and increased the number of potentiometers to nine. In addition to providing a unique handle pose, the extra potentiometers also provide an opportunity to utilize the redundant sensing for the implementation of the proposed sensor failure diagnosis algorithm on the hand controller.

D.2.1 Connection to Power Supply and Voltage Regulator (Blue Box)

To incorporate the three potentiometers on the second joint axes, the hand controller branches had to be taken apart and later reassembled. The wiring of the hand controller was changed as well. The new wiring was made according to the format being used by the RSI Research Ltd. on their new version of hand controller which utilizes nine joint sensors, refer to Table D.1.

D.2.2 Connection to RTI600 A/D Converter

The last fourteen channels of the RTI600 analog to digital converter were specified for the hand controller, where channels 18-26 were used to read the displacements of the main-arm joints (potentiometer rotation) and the last five channels, i.e., channels 27-31, were connected to the switches on the hand controller (Table D.1). The order of the joint potentiometers connected to the channels 18-26 is as follows. Channels 18-20 are used for the first, the second, and the third joint of branch one. Channels 21-23 and 24-26 are connected to the potentiometers of the second and the third branches, respectively, with channel 21 corresponding to the first joint of the second branch and so on.

D.2.3 Resolution of Joints

The RTI600 analog to digital converter is supplied with regulated voltage of ± 10 volts. The RTI600 A/D converter has 12-bit precision which gives $2^{12} = 4096$ counts where 0, 2048, and 4096 counts correspond to -10, 0, and $+10$ volts, respectively. However, the voltage input to the potentiometers is currently ± 5 volts. Hence, -5, 0

and +5 volts will respectively correspond to 1024, 2048 and 3072 counts. Note that the A/D converter of the RSI Research Ltd. is supplied with regulated ±5 volts with 12-bit precision, and hence, their −5, 0 and +5 volts correspond to 0, 2048 and 4096 counts, respectively.

D.2.4 Approximate Values of Potentiometers' Offsets and Gains

The relationship between the joint displacement θ_j and the potentiometer signal η_j is modeled to be a linear function

$$\theta_j = k_{1_j}\eta_j + k_{2_j} \tag{D.1}$$

The approximate values of the joint angle gain k_{1,app_j} and the joint offset k_{2,app_j} can be calculated as described in the following paragraph.

The electrical angle of the Midori CP-2FCB potentiometer is specified as 340°. The A/D converter has 12 bit precision for the range of ±10 volts and because the voltage regulation of the potentiometers is ±5 volts, the precision of the potentiometers will be 11 bit (2^{11} = 2048 counts). The approximate gain of the potentiometers is $k_{1,app}$ = (340°)(π/180)/(2048) = 0.0029 radian/count. Based on the zero-configuration of the branches and also the assigned direction of the joint axes, it was determined that the approximate gain of the first and the second joint potentiometers are −0.0029 radian/count, i.e., these potentiometers are connected in the negative sense.

During assembly the potentiometers were rotated and clamped to give approximately 0 volt output corresponding to a 2048 count when the hand controller was in

the rest position. The approximate potentiometer offsets at the rest position can be obtained by rearranging equation (D.1) as

$$k_{2,app_j} = \theta_{rest_j} - k_{1,app_j}\eta_{rest} \tag{D.2}$$

where θ_{rest_j} is the theoretical j-th joint angle at the rest position and $\eta_{rest} = 2048$ counts. Therefore, the potentiometer offsets of the first, the second and the third main-arm joints of the branches are respectively, 6.354, 3.963, and -4.363 radians. These values were used to check the forward displacement program before calibrating the potentiometers of the hand controller.

D.3 Redesign - Limiting and Modeling Potential Error Sources

To reduce the potentiometers noise for the calibration procedure, the A/D channel data corresponding to the readings of the potentiometers were filtered by averaging twenty samplings using *moving window averaging* (Press et al. (1992)). The basic idea of averaging values locally is that rapid variations from point to point will be averaged out and slow variations will be retained, corresponding to smoothing or lowpass filtering the original reading.[1] Because at each configuration the joint sensor reading is constant, no bias was introduced into the readings to obtain the moving average results. For other uses the filtering of the potentiometer readings was achieved by five-sampling moving average in order to limit errors resulting from longer response time. This will reduce the bias which could be introduced at a local maximum where

[1]The moving-average filter can be generalized by forming a weighted average of n samples (instead of weighting each sample by $1/n$) in order to obtain a sharp cutoff frequency.

the moving window averaging always reduces the sensor readings. The clearances of the joints were reduced by either tightening the joints or by adding shims. This slightly reduced the error of the distance between the spherical joint centers during the motion of the mobile platform by eliminating backlash.

The calibration fixture of the RSI Research Ltd. was used to measure the end effector pose of the hand controller. The twelve poses of the fixture correspond to the end effector positions with negative z coordinates (in the hand controller base reference frame). Another block with a length of 4 inches was machined to obtain positive z coordinates and to increase the number of data from twelve to eighteen. It was observed that the potentiometer calibration parameters obtained from these eighteen poses reduces the error in positive z direction but increases the error in negative z direction (compared to the parameters calculated using the original twelve poses which result in a locally accurate model). The number of fixture poses was further increased by rotating the fixture by $\frac{2\pi}{3}$ and $\frac{4\pi}{3}$ radians about the Z_0-axis of the base reference frame. It should be noted that the errors can be reduced but not eliminated even with large number of measurements, due to the measurement and fixture assembly related tolerances.

To allow restriction of the workspace of the hand controller, adjustable joint limits were prepared and used on the first and the third main-arm joints of each branch. These limits allow the effect of the size of the work volume on the calibration procedure to be studied. It can also provide a specific workspace for testing the sensor fault detection schemes.

To increase the precision of the hand-controller, the primary sources of inaccuracy should be identified and eliminated. An appropriate kinematic model of the hand controller is essential and the exact location of the mobile platform at each pose might be necessary for a successful calibration. The kinematic model could include

the radii of the base and the mobile platform circles, the location of each branch end on these circles (or the location of branch bases/ends on these platforms if the circles are not perfect), the pose of the end-effector corresponding to these branch end locations since the end-effector location on the mobile platform might not correspond to the centroid of the branch end locations, and the link lengths of the branches. A more sophisticated model might also take into account the link lengths, joint offsets, and link twist angles resulting from the machining and assemblying tolerances. If these parameters cannot be measured, their values can be identified from the kinematic calibration of the hand-controller (as is performed in Chapter 5).

The BHN710 coordinate measuring machine in the CMM Lab, University of Victoria, has a resolution of 0.00002 inches and was used to measure the location of the branch ends on the mobile platform, and also to measure the relative position of different mobile platform configurations on the calibration fixture. It was verified that the branch ends are located on a circle with a radius of 1.5 inches and a spacing of 120°. The measured error for the circle radius was less than 0.004 inches and for the branch end spacing was 0.04°. It was also found that the end-effector (mobile platform frame) is located at the centroid of the branch ends p_1, p_2, and p_3 within ± 0.004 inches tolerance. Furthermore, the errors of the distance between branch ends were measured to be very small, the maximum error being 0.35% (0.009 inches of the nominal value. During measurements it was noticed that the plane of the calibration fixture is not exactly a horizontal plane, and that the end effector obtainable positions are not that perfect.

Appendix E

Joint Sensor Calibration Model

E.1 Calibration Models

The purpose of joint sensor calibration is to relate the signal from the joint displacement transducer to the actual joint displacement. In many cases, this procedure must be done after the assembly of the manipulator and also calibration must be repeated if the joint has been disassembled for maintenance or part replacement. There are a variety of joint displacement transducers. These transducers are usually rotary or linear and they produce a digital signal or an analog voltage. If the transducer is mounted to the joint axis directly the model is simple and it relates the transducer signal to the joint displacement. When the position transducers are on a prime mover such as a motor shaft, the model includes the kinematics of the drive system. The relationship between the joint displacement θ_j and the transducer signal (analog input data) η_j can be defined as

$$\theta_j = f_j(\eta_j, \gamma_j) \tag{E.1}$$

where γ_j represents the vector of parameters in the function $f_j(\eta_j, \gamma_j)$. If function $f_j(\eta_j, \gamma_j)$ is assumed to be linear then

$$\theta_j = k_{j_1}\eta_j + k_{j_2} \tag{E.2}$$

The purpose of calibration is to determine the values of the joint angle gain k_{j_1} and the joint offset k_{j_2}, i.e., $\gamma_j = \{k_{j_1}, k_{j_2}\}^T$.

When a rotary potentiometer is used as a position feedback transducer, the displacement of the joint is converted by the potentiometer into a proportional voltage that is used as a feedback signal in the controller. The analog voltage must be converted into a digital value to be used by digital computers which are used to control manipulators. If the analog to digital (A/D) converter has a resolution of 12 bits, the entire range of joint motion is expressed in 2^{12} or 4096 increments. If the joint range is 360°, any joint motion less than 360°/4096 cannot be sensed.[1]

The output of an incremental encoder is a pulse count n. If the encoder is connected directly to a revolute joint axis the joint angle is $\theta = k_1 n + k_2$, where k_1 is the angle represented by each pulse and k_2 is the joint angle when the pulse count is zero. The value of k_1 can be determined by obtaining the number of lines on the encoder and checking to see if the electronic counter in the controller multiplies the count by 1, 2, or 4. For example, for a device with m lines and a count multiplier of 2 there will be $2m$ counts per revolution and if the device is connected to the joint shaft $k_1 = 360/2m$ degree per count. k_1 may be treated as constant and not included in the calibration process. The value of k_2 corresponds to the joint angle when the pulse is zero. This value must be set every time the controller is powered up since the encoder gives a relative pulse count and not an absolute reading of joint angle.

[1]The smallest signal change that can be both sensed and acted on by the controller is called the resolution of the joint.

k_2 is usually referred to as the joint offset and can be determined by moving the joint to a known angle and resetting the pulse counter. Many robots do this as a part of start-up sequence and the process is referred to as the homing or initialization procedure.

For cases which require high precision, a more sophisticated model is required to describe the relationship between the transducer signal and the joint displacement, e.g., to include drive train kinematics. Note that the design of the joint and type of the transducer might dictate the form of the model used. However, the particular type of involved nonlinearities must be deduced from experimental data. When a revolute joint is driven by a dc motor through a gear train, if the joint transducer is an encoder mounted on the motor shaft rather than the joint axis, nonlinearities in the gear train between the motor and the joint axis will affect the relationship between the joint angle and the encoder.

The measurement process may consist of either using some external measurement device to determine the actual joint angle accurately, e.g., use of a fixture to ensure that a joint is at a known displacement, or moving the joint to some "known" configuration, e.g., when a link is "straight up".

The signal that comes from the joint transducer is converted to the actual joint displacement by the controller in the software. This conversion is accomplished employing the identified parameters. For a linear joint sensor calibration model, linear regression analysis can be employed to identify the joint angle gains and offsets. Regression analysis deals with the relationship among measured variables. This relationship is expressed in terms of an equation relating one dependent variable to one or more independent variables.[2] A typical situation is that of fitting a straight line to a

[2]If the number of independent variables is one the analysis is called *simple regression* compared to *multiple regression* for several independent variables. If the relation is linear in terms of the

set of measured points on a plane. The decision with regard to which variable should be taken as the dependent variable depends on the physical nature of the problem.

E.2 Potentiometers

Potentiometers are one of the simplest devices available for measuring displacement. A potentiometer consists of a resistive element and a wiper that contacts the resistive element. The resistive element which is a coil of resistive wire is wrapped around a nonconducting base. A voltage is applied across the resistive winding and the voltage sensed by the wiper is proportional to the position of the wiper contact point. If the wiper is attached to the moving portion of the robot joint, then the wiper voltage will vary in proportion to the joint displacement. When the wiper is sliding from one coil to the next the voltage change will be a discrete variation (rather than continuous). The wire winding can be replaced with a thin resistive film to obtain a high (theoretically infinite) resolution. However, the electrical noise between the wiper and the film as well as the nonlinearities in the resistance of the film significantly limit the variation in voltage that can practically be determined. Note that since the displacement signal of a potentiometer is an analog voltage, any variation in the voltage level will be perceived as joint motion, e.g., the controller might sense a wrong displacement because of electrical noise in the environment or due to a slight variation of the reference voltage (± 5 volt for the RSI hand controller), Mooring et al. (1991).

unknown coefficients, the analysis is referred to as *linear regression analysis* and the coefficients are called the regression coefficients which can be estimated using least-squares.

VITA

Surname: Notash Given Names: Leila

Educational Institutions Attended:

University of Victoria	1991 to 1995
University of Toronto	1989 to 1990
Middle East Technical University	1984 to 1988

Degrees Awarded:

M.A.Sc.	University of Toronto	1991
B.Sc. (High Honour)	Middle East Tech. University	1988

Honours and Awards:

UVic. Charles S. Humphrey Award	1993–1994
U. of T. Open Fellowship	1989–1990
U. of T. Differential Fee Waiver	1989–1990

Publications:

1. L. Notash and R. P. Podhorodeski. Sensor Fault Detection Scheme for Fault Tolerance Operation of Parallel Manipulators. to be presented at *IEEE Int. Conf. on Sys. Man and Cyber.*, Vancouver, October 1995.

2. L. Notash and R. P. Podhorodeski. Kinematic Calibration of a Parallel Manipulator Based Hand Controller. In *Proc. of 15th CANCAM Conf.*, Victoria, pp. 872–873, May 1995. (The full paper will be presented at *IEEE Int. Conf. on Sys. Man and Cyber.*, Vancouver, October 1995).

3. L. Notash and R. P. Podhorodeski. Forward Displacement Analysis and Uncertainty Configurations of Parallel Manipulators with a Redundant Branch. submitted to *J. Robotic Systems*, October 1994.

4. L. Notash and R. P. Podhorodeski. On the Forward Displacement Problem of Three-Branch Parallel Manipulators. *J. Mech. Mach. Theory*, 30(3):391–404, 1995.

5. L. Notash and R. P. Podhorodeski. Uncertainty Configurations of Three-Branch Parallel Manipulators - Identification and Elimination. In *Proc. of ASME 23rd Biennial Mechanisms Conf.*, Minneapolis, volume DE-Vol. 72, pages 459–466, 1994.

6. L. Notash and R. P. Podhorodeski. Complete Forward Displacement Solutions for a Class of Three-Branch Parallel Manipulators. *J. Robotic Systems*, 11(6):471–485, September 1994.

7. J. K. Mills, L. Notash, and R. G. Fenton. Optimal Design and Sensitivity Analysis of Flexible Cam Mechanisms. *J. Mech. Mach. Theory*, 28(4):563–581, 1993.

8. L. Notash and R. G. Fenton. A Comparison of the Efficiency of the Various Representations of Rigid Body Displacements and their Applications in Robotics. In *Proc. Int. Conf. on Engineering Applications of Mechanics*, Iran, pp. 274–281, 1992.

9. L. Notash, R. G. Fenton, and J. K. Mills. Sensitivity Analysis of Systems Coefficients to Aid the Design of Cam Mechanisms. In *Proc. of 2nd National Applied Mechanisms and Robotics Conf.*, Cincinnati, Vol. 1, IVA.6, 1991.

10. L. Notash, R. G. Fenton, and J. K. Mills. Optimal Design of Flexible Cam Mechanisms. In *Proc. of 8th World Congress on the Theory of Machines and Mechanisms*, Czechoslovakia, pp. 695–698, 1991.

PARTIAL COPYRIGHT LICENSE

Title of Dissertation:

Kinematic Solutions for the Effective Implementation of Parallel Manipulators

Author: _____

Leila Notash

July 4, 1995

Date